Silesian University of Technology

Investigation of non-toxic dye-sensitized solar cell materials for circular design approaches

Fabian Schoden

PhD dissertation written under guidance of
Prof. Dr. hab. Tomasz Błachowicz and
Prof. Dr.-Ing. Eva Schwenzfeier-Hellkamp

June 7, 2023

Contents

Acknowledgments

I thank Prof. Dr. hab. Tomasz Błachowicz, Prof. Dr.-Ing. Eva Schwenzfeier-Hellkamp, Prof. Dr. Dr. hab. Andrea Ehrmann and my colleagues for supporting me during my scientific work. I also thank my family and friends for motivating and supporting me.

Abstract

The climate crisis and the natural resource crisis are great challenges of our current time. In order to address the problems arising from this, it is necessary to increase the use of renewable energy resources and use them more efficiently. Dye-sensitized solar cells (DSSCs), being the main subject of the current work, are based on technology that supports the move to a more resource-efficient green energy supply. The presented doctorate has interdisciplinary character, covering two main research disciplines: materials engineering and related business activities.

The thesis presents a holistic design approach related to the circular economy, based on non-toxic materials for the manufacturing of DSCCs. The literature review using state-of-the-art support tools such as the VOSviewer tool revealed the research gap in the field of DSSC recycling and remanufacturing.

To fill this research gap, experiments with mechanical grinding and melting of materials were carried out. Several methods used in materials engineering, electronics and solid state physics were used to characterize the investigated materials. Specifically, the glass substrate of the used DSSCs was investigated using inductively coupled plasma optical emission spectrometry (ICP-OES), and the glass' surface was examined by scanning electron microscopy energy dispersive X-ray (SEM-EDX) and atomic force microscopy (AFM). AFM is the latest method for studying the surface morphology of individual DSSC layers.

The research methodology included quantitative identification of elements and compounds and a preliminary evaluation of the relationship between the roughness of the layers, including the TiO_2 semiconductor layer, and the resulting cell current-voltage characteristics as well as the power conversion efficiency.

On top of analyzing the DSSC materials and performing recycling experiments a series of remanufacturing experiments was performed. In these experiments, old DSSCs were disassembled and their conductive glass substrates were reused to build new DSSCs. This process is promising, since the remanufactured DSSCs have comparable efficiencies to newly-manufactured DSSCs and can be remanufactured multiple times.

In the final investigation, a potential circular DSSC was illustrated using the Circo method. This method is a framework to transform a linear product into a circular one coupled with a suitable business model. The business model described is a performance-contracting model, integrating DSSCs into a customer's building and offering green energy as a service. The circular design of a product is key to enable an efficient recycling or remanufacturing process.

The thesis consists of six main chapters. The introduction presents the main ideas of the thesis. In chapter two the theoretical foundations about the materials and fabrication methods for DSCCs are described. Chapter three describes the methodology of the experiments performed and the equipment used. The fourth chapter presents the results of the research, while the fifth chapter contains a discussion of the results, in particular, the business model is presented in its last sub-chapter. The last chapter contains the final conclusions of the conducted research.

Streszczenie

Kryzys klimatyczny i kryzys zasobów naturalnych to wielkie wyzwania obecnych czasów. Aby zaradzić problemom z tego wynikającym, konieczne jest zwiększenie wykorzystania zasobćw energii odnawialnej oraz jej bardziej efektywne wykorzystanie. Ogniwa słoneczne uczulane barwnikiem (DSSC, Dye-Sensitized Solar Cell), będące przedmiotem obecnej pracy, są technologią, która wspiera tego rodzaju postulat. Przedstawiana pracy ma charakter interdyscyplinarny, obejmujący dwa zasadnicze obszary: inżynierię materiałową oraz powiązane z tym planowanie działań biznesowych.

W rozprawie przedstawiono całościowe podejście projektowe związane z gospodarką o tzw. cyklu zamkniętym, oparte o nietoksyczne materiały służące do wytwarzania ogniw DSCC. Uzasadnieniem badań w zakresie inżynierii materiałowej ogniw był wnikliwy przegląd literaturowy, z wykorzystaniem nowoczesnych narzędzi wspomagających typu VOS-viewer, nawiązujący do niespotykanych szeroko etapów obróbki technologicznej związanych z regeneracją ogniw lub odzyskiem i ponownym wykorzystaniem nietoksycznych materiałów fotowoltaicznych. Aby wypełnić tę lukę badawczą, przeprowadzono eksperymenty z mechanicznym mieleniem i topnieniem materiałów. Do charakteryzacji materiałów wykorzystano kilka metod stosowanych w inżynierii materiałowej, elektronice i fizyce ciała stałego. Były to przede wszystkim: optyczna spektrometria emisyjna z wykorzystaniem plazmy sprzężonej indukcyjnie (ICP-OES), skaningowa mikroskopia elektronowa z dyspersją energii promieniowania rentgenowskiego (SEM-EDX) oraz mikroskopia optyczna oraz mikroskopia siły atomowej (AFM) do badania morfologii powierzchni poszczególnych warstw tworzących ogniwo. W trakcie prac dokonano identyfikacji ilościowej pierwiastków i związków a także dokonano wstępnej oceny relacji pomiędzy chropowatością warstw, w tym półprzewodnikowej warstwy TiO_2, a otrzymywanymi charakterystykami prądowo-napięciowymi ogniw oraz współczynnikiem wydajności fotokonwersji PCE.

Procedury regeneracji lub recyklingu były powtarzane kilkukrotnie a następnie przeprowadzono wszechstronną charakteryzację porównawczą w odniesieniu do materiałów nowych lub pochodzących z różnych okresów w przeszłości.

W końcowym etapie badań, przedstawiono potencjalny proces produkcji, zgodny z zasadami obiegu zamkniętego i zilustrowany przy użyciu metody Circo. Podejście to stanowi nowy przykład przekształcenia klasycznego liniowego procesu produkcyjnego w proces obiegu zamkniętego, w połączeniu z odpowiednim modelem biznesowym. Opisany model biznesowy to procedura oparta o kryterium wydajności energetycznej ogniwa, zamontowanego w budynku klienta i oferujący zieloną energię jako usługę.

Praca składa się z sześciu głównych rozdziałów. We wprowadzeniu przedstawiono główne założenia pracy doktorskiej. Rozdział drugi ma charakter teoretyczny i zawiera opis materiałów i metod wytwarzania ogniw słonecznych uczulanych barwnikiem (DSCC). W rozdziale trzecim opisano metodologię stosowanych badań a także zaprezentowano aparaturę eksperymentalną. Rozdział czwarty przedstawia wyniki badań, natomiast rozdział piąty zawiera dyskusję wyników, w szczególności w ostatnim jego podrozdziale przedstawiony jest model biznesowy. Ostatni, krótki rozdział zawiera wnioski końcowe z przeprowadzonych prac badawczych.

Rozszerzone streszczenie pracy doktorskiej

I Cel badań

Ludzkość stoi w obliczu poważnego kryzysu klimatycznego [1] związanego z nadmierną produkcją gazów cieplarnianych, w tym dwutlenku węgla. Istotnie ważnym czynnikiem redukcji emisji dwutlenku węgla jest przejście na odnawialne źródła energii [2]. Niestety, podejście takie jest często źródłem produkcji mnóstwa odpadów na zakończenie okresu użytkowania danego systemu energetycznego. Połączone jest to ze słabymi możliwościami ponownego wykorzystania materiałów [3,4]. Generalnie, wpływa to wszystko niekorzystnie na stan zasobów naturalnych, co jest w konsekwencji źródłem kolejnego kryzysu. Kryzys zasobów staje się widoczny, na przykład, w zaburzeniu łańcucha dostaw materiałów do produkcji elementów półprzewodnikowych lub w rosnących cenach drewna traktowanego jako klasyczne źródło energii [5, 6]. Przeróbka materiałów i ich ponowne wykorzystanie mają więc sens nie tylko środowiskowy, ale również ekonomiczny. W związku z tym, przejście funkcjonowania przemysłu na wykorzystanie metod gospodarki cyrkularnej - inaczej gospodarki obiegu zamkniętego - może wnieść znaczący wkład w rozwiązanie powyższych problemów. W gospodarce cyrkulacyjnej produkty i materiały krążą dzięki takim działaniom technologicznym jak naprawa, ponowne użycie, regeneracja oraz recykling [7]. Koncepcja gospodarki cyrkularnej przeciwstawia się istniejącemu systemowi tzw. gospodarki linearnej lub gospodarce typu „take, make and waste" [8].

Obiecującym podejściem, wpisującym się w szeroko rozumiane gospodarowanie w obiegu zamkniętym, które zostało badane w tej pracy, jest technologia wytwarzania ogniw słonecznych uczulonych barwnikiem (Dye Sensitized Solar Cell, DSSC). Technologia ta może być oparta na materiałach nietoksycznych - przy niskim zapotrzebowaniu na energię w trakcie produkcji – oraz może być oparta na wysokiej czystości procesów wytwarzania, co pozwala na jej lokalizację w obszarach wiejskich lub w krajach rozwijających się o niskim poziomie skażenia środowiska [9–12]. Z drugiej strony, wydaje się, że ogniwa DSSC nie zastąpią klasycznej fotowoltaiki opartej na krzemie, ale mogą ją uzupełniać [13]. Obecne prowad-

zone w tym zakresie badania nad ogniwami DSSC koncentrują się głównie na poprawie stabilności mechanicznej elektrolitu, będącego istotnym elementem konstrukcji ogniwa DSSC, na zwiększeniu sprawności konwersji mocy (Power, Conversion Efficiency, PCE) oraz na zastosowaniu materiałów „zrównoważonych". Wymaga to jednak prowadzenia intensywnych prac badawczych, zanim technologia ta będzie mogła osiągnąć poziom umożliwiający produkcję przemysłową [14, 15].

Same badania nad materiałami właściwymi dla gospodarki zrównoważonego rozwoju koncentrują się na ocenie ich cyklu życia (LCA, Life Cycle Assessment) oraz na ekoprojektowaniu i wykorzystaniu tzw. zielonej chemii [16] czyli materiałów nietoksycznych [17–19]. Co ważne, wykazano już wcześniej, że recykling materiałów DSSC może mieć pozytywny wpływ na środowisko naturalne [18], jednak badania tego typu nie są prowadzone w wystarczająco szerokim zakresie [16, 20].

Celem obecnej pracy doktorskiej było zbadanie materiałów używanych do produkcji ogniw DSSC, które można wielokrotnie wykorzystać. W konsekwencji, sformułowano następującą hipotezę badawczą: materiały do produkcji ogniw DSSC, mogą podlegać cyklicznym procesom technologicznym tak, aby uzyskana stabilność parametrów strukturalnych, optycznych i elektrycznych, dawała możliwość ich ponownego wykorzystania w urządzeniach fotowoltaicznych.

W czasie badań prowadzonych w ramach obecnej pracy doktorskiej stało się jasne, że w projektowaniu nowych urządzeń wytwarzających tzw. zieloną energię, istotną rolę odgrywa materiałoznawstwo. Dzięki temu można wyprodukować nietoksyczne dla środowiska oraz zgodne z podejściem gospodarki cyrkularnej ogniwa barwnikowe DSSC. Co warte jest podkreślenia, produkcja fotowoltaiki krzemowej jest procesem bardzo energochłonnym, podczas gdy ogniwa DSSC mogą być wytwarzane w sposób niskoemisyjny i niskoenergetyczny [15]. Nie oznacza to jednak, że metody proekologiczne nie mogą być również stosowane w produkcji krzemowych modułów fotowoltaicznych [21].

Ogniwo barwnikowe DSSC zostało wynalezione przez Michaela Grätzela i Briana O'Regana w roku 1991 [22]. W tym czasie produkcja ogniw krzemowych z krystalicznego krzemu (c-Si) była bardzo droga, a technologia DSSC stanowiła tańszą alternatywę. Jednak w lat-

ach 2005-2015 koszty produkcji ogniw c-Si zostały drastycznie obniżone. Spowodowane to było to budową przez Chiny nowego programu produkcji ogniw c-Si PV. Dlatego też, z powodów komercyjnych, nie ma obecnie przemysłowych zastosowań dla ogniw DSSC, które mogłyby zastąpić moduły c-Si [23]. Możliwe obszary zastosowań materiałów DSSC to ich integracja w budynkach, np. jako okna lub fasady. Ponadto, ogniwa te mogą być wykorzystane jako źródła energii w przenośnych urządzeniach małej mocy, takich jak zegarki. Przykładowo, szwajcarskie firmy Asulab i Leclanché, wypuściły na rynek prototypy takich produktów w połowie lat 90-tych [23].

Trendem, który może jeszcze bardziej zwiększyć zapotrzebowanie na ogniwa DSSC w urządzeniach małej mocy jest tzw. Internet Rzeczy. Przy szybkim wzroście zapotrzebowania na tego typu urządzenia, zintegrowane ogniwa DSSC mogłyby znaleźć swoje kolejne, niszowe zastosowania. Aby produkty te były konkurencyjne w stosunku do rozwiązać klasycznych, ich żywotność musiała by dochodzić do 5 lat - dla urządzeń typu przenośnego (wearable) - oraz do około 20 lat dla zastosowań w sektorze budowlanym [18, 24]. Kolejnymi przykładami zastosowań mogą być bezprzewodowy multisensor firmy Fujikura Ltd. z Japonii lub urządzenia medyczne i sportowe firmy 3GSolar Photovoltaics Ltd. z Izraela. Oprócz przewagi tych ogniw związanej z możliwością przetwarzania światła o niskim natężeniu, również inne czynniki, takie jak cena, kolor i elastyczność, odgrywają ważną rolę w komercjalizacji ogniw DSSC.

Konstrukcja ogniwa barwnikowego DSSC, jak również zasada jego działania, jest wyjaśniona na Rys. 1.

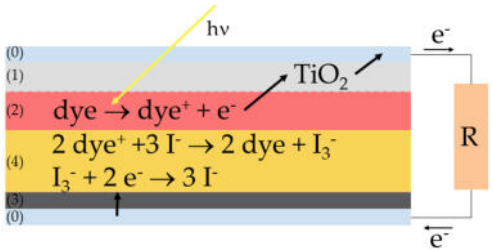

Rysunek 1: Zasada działania ogniwa barwnikowego DSSC, zaczerpnięta z pracy [16]. Oznaczenia: 0 – warstwa FTO (SnO_2:F), 1- TiO_2, 2 – barwnik, 3 – grafit lub platyna, 4 – KI (jodek potasu).

W typowym ogniwie, wymagane są przede wszystkim dwa przewodzące podłoża. Powszechnie stosowanym materiałem jest podłoże szklane pokryte tlenkiem cyny z domieszką fluoru (FTO). Elektroda górna jest pokryta materiałem półprzewodnikowym - najczęściej jest to TiO_2. Następnie na porowatą warstwę TiO_2 nakładany jest barwnik, który jest materiałem fotoaktywnym. Elektroda dolna składa się z drugiego przewodzącego elementu szklanego, który jest pokryty katalizatorem, takim jak grafit lub platyna. Pomiędzy grafitem a barwnikiem umieszcza się barwnik - często używa się tutaj jodu i jodku potasu. Pod wpływem światła elektrony w barwniku ulegają wzbudzeniu i są wstrzykiwane do pasma przewodnictwa półprzewodnika, aż w końcu docierają do warstwy FTO szklanej elektrody. Stamtąd, wytworzone nośniki przepływają przez obwód zewnętrzny. Następnie, elektrony w drodze powrotnej przepływają przez warstwę grafitu lub platyny. Warstwa katalizatora redukuje elektrolit, który transportuje elektrony z powrotem do cząsteczek barwnika i regeneruje barwnik [22].

Mało intensywnie rozwijanymi do tej pory elementami badań w inżynierii materiałowej ogniw DSSC są:

- eksperymenty recyklingowe;
- eksperymenty z regeneracją ogniw;
- ekonomiczne koncepcje obiegu zamkniętego wraz z adekwatnymi modelami biznesowymi.

Są to jednocześnie główne zagadnienia badawcze tejże rozprawy.

II Metodologia badań

Metodologia badań składa się z kilku etapów testujących hipotezę postawioną w pracy. Po pierwsze, w pracy przeanalizowano znaczenie zrównoważonego rozwoju w kontekście badań naukowych nad ogniwami DSSC. Dokonano tego przez analizę źródeł bibliograficznych z wykorzystaniem narzędzia VOSviewer. Po drugie, przeprowadzono eksperymenty recyklingowe z wykorzystaniem materiałów pochodzących z ogniw DSSC oraz ogniw żelowo-elektrolitowych. Po trzecie, przeprowadzono eksperymenty wielkokrotnej regeneracji starych ogniw. W trakcie prac, badane ogniwa były testowane pod kątem zmiennego w czasie współczynnika fotokonwersji (PCE). Dokonano także analizy strukturalnej badanych materiałów.

Badania bibliograficzne

Na początku realizacji pracy doktorskiej przeprowadzono analizę bibliograficzną w celu wykazania przydatności badań nad zrównoważonym rozwojem w dziedzinie ogniw barwnikowych DSSC. W związku z tym wykorzystano narzędzie VOSviewer (VOSviewer wersja 1.6.16) z Uniwersytetu w Leiden. Narzędzie zostało opracowane przez Nees van Ecka i Ludo Waltmana [25]. Aby przeprowadzić analizę informacje o publikacjach muszą być pobrane z bazy Web of Science - Baza została przeszukana za pomocą terminu „dye sensitized solar cell".

Recykling

Do eksperymentów topnienia, związanych z recyklingiem, użyto ogniw DSSC wyprodukowanych w latach 2018 - 2020 [26]. Podłoża szklane z 2018 roku miały grubość 2 mm. Podłoża szklane z roku 2020 miały grubość 3 mm. Do badania powierzchni podłoży stosowano skaningową mikroskopię elektronową z dyspersją energii promieniowania rentgenowskiego (SEM-EDX). Pomiary przeprowadzono aparatem EVO MA10 firmy Carl Zeiss AG (Oberkochen, Niemcy). Pomiar umożliwił wyznaczenie składu chemicznego materiałów. Przygotowanie próbek i wykonanie pomiarów SEM-EDX przeprowadzono zgodnie z normą ISO 22309:2011 „Microbeam analysis – Quantitative analysis using energy-dispersive spectrometry (EDS) for elements with an atomic number of 11 (Na) or above"

[27]. Podłoża szklane zostały oczyszczone mechanicznie a następnie rozdzielone na dwie grupy próbek. Jedna część została zbadana w niezmienionej postaci za pomocą mikroskopu SEM-EDX, natomiast druga połowa została wcześniej wytrawiona mieszaniną stężonego kwasu siarkowego i stężonego kwasu fluorowodorowego. Proces trawienia posłużył do sprawdzenia, jakie pierwiastki można ewentualnie usuwać z obszarów przypowierzchniowych próbek.

Dodatkowo, do określania składu chemicznego materiału zastosowano optyczną spektrometrię emisyjną z plazmą sprzężoną indukcyjnie (ICP-OES). Do badań ICP-OES wykorzystano urządzenie iCAP 6300 Duo firmy Thermo Fischer Scientific Inc. (Waltham, USA). Eksperymenty przeprowadzono zgodnie z normą DIN 51086-2 „Testing of oxidic raw materials and materials for ceramics, glass and glazes Part 2: Determination of Ag, As, B, Ba, Be, Bi, Ca, Cd, Ce, Co, Cr, Cu, Er, Eu, Fe, La, Mg, Mn, Mo, Nd, Ni, P, Pb, Pr, S, Sb, Se, Sn, Sr, Ti, V, W, Y, Yb, Zn, Zr by optical emission spectrometry with inductively coupled plasma (ICP OES)" [28].

Istotnym elementem badań recyklngowych był etap kruszenie szkła, który wykonywano za pomocą młyna Mixer Mill MM 400 firmy Retsch GmbH (Haan, Niemcy). Uzyskana średnica stłuczki szklanej wynosiła około 8,0 mm. Po pokruszeniu próbek stłuczkę suszono za pomocą pieca UF260 firmy Memmert GmbH and Co. KG (Schwabach, Niemcy).

Dla zbadania wpływu topnienia materiałów na wydajność ogniw, przetestowano różne zestawy stopów, aby sprawdzić, czy i w jakim stopniu standardowe ogniwa barwnikowe DSSC oraz ogniwa DSSC z żelowym elektrolitem mogą być wykorzystane w do budowy kolejnych ogniw. Analizowano cztery rodzaje próbek:

Melt A: 60 wt% białej stłuczki i 40 wt% surowca (próbka referencyjna).

Melt B: 60 wt% stłuczka DSSC z żel-elektrolitem (17 wt% PEO o masie cząsteczkowej (MW) 600 kg/mol PEO i 38 wt% glicerol) i 40 wt% surowiec.

Melt C: 60 wt% Stłuczka DSSC z żel-elektrolitem (8 wt% PEO z 600 kg/mol PEO i 47 wt% glicerolu) i 40 wt% surowca.

Melt D: 60 wt% stłuczki DSSC z elektrolitem jodowo-potasowym i 40 wt% surowca.

Ogniwa DSSC w stopach B, C i D składały się ze szklanych podłoży z powłoką FTO firmy Man Solar. Do ekstrakcji użytego w ogniwach barwnika użyto herbaty z owoców leśnych firmy Mayfair.

W stopionym materiale D jako warstwę katalizatora zastosowano grafit z ołówka 6B firmy J. S. Staedtler. W materiałach B i C użyto grafitu w sprayu firmy CP-Graphitprodukte GmbH.

Ogniwa do topnienia mieszaniny B przechodziły przez symulowany proces wietrzenia. W prawdziwym zakładzie recyklingu, stłuczka szklana jest traktowana przez światło słoneczne i deszcz, które działają oczyszczająco. Aby zasymulować ten proces, ogniwa były myte wodą z kranu i suszone w uniwersalnym piecu UF260 firmy Memmert GmbH and Co. KG w temperaturze 115 °C. Ogniwa ze stopu C i D nie przechodziły procesu wietrzenia. Wszystkie ogniwa zostały rozdrobnione za pomocą młynka Mixer Mill MM 400 firmy Retsch GmbH. Średnica stłuczki wynosiła około 0,8 mm. Stopy ogrzewano za pomocą laboratoryjnego pieca komorowego-CWF firmy Carbolite Gero GmbH & Co. KG (Neuhausen, Niemcy) do temperatury 1300 °C.

Proces regeneracji ogniw barwnikowych DSSC składał się z kilku etapów. Polegał na wstępnym oczyszczeniu elektrod, naniesieniu TiO_2, barwnika i grafitu, złożeniu elektrod oraz na dodaniu elektrolitu. Podobnie jak w eksperymencie recyklingowym, wykorzystane zostały szklane podłoża z powłoką FTO firmy Man Solar.

W celu zdjęcia charakterystyk prądowo-napięciowych ogniw stosowano miernik Keithley 2450 firmy Tektronix Inc (Beaverton, USA). W mierniku zastosowano tzw. podwójne przemiatanie. Procedura ta polegała na tym, że napięcie było zwiększane od wartości zerowej do 0,6 V, a następnie zmniejszane do 0 V w krokach co 0,005 V. Pomiędzy każdym krokiem pomiarowym występowało opóźnienie 0,1 s. Do pomiaru współczynnika wydajności fotokonwersji PCE wykorzystano tylko przemiatanie napięcia wstecz, czyli od 0,6 V do 0 V, ze względu na bardziej stabilne wskazania miernika.

Obszar aktywny DSSCs o powierzchni 6 cm^2 był oświetlany za pomocą symulatora słonecznego LS0500 firmy LOT-Quantum Design GmbH (Darmstadt, Niemcy). Źródło światła oświetlało ogniwo wiązką o natężeniu 100 mW/cm^2.

Przy zmierzonym prądzie i napięciu, można było wyznaczyć generowaną moc ($P = UczasI$). Przy aktywnej powierzchni ogniwa wynoszącej $0,6\ cm^2$ i natężeniu oświetlenia $100\ mW/cm^2$ można było wyznaczyć współczynnik PCE, rozumiany jako stosunek mocy uzyskanej do mocy światła padającego na ogniwo. Oprócz pomiarów prądowo-napięciowych, regenerowane podłoża były sprawdzane wizualnie za pomocą mikroskopu optycznego Axio Observer 7 firmy Carl Zeiss Microscopy GmbH.

Regeneracja

W ramach pracy doktorskiej przeprowadzono trzy rodzaje eksperymentów związanych z regeneracją ogniw:

1. ogniwa DSSC z komercyjnie stosowanymi warstwami TiO_2. W eksperymencie tym użyto nowych podłoży szklanych (Man Solar) – elektrody przednie miały już gotowe warstwy TiO_2. Sześć próbek w tej serii eksperymentów otrzymało oznaczenia od G1.1 do G1.6. Po zmniejszeniu się współczynnika PCE ogniwa były ponownie regenerowane. Polegało to na dodaniu nowego elektrolitu. Nowa generacja ogniw otrzymywała wtedy oznaczenia G2.1 do G2.6. Proces ten powtarzano aż do czwartej generacji (G4.1 do G4.6), którą również charakteryzowano aż do momentu zaniku współczynnika PCE.
2. ogniwa DSSC z ręcznie nakładanymi warstwami TiO_2. Podłoża szklane dla próbek w tym eksperymencie zostały odzyskane ze starych DSSC. Dwanaście próbek otrzymało oznaczenia od T1.1 do T1.12. Po spadku współczynnika PCE, były one ponownie nawadniane elektrolitem i mierzone, do momentu, kiedy współczynnik PCE spadł poniżej 0,01 - próbki takie były oznaczane jako T1.1rehy – T1.12rehy. Następnie sześć wybranych próbek zostało ponownie nawodnionych (T1.1rehyII – T1.6rehyII). Pozostałe sześć próbek wykorzystano do regeneracji i wytworzenia nowej generacji (T2.1 – T2.6). Eksperyment ten został przeprowadzony w celu sprawdzenia różnic pomiędzy prostym nawodnieniem a złożonym remanufakturingiem (rekonstrukcją) komórek.

3. ogniwa DSSC, starsze, pochodzące z roku 2015. W trzeciej konfiguracji eksperymentalnej wykorzystano 18 ogniw. Sześć z nich nawodniono elektrolitem, aby zbadać, czy tak stare ogniwa można po prostu pobudzić do pracy poprzez ponowne nawodnienie elektrolitu (oznaczenia próbek: Reviv1 – Reviv6). Kolejne sześć ogniw wykorzystano do regeneracji (rekonstrukcji), przy czym zachowano w nich starą warstwę TiO_2, a na wierzchu starej warstwy spiekano dodatkową nową warstwę TiO_2 – oznaczenia próbek: Over1 – Over6. Ostatnie sześć ogniw wykorzystano do jeszcze innego procesu regeneracji. Starą warstwę TiO_2 zmyto przed nałożeniem nowej warstwy – oznaczenia próbek: New1 – New6. Wszystkie ogniwa zostały pomierzone w taki sam sposób, jak to opisano powyżej, czyli w szczególności zdjęto charakterystyki prądowonapięciowe.

Poniżej przedstawiono zestawienie eksperymentów przeprowadzonych w pracy doktorskiej (Tab. 1):

Tabela 1: Przegląd eksperymentów z regeneracją.

Nr	nazwa próbek	Pochodzenie warstwy TiO_2	nawodniony	ilość pokoleń
1	G1.1-G4.6	stosowane komercyjnie	nie	4
2	T1.1-T1.12 and T2.1-T2.6	stosowane ręcznię	nie	2
2	T1.1rehy-T1.12rehy and T1.1rehyII-T1.6rehyII	stosowane ręcznię	tak	2
3	Reviv1-Reviv6	używana istniejąca warstwa (stosowane ręcznię)	tak	1
3	Over1-Over6	używana istniejąca warstwa (dodatkowo zastosowana nowa warstwa)	nie	1
3	New1-New6	stosowane ręcznię	nie	1

III Wyniki badań

Ważnym elementem doktoratu, uzasadniającym podjęcie tego typu prac badawczych, była analiza danych literaturowych. Analizę tę wykonano z wykorzystaniem narzędzia VOSviewer, dzięki któremu powstaje mapa terminów z bardzo obrazowym sposobem ilości ich wystąpień (Rys. 2).

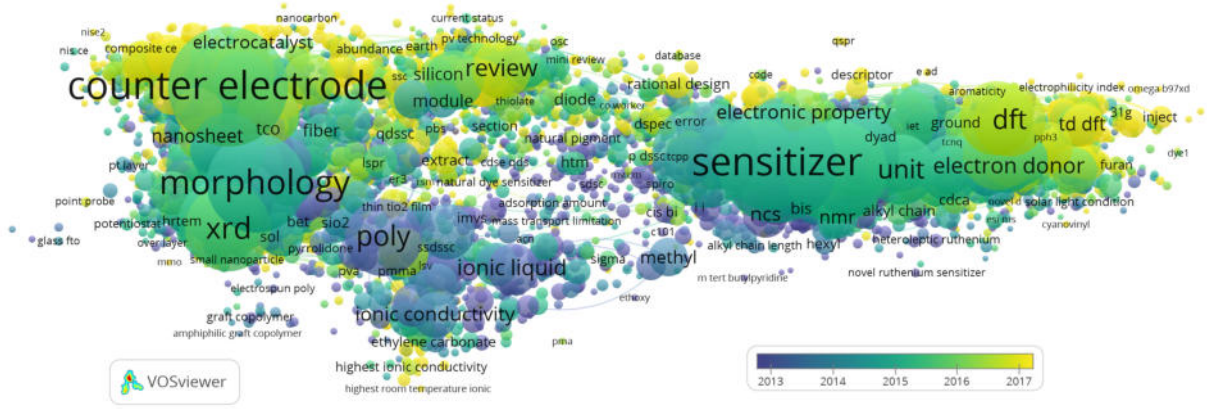

Rysunek 2: Terminy i częstotliwość ich występowania – w grupie recykling ogniw słonecznych.

W tabeli poniżej (Tab. 2) zestawiono terminy, które w związku z kontekstem prowadzonych prac badawczych, pojawiły się najczęściej w analizie bibliograficznej.

Tabela 2: Ważne słowa kluczowe i ilość ich wystąpień.

Nr	termin	15 marca 2021 r. ilość wystąpień	6 grudnia 2022 r. ilość wystąpień
1	counter electrode	2769	3048
2	sensitizer	2810	3043
3	molecule	2086	2389
4	group	2263	2273
5	morphology	1899	2087
6	xrd (x ray diffraction)	1316	1574
7	series	1357	1527
8	organic dye	1474	1517
9	complex	1316	1513

Badania materiałowe

SEM-EDX

Na rysunku poniżej (Rys. 3) przedstawiono przykładowe wyniki analizy SEM-EDX (Energy-Dispersive X-ray Spectroscopy) dla elektrody górnej w materiale pochodzącym z roku 2018 przed jej wytrawianiem.

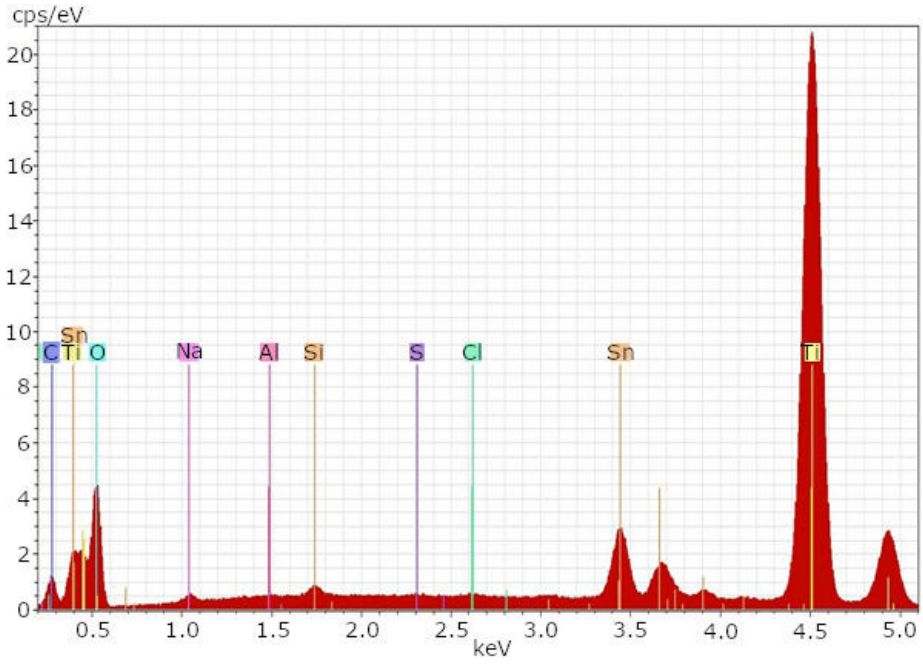

Rysunek 3: Wynik badania SEM-EDX podłoży szklanych DSSC z roku 2018 – przed wytrawianiem [29].

Oś pionowa wykresu jest miarą ilość fotonów rejestrowanych na sekundę, na jednostkę energii, w danym zakresie energetycznym (oś pozioma). Dwa piki po prawej stronie, Ti (tytan) i Sn (cyna), wskazują na występowanie warstwy TiO_2 oraz warstwy FTO naniesionej na elektrodę górną - sygnały te są dominujące. Sygnały widziane na lewo od Sn to typowe pierwiastki występujące w szkłach, takie jak: Si (krzem), Al (aluminium), Na (sód), O (tlen), Sn (cyna), Ti (tytan) i C (węgiel). Pierwiastki te występują zasadniczo w niższych stężeniach od tych, które występują w elektrodzie górnej ogniw.

Na Rys. 4 przedstawiono wynik analizy SEM-EDX przeprowadzonej dla elektrody górnej po zakończonym procesie trawienia mieszaniną kwasu siarkowego i kwasu fluorowodorowego (w stosunku 1:1) w ciągu 10 minut.

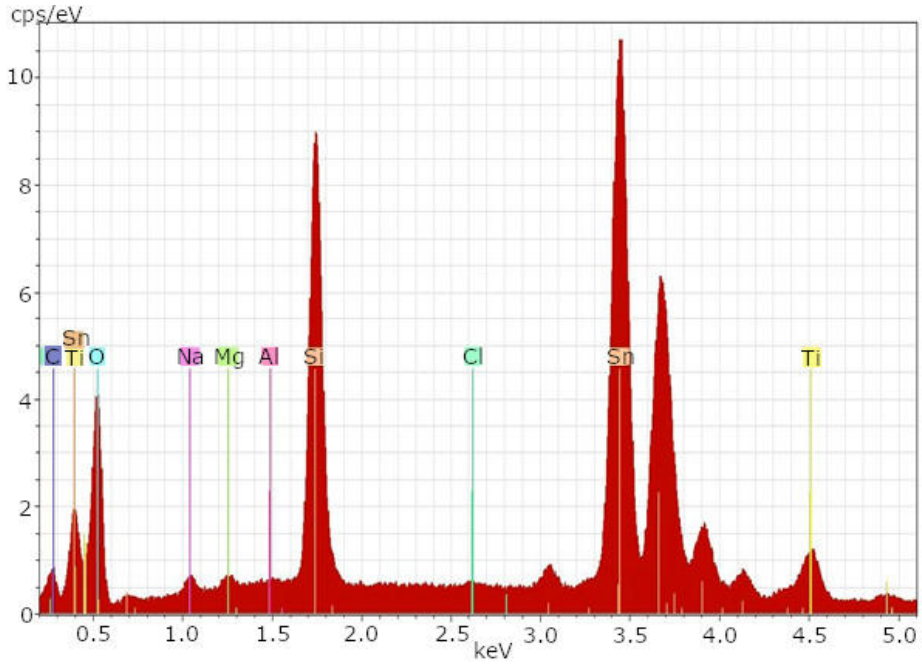

Rysunek 4: Wynik badania SEM-EDX podłoży szklanych ogniw barwnikowych DSSC po procesie trawienia [29].

Z rysunku wynika, że sygnał od tytanu jest znacznie niższy w stosunku do sytuacji przed trawieniem. Obecność cyny jest w dalszym ciągu wykrywalna. Pozostałe, typowe składniki szkła są również obecne. Wyniki te potwierdzają, że warstwa TiO_2 jest usuwana za pomocą opisanego powyżej procesu trawienia, natomiast warstwa FTO nie może być usunięta.

ICP-OES

Kolejna tabela (Tab. 3) przedstawia zestawienie wyników badań metodą Emisyjnej Spektroskopii Optycznej Indukcyjnie Wzbudzanej Plazmy (Inductively Coupled Plasma Optical Emission Spectroscopy, ICP-OES) opublikowane już wcześniej w pracy autora dysertacji [29]. Czwarta kolumna tabeli pokazuje skład procentowy szkła produkowanego

Tabela 3: Wyników badań składu chemicznego szkieł metodą Emisyjnej Spektroskopii Optycznej Indukcyjnie Wzbudzanej Plazmy (ICP-OES) – porównanie próbek z lat 2018 i 2020 – wyrażony udziałem masowym wt w procentach.

Element	Szkło DSSC od 2018 r. (wt%)	Szkło DSSC od 2020 r. (wt%)	Szkło patentowe (wt%) [30]
Al_2O_3	0.540	0.070	4.7-19
Fe_2O_3	0.009	0.100	0-0.5
CaO	8.950	8.880	0-5
MgO	4.260	3.960	0-6
SrO	0.005	0.006	0-7
Na_2O	13.800	13.640	10-18
K_2O	0.050	0.040	0-8
Li_2O	0.003	0.002	0-4
BaO	0.001	0.001	0-10
PbO	0.000	0.000	-
TiO_2	0.005	0.010	0-6
Cr_2O_3	0.000	0.001	-
Mn_2O_3	0.001	0.006	-
NiO	0.001	0.000	-
SnO_2	0.013	0.024	-
ZnO	0.002	0.003	0-0.3
ZrO_2	0.000	0.010	0-0.5
SO_3	0.220	0.218	-
SiO_2	72.140	73.030	49-69

przez firmę Schott AG – skład ten jest jednak chroniony prawami własności intelektualnej i nie jest ujawniany oficjalnie [30].

Dla związku Al_2O_3, szkło f-my Schott posiada znacznie wyższe wartości udziału masowego w porównaniu do podłoży szklanych DSSC firmy Man Solar. Podłoża szklane z roku 2018 ma wyższą zawartość Al_2O_3 w porównaniu do podłoży szklanych z roku 2020.

Jednak oba te podłoża szklane mają wyższe zawartości CaO niż to podano w powyższym opisie patentowym.

Stężenie związku Fe_2O_3 w podłożach szklanych z roku 2020 jest wyższe niż w podłożach szklanych z roku 2018. Jednak wartości Fe_2O_3 z obu podłoży szklanych znajdują się w przedziale wartości określonych w patencie.

Stwierdzony, różny skład chemiczny szkła, pochodzący z różnych partii, może stanowić potencjalny problemem dla przebiegu procesu recyklingu. Problem ten jest znany w recyklingu klasycznych, krzemowych modułów fotowoltaicznych c-Si.

Procesy topnienia materiałów

Na Rys. 5 pokazano topiony materiał próbek oznaczonych od A do D po czasie 5, 20 i 50 minut w piecu indukcyjnym [29]. Po czasie topnienia wynoszącym 20 minut,

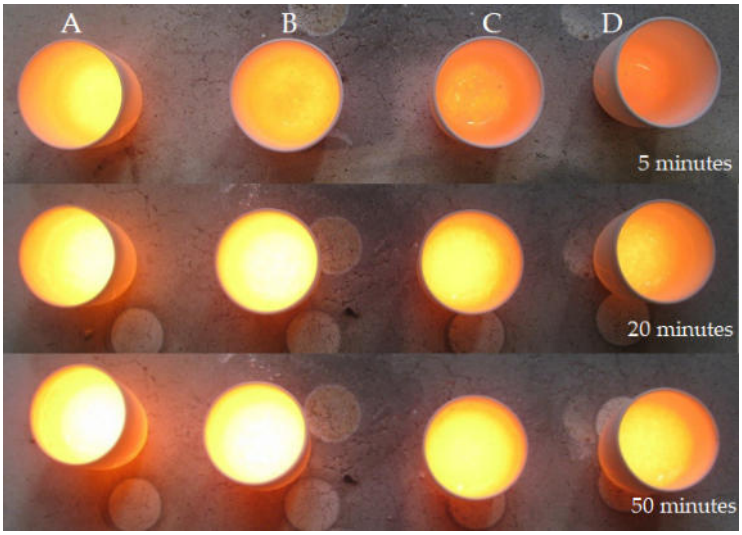

Rysunek 5: Wygląd topionych próbek, oznaczonych literami od A do D po czasie 5, 20 i 50 minut przebywania w piecu indukcyjnym [29].

osobne ziarna oraz niestopiony materiał były nadal widoczne we wszystkich materiałach, jednak różnorodny wygląd próbek wynikał z ich lokalizacji wewnątrz pieca – próbki A i B znajdowały się w środkowej części, natomiast próbki C i D umiejscowiono bliżej drzwi. W próbkach można wyróżnić trzy rodzaje obszarów strukturalnych: ziarna, niestopione fragmenty materiału, pęcherzyki gazu. Na Rys. 6 pokazane są końcowe wytopy próbek widziane pod mikroskopem optycznym.

W badanych stopach nie zaobserwowano kawałków ceramiki lub metalu.

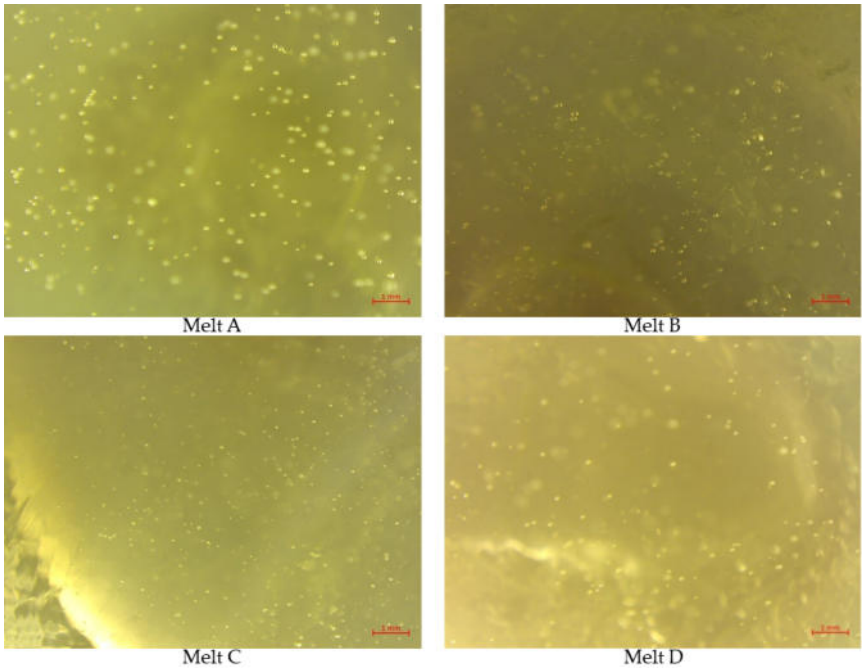

Rysunek 6: Wyniki eksperymentu z topnieniem materiałów szklistych widziane pod mikroskopem optycznym o 10-krotnym powiększeniu (adaptacja z [29]).

W przeprowadzonym eksperymencie zastosowano względnie proste ogniwa barwnikowe. Jednak w przypadku występowania większej ilości składników metalicznych, takich jak platyna czy srebro, recykling szkła wydaje się być znacznie trudniejszy. Dlatego w przyszłych rozwiązaniach, należałoby zastanowić się nad alternatywnymi podejściami technologicznymi, np. nad stosowaniem nanorurek węglowych, jako opcji dla materiału przewodzącego [31].

Regeneracja ogniw

W tym miejscu przedstawiono skrótowo wyniki wszystkich eksperymentów związanych z procesem regeneracji ogniw, koncentrując się głównie na analizie współczynnika fotokonwersji PCE. Rodzaje próbek zostały opisane w poprzedniej części streszczenia, w szczególności sposób oznaczania kolejnych generacji wytworzonych ogniw. Na Rys. 7 przedstawiono czasowe zmiany średniego współczynnika fotokonwersji (PCE) dla różnych generacji ogniw barwnikowych z komercyjnie naniesionymi warstwami TiO_2. Kolejne generacje ogniw, od 1 do 4, wskazują na to, że nowe, kolejne generacje ogniw wykazują nieznacznie wyższą wydajność PCE. Ponadto, dla kolejnych generacji ogniw, ich PCE utrzymuje się na wyższym poziomie przez dłuższy okres czas. Na Rys. 8-9 przedstawiono wyniki pomiarów współczynnika PCE dla ogniw barwnikowych z ręcznie naniesionymi warstwami TiO_2.

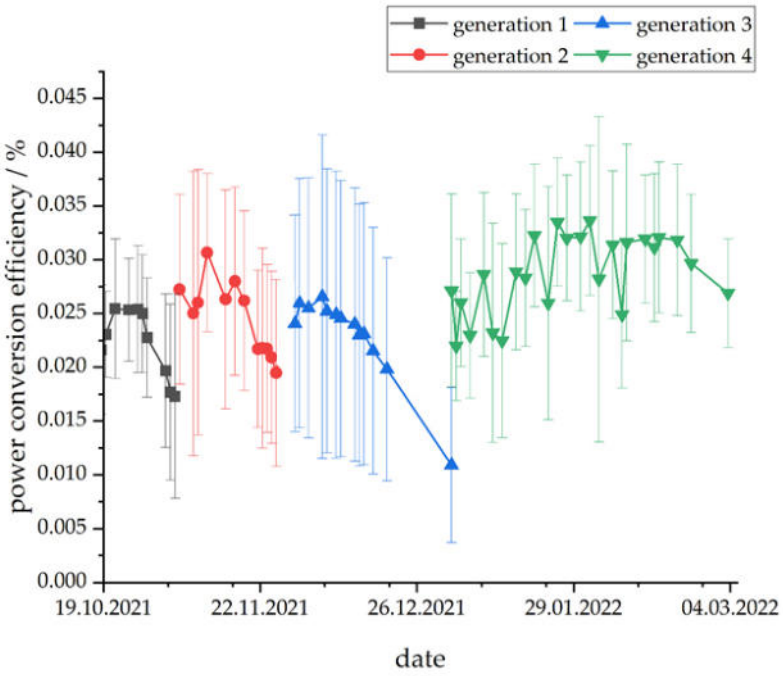

Rysunek 7: Czasowe zmiany współczynnika fotokonwersji (PCE) dla ogniw barwnikowych z komercyjnie stosowanym TiO_2 – przedstawiono cztery generacje ogniw [21].

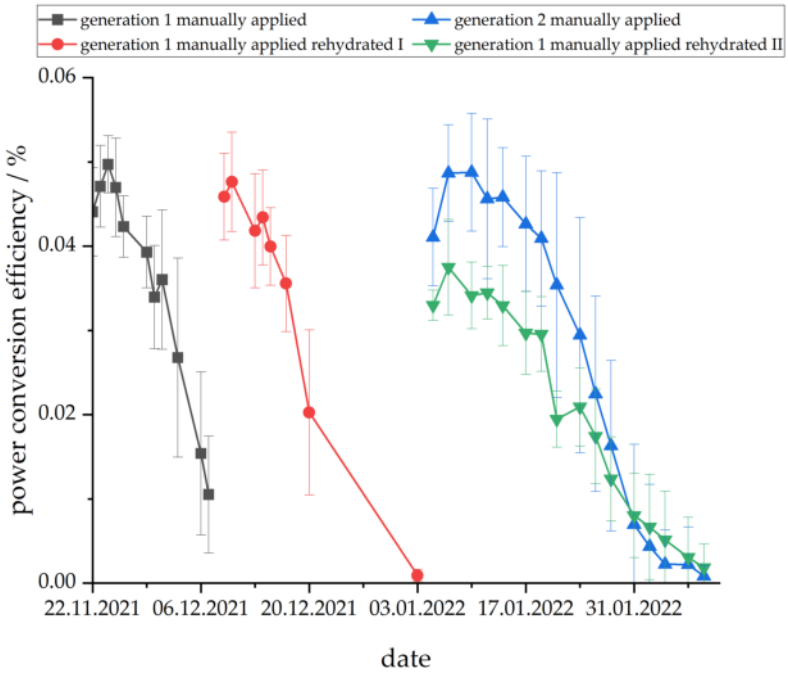

Rysunek 8: Zmiany współczynnika PCE dla ręcznie naniesionej warstwy TiO_2 – pokazano wyniki dla linku wybranych generacji [21].

Badania morfologiczne z wykorzystaniem AFM

W tabeli 4 pokazano zbiorcze zestawienie parametrów elektrycznych ogniw oraz wyniki pomiaru stanu chropowatości powierzchni (oznaczane w literaturze jako Rq lub rms – pierwiastek ze średniego odchylenia wartości kwadratowej od wartości średniej) podłoży szklanych, na których wytworzono ogniwa. W tabeli pokazano wybrane przypadki a wcześniej zdefiniowane oznaczenia zawierają, między innymi, informację o kolejnych generacjach próbek. Próbka „T1.1rehyII" ma względnie dużą chropowatość podłoża szklanego FTO i niski współczynnik wypełnienia FF, ale próbka „G4.3", z najwyższym współczynnikiem FF nie ma względnie niskiej chropowatości warstwy szklanej FTO. Ponadto, chropowatość warstw tlenku tytanu TiO_2 „T1.1rehyII" i „New1" jest podobna, natomiast oba te ogniwa są jednak elektrycznie podobne tylko pod względem wartości napięcia obwodu otwartego Voc.

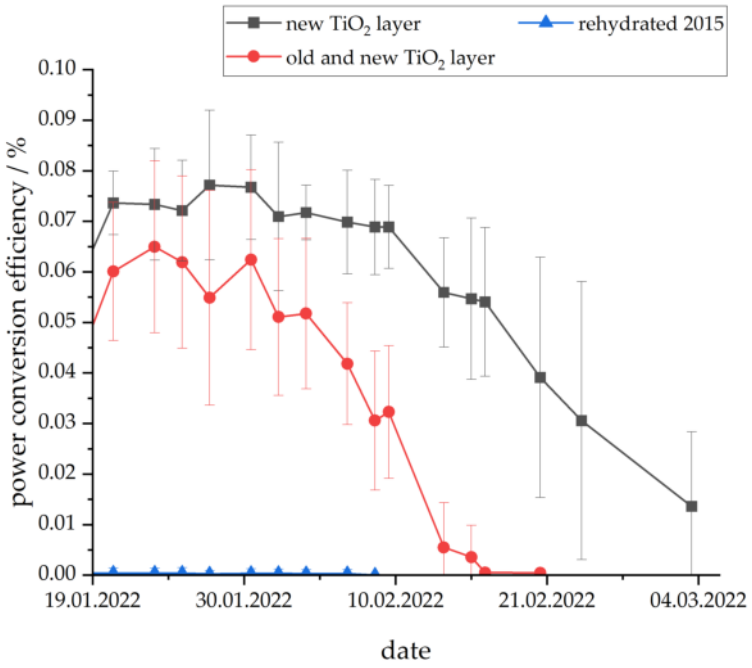

Rysunek 9: Średnie wartości współczynnika fotokonwersji PCE ogniw barwnikowych wyprodukowanych pierwotnie w roku 2015 z ręcznie naniesioną warstwą TiO_2 – oznaczenia kolorem szarym: ogniwa z nową warstwą TiO_2, oznaczenia czerwone: ogniwa z dodatkową warstwą TiO_2 położoną na warstwę starą, oznaczenia niebieskie: ogniwa barwnikowe, które tylko ponownie uwodniono elektrolitem [21].

Tabela 4: Właściwości elektryczne próbek DSSC i średnia chropowatości kwadratowej badane za pomocą AFM. Oznaczenia: J_{sc} – prąd zwarcia, V_{oc} – napięcie obwodu otwartego, PCE – współczynnik fotokonwersji, FF – współczynnik wypełnienia (stosunek maksymalnej mocy uzyskanej z ogniwa do iloczynu prądu zwarcia i napięcia obwodu otwartego, R_q FTO – chropowatość średniokwadratowa podłoża FTO, R_q TiO_2 – chropowatość średniokwadratowa warstwy TiO_2, R_q C – chropowatość średniokwadratowa warstwy katalizatora grafitowego.

Oznaczenie próbki	J_{sc} (mA)	V_{oc} (mV)	PCE (%)	FF (%)	R_q FTO (nm)	R_q TiO_2 (nm)	R_q C (nm)
G4.2	2.26	400	0.05	29.79	6.48	10.59	4.37
G4.3	1.00	415	0.03	38.51	6.63	10.26	2.23
T2.5	3.64	490	0.06	19.69	7.09	16.01	1.62
T1.1rehyII	3.06	450	0.04	17.95	10.10	18.28	3.04
New1	4.06	455	0.10	32.28	6.75	17.26	6.67
Over3	3.31	480	0.05	18.41	6.55	9.43	4.69
Virgin glass	–	–	–	–	7.54	12.02	–

Pobieżny ogląd tych danych nie pozwala na jednoznaczną odpowiedź o związki pomiędzy pokazanymi parametrami. Dlatego, aby przeprowadzić ilościową ocenę zaistniałej sytuacji, wykonano obliczenia korelacji liniowych dla danych z tabeli, z pominięciem czystego szkła (Virgin glass). W podejściu tym kolejne wiersze tabeli traktujemy jako wektory 7-dmio składnikowe a kolumny jako zależne od sytuacji sygnały.

Oszacowane korelacje pokazane są w kolejnej tabeli (Tab. 4).

Korelację liniową pomiędzy dowolnymi, dwoma sygnałami x i y obliczono, korzystając ze standardowego wzoru:

$$r_{xy} = \frac{\overline{x \cdot y} - \overline{x} \cdot \overline{y}}{sd(x) \cdot sd(y)},$$

gdzie sd(x) oznacza odchylenie standardowe np. dla sygnału x, natomiast poziome kreski nad symbolami oznaczają odpowiednie wartości średnie.

Z tabeli wynika, że istnieje znacząca, dodatnia korelacja pomiędzy chropowatością warstwy katalizatora grafitowego i współczynnikiem fotokonwersji PCE, umiarkowane (0.5-0.6), dodatnie korelacje pomiędzy chropowatością warstwy grafitowej i tlenku tytanu TiO_2 a prądem zwarcia oraz chropowatością warstwy TiO_2 a współczynnikiem fotokonwersji PCE. Istnieje również zauważalna anty-korelacja pomiędzy chropowatością warstwy elektrodowej FTO oraz współczynnika wypełnienia FF. Ponieważ półprzewodnikowy materiał TiO_2 pojawia się w powyższym zestawieniu dwukrotnie, można przypuszczać, że morfologia stanu powierzchni tej warstwy może mieć duży wpływ na efektywność przemiany energii świetlnej na elektryczną. Z atomowego punktu widzenia morfologia powierzchniowa i objętościowa materiału półprzewodnikowego wpływa na charakter przerwy energetycznej pomiędzy pasmem walencyjnym i przewodnictwa – jej szerokość i rozmycie tej szerokości zależy od tego, czy mamy do czynienia z materiałem amorficznym, z jednej strony, czy z materiałem krystalicznym o bardzo dobrze określonym, długo-zasięgowym uporządkowaniu struktury, z drugiej strony.

Tabela 5: Korelacje pomiędzy wartościami parametrów elektrycznych i chropowatości powierzchni warstw ogniwa barwnikowego DSCC. Oznaczenia obszarów: parametry elektryczne (niebieski), chropowatości (zielony), korelacja pomiędzy chropowatością warstwy katalizatora grafitowego i współczynnikiem fotokonwersji (czerwony), korelacje pomiędzy chropowatością warstwy grafitowej i tlenku tytanu TiO_2 a prądem zwarcia oraz chropowatością warstwy TiO_2 a współczynnikiem fotokonwersji PCE (żółty), anty-korelacja pomiędzy chropowatością warstwy FTO oraz współczynnika wypełnienia FF (szary).

	J_{sc}	V_{oc}	PCE	FF	R_q FTO	R_q TiO_2	R_q C
J_{sc}	1.00	0.79	0.77	-0.56	0.08	0.57	0.52
V_{oc}	0.79	1.00	0.35	-0.78	-0.09	0.17	0.06
PCE	0.77	0.35	1.00	0.10	-0.29	0.47	0.75
FF	-0.56	-0.78	0.10	1.00	-0.47	-0.24	0.14
R_q FTO	0.08	-0.09	-0.29	-0.47	1.00	0.63	-0.22
R_q TiO_2	0.57	0.17	0.47	-0.24	0.63	1.00	0.11
R_q C	0.52	0.06	0.75	0.14	-0.22	0.11	1.00

W przypadku badanych struktur mamy niewątpliwie do czynienia z fazą nieuporządkowaną. Kolejne etapy, szczególnie recyklingu, zmieniają stopień tego nieuporządkowania. Istnienie pewnej dodatniej korelacji pomiędzy morfologią warstwy TiO_2 w współczynnikiem PCE może być związany ze zmianą charakterystyki wspomnianej przerwy energetycznej. Mianowicie, w półprzewodnikach amorficznych dochodzi do pojawienia się na krawędziach przerwy energetycznej tzw. dyfuzyjnych stanów ogonowych oraz – wskutek istnienia obcych wtrąceń i zanieczyszczeń – dodatkowych stanów ulokowanych w przerwie energetycznej. Stany te mogą być źródłem dodatkowych nośników w pasmie przewodnictwa [32]. Wniosek ten należy traktować, jako wstępny, wymagający dalszych badań. Badanie struktury energetycznej materiału półprzewodnikowego TiO_2 nie było jednak głównym, wiodącym wątkiem obecnego doktoratu.

IV Podsumowanie

Niniejsza praca wykazała, że nietoksyczne ogniwa barwnikowe DSSC mogą być regenerowane bez negatywnego wpływu na wydajność fotokonwersji a ich potencjalne wykorzystanie w konwencjonalnym recyklingu szkła jest obiecujące. Ponadto wskazano, że cyrkularny model biznesowy jest kluczowym dla wdrożenia technologii wytwarzania ogniw barwnikowych do produkcji przemysłowej i zmniejszenia jej wpływu na środowisko.

Ponieważ ogólnie, nie prowadzono do tej pory regularnych eksperymentów dotyczących regeneracji i recyklingu ogniw barwnikowych, w niniejszej pracy uczyniono pierwszy krok do wypełnienia tej luki.

Wyniki przeprowadzonych prac badawczych pokazały, że rehydratacja elektrolitu może przedłużyć żywotność DSSC i że zastosowanie elektrolitów stałych lub żelowych jest rozwiązaniem pozwalającym na dalsze udoskonalenie DSSC. Analiza spektroskopowa typu Emisyjnej Spektroskopii Optycznej Indukcyjnie Wzbudzanej Plazmy (ICP-OES) wykazała, że skład badanych w pracy podłoży szklanych, pochodzących z różnych lat, wykazuje dużą różnorodność. Na przykład wartość Fe_2O_3 podłoża szklanego z roku 2018 wynosiła 0,009 wt%, a wartość Fe_2O_3 podłoża szklanego z roku 2020 wynosiła 0,100 wt%. Dlatego dla kontrolowanego zarządzania przyszłym procesem recyklingu skład szkła powinien być jednoznacznie identyfikowany, na przykład poprzez wdrożenie paszportu materiałowego wraz etykietą produktu.

Proces recyklingu ogniw barwnikowych DSSC zawierających barwniki rutenowe nie został do tej pory zbadany. Jednak w trakcie prac badawczych zauważono, że możliwe jest wstępne czyszczenie i usunięcie składników toksycznych przed rozpoczęciem właściwego recyklingu ogniw barwnikowych. Okazuje się, że w ten sposób, na każdej tonie stłuczki ogniw barwnikowych zastępującej materiał pierwotny, można by zaoszczędzić około 84 EUR oraz 0,13 ton CO_2 w postaci tzw. śladu węglowego.

Wyniki eksperymentu z topnieniem materiałów są obiecujące. Stopy są wizualnie podobne i można zidentyfikować jedynie niewielkie różnice w wybarwieniu materiałów. Za pomocą symulowanego procesu wietrzenia, związki organiczne i inne pozostałości zostały

wymyte z badanych ogniw.

Aby stwierdzić, czy stłuczka zużytych ogniw barwnikowych może być wykorzystana w produkcji szkła konieczne są dalsze testy - zbadanie powinny być takie właściwości materiału, jak przezroczystość, lepkość i odporność chemiczna. Najlepszym sposobem wykorzystania szkła z ogniw barwnikowych, lub ogólnie szkła z zastosowań fotowoltaicznych, byłoby ponowne wykorzystanie szkła ubogiego w żelazo.

Aby jeszcze bardziej poprawić stabilność czasową wydajności ogniw, podłoża szklane powinny być regenerowane zamiast poddawane recyklingowi. W pracy, dla ogniw wykonanych z materiałów nietoksycznych, opisano udaną procedurę regeneracji. Proces regeneracji okazał się przewyższać standardową hydratację ogniw barwnikowych z punktu widzenia otrzymanych wartości wydajności fotokonwersji oraz ich długoterminowej stabilności. Procesy wytwarzania i przetwarzania badanych ogniw są zawsze związane z przemianami materiałowymi, które można odnieść do skali atomowej. W pracy dokonano analizy strukturalno-chemicznej materiałów a poprzez badania morfologii powierzchni wykazano wstępnie, że istnieje wytłumaczenie poprawy wydajności ogniw poddanych kolejnym procesom przetwarzania, które można wyjaśniać związkiem pomiędzy amorficznością materiału a charakterem przerwy energetycznej materiału półprzewodnikowego TiO_2.

W tym momencie staje się jasne, że zdolność do recyklingu, regeneracji i ponownego wykorzystania materiałów zależy w dużej mierze od całościowego procesu powstawania produktu, analizowanego również z ekonomicznego punktu widzenia.

W pracy wykazano, że model biznesowy, oparty o metodę Circo, może być stosowany przez firmy tak, aby wdrożyć lub poprawić transformację procesów produkcyjnych w kierunku gospodarki cyrkularnej. W tym przypadku, w pracy, opisano jedynie fikcyjnego producenta modułów DSSC, a więc w centrum uwagi znalazły się zasady projektowania cyrkularnego i modele biznesowe, a nie realizacja konkretnych pomysłów. Wykazano, że dzięki kluczowym procesom cyrkularnego modelu biznesowego, czyli regeneracji i recyklingowi, można uzyskać tzw. zamknięte pętle materiałowe a nietoksyczne ogniwa barwnikowe DSSC są obiecującą technologią wytwarzania zielonej energii, która potencjalnie może być zintegrowana z cyklami materiałowymi gospodarki cyrkularnej.

Literatura

[1] IPCC. Climate Change 2022 Impacts, Adaption and Vulnerability. Technical report, The Intergovernmental Panel on Climate Change, 2022.

[2] Larry E. Erickson and Gary Brase. Paris Agreement on Climate Change. Technical report, 2019.

[3] Roland Pohl and Benedikt Heitmann. Aufarbeitung von Altmodulen und Rückführung von Wertstoffen in den Stoffkreislauf. Technical report, Reiling Glas Recycling GmbH & Co. KG, 2019.

[4] John A. Tsanakas, Arvid van der Heide, Tadas Radavičius, Julius Denafas, Elisabeth Lemaire, Ke Wang, Jef Poortmans, and Eszter Voroshazi. Towards a circular supply chain for PV modules: Review of today's challenges in PV recycling, refurbishment and re-certification. *Progress in Photovoltaics: Research and Applications*, 28(6):454–464, 2020.

[5] Lance Lambert. Why lumber prices are suddenly rising again | Fortune. https://fortune.com/2021/09/27/lumber-prices-rising-2021-covid/, last accessed 01/11/2023.

[6] Saheli Roy Choudhury. JPMorgan on semiconductor shortage and outlook for 2022, 2023. https://www.cnbc.com/2021/11/19/jpmorgan-on-semiconductor-shortage-and-outlook-for-2022-2023.html, last accessed 01/11/2023.

[7] The Ellen MacArthur Foundation. Towards the Circular Economy Vol. 1: an economic and business rationale for an accelerated transition. *Ellen MacArthur Found.*, 1:96, 2013.

[8] Ellen MacArthur Foundation. The Circular Economy In Detail. https://www.ellenmacarthurfoundation.org/explore/the-circular-economy-in-detail, last accessed 01/11/2023.

[9] Sophia Kohn, Christina Großerhode, Jan Lukas Storck, Georg Grötsch, Carsten Cornelißen, Almuth Streitenberger, Carsten Grassmann, Anne Schwarz-Pfeiffer, and Andrea Ehrmann. Commercially available teas as possible dyes for dye-sensitized solar cells. *Optik*, 185:178–182, 2019.

[10] Katrin Gossen, Jan Lukas Storck, and Andrea Ehrmann. Influence of solvents on Aloe vera gel performance in dye-sensitized solar cells. *Optik*, 180:615–618, 2019.

[11] Jan Lukas Storck, Timo Grothe, Marius Dotter, Sonia Adabra, Michelle Surjawidjaja, and Bennet Brockhagen. Long-term stability improvement of non-toxic dye-sensitized solar cells via poly(Ethylene oxide) gel electrolytes for future textile-based solar cells. *Polymers*, 12(12):1–15, 2020.

[12] Fabian Schoden, Alina Siebert, Alparslan Keskin, Konstantin Herzig, Majkel Straus, and Eva Schwenzfeier-Hellkamp. Building a wind power plant from scrap and raising public awareness for renewable energy technology in a circular economy. *Sustainability (Switzerland)*, 12(1):1–11, 2020.

[13] J Kawakita. Trends of research and development of dye-sensitized solar cells. *Sci Technol Trends*, 35:70–82, 2010.

[14] Fabian Schoden, Marius Dotter, Dörthe Knefelkamp, Tomasz Blachowicz, and Eva Schwenzfeier-Hellkamp. Review of State of the Art Recycling Methods in the Context of Dye Sensitized Solar Cells. *Energies*, 14(13):3741, 2021.

[15] Andrea Ehrmann and Tomasz Błachowicz. Solarstrom aus Früchtetee. *Physik in unserer Zeit*, 51(4):196–200, 2020.

[16] Fabian Schoden, Marius Dotter, Dörthe Knefelkamp, Tomasz Blachowicz, and Eva Schwenzfeier-Hellkamp. Review of State of the Art Recycling Methods in the Context of Dye Sensitized Solar Cells. *Energies*, 14(13):3741, 2021.

[17] Paul Anastas and C. John Warner. *Green Chemistry: Theory and Practice*. Oxford University Press, 2000.

[18] M. L. Parisi, S. Maranghi, L. Vesce, A. Sinicropi, A. Di Carlo, and R. Basosi. Prospective life cycle assessment of third-generation photovoltaics at the pre-industrial scale: A long-term scenario approach. *Renewable and Sustainable Energy Reviews*, 121:109703, 2020.

[19] Kati Miettunen and Annukka Santasalo-Aarnio. Eco-design for dye solar cells: From hazardous waste to profitable recovery. *Journal of Cleaner Production*, 320:128743, 2021.

[20] M. J. de Wild-Scholten and A. C. Veltkamp. Environmental life cycle analysis of large area dye sensitized solar modules; status and outlook. *Presented at: 22nd European Photovoltaic Solar Energy Conference and Exhibition*, 3:3–7, 2007.

[21] Fabian Schoden, Joscha Detzmeier, Anna Katharina Schnatmann, Tomasz Blachowicz, and Eva Schwenzfeier-Hellkamp. Investigating the Remanufacturing Potential of Dye-Sensitized Solar Cells. *Sustainability (Switzerland)*, 14(9):5670, 2022.

[22] Brian O'Regan and Michael Grätzel. A low-cost, high-efficiency solar cell based on dye-sensitized colloidal TiO2 films. *Nature*, 354:737–740, 1991.

[23] Ana Belén Muñoz-García, Iacopo Benesperi, Gerrit Boschloo, Javier J. Concepcion, Jared H. Delcamp, Elizabeth A. Gibson, Gerald J. Meyer, Michele Pavone, Henrik Pettersson, Anders Hagfeldt, and Marina Freitag. Dye-sensitized solar cells strike back. *Chemical Society Reviews*, 50(22):12450–12550, 2021.

[24] Jason B. Baxter. Commercialization of dye sensitized solar cells: Present status and future research needs to improve efficiency, stability, and manufacturing. *Journal of Vacuum Science & Technology A: Vacuum, Surfaces, and Films*, 30(2):020801, 2012.

[25] Nees Jan van Eck and Ludo Waltman. Software survey: VOSviewer, a computer program for bibliometric mapping. *Scientometrics*, 84(2):523–538, 2010.

[26] Jan Lukas Storck, Marius Dotter, Bennet Brockhagen, and Timo Grothe. Evaluation of Novel Glycerol/PEO Gel Polymer Electrolytes for Non-Toxic Dye-Sensitized Solar

Cellswith Natural Dyes Regarding Long-Term Stability and Reproducibility. *Crystals*, 10:1158, 2020.

[27] DIN German Institute for Standardization. Microbeam analysis – Quantitative analysis using energy-dispersive spectrometry (EDS) for elements with an atomic number of 11 (Na) or above (ISO 22309:2011). November, 2015.

[28] DIN German Institute for Standardization. Testing of oxidic raw materials and materials for ceramics, glass and glazes – Part 2: Determination of Ag, As, B,..., W, Y, Yb, Zn, Zr by optical emission spectrometry with inductively coupled plasma (ICP OES). July, 2004.

[29] Fabian Schoden, Anna Katharina Schnatmann, Emma Davies, Dirk Diederich, Jan Lukas Storck, Dörthe Knefelkamp, Tomasz Blachowicz, and Eva Schwenzfeier-Hellkamp. Investigating the recycling potential of glass based dye-sensitized solar cells – melting experiment. *Materials*, 14(21):6622, 2021.

[30] Schott Ag. * DE102010023366B420170921 * patent, 2017.

[31] Jiawei Gong, Jing Liang, and K. Sumathy. Review on dye-sensitized solar cells (DSSCs): Fundamental concepts and novel materials. *Renewable and Sustainable Energy Reviews*, 16(8):5848–5860, 2012.

[32] Norio Sato. *Electrochemistry at Metal and Semiconductor Electrodes*. Elsevier, 1998.

1 Introduction

Mankind is facing several major crises, one of which is the climate crisis [1]. A massive lever for reducing carbon emissions is switching to renewable energy sources. Wind turbines and crystalline silicon photovoltaic (c-Si PV) are well-established technologies that are core elements of the transition to a society powered by renewable energy [2]. However, these technologies become waste at the end of their useful life – with few possibilities for recycling or reuse of materials [3,4]. That is worsening a second crisis of humanity, namely the resource crisis – valuable materials are wasted, burned and disposed of. The resource crisis becomes visible in supply chain bottlenecks for semiconductor material or rising wood and energy prices [5,6]. Other problems, such as pandemics, war, or inflation, worsen this crisis. Therefore, not only does it make sense from an environmental perspective to reuse and recycle materials, but also from an economic perspective. Moving industry to a circular economy can yield tremendous improvements in supply chain resilience and thus business resilience. In a circular economy, products and materials circulate thanks to concepts like repairing, reusing, remanufacturing or recycling [7]. The concept of the circular economy contrasts with the existing system, the linear economy or the "take, make and waste" economy [8]. When facing multiple crises, multisolving becomes essential – which means to find solutions which solve several problems at a time. In this case we need to develop technologies which harness renewable energies and are designed for a circular economy at the same time.

A promising technology that was investigated in this work is dye-sensitized solar cells (DSSCs). This technology can potentially be made from non-toxic material and has low energy and purity requirements during the production phase, allowing production in rural areas or developing countries [9–12]. DSSC technology is unlikely to replace c-Si PV, but will complement it, as this technology can be used in lower-light-intensity conditions such as indoors or in the morning or evening hours [13]. Integrated in windows of buildings or cars, entire facades, backpacks or tents are possible applications [14, 15]. Research is focusing on improving stability of the electrolyte, increasing the power conversion efficiency

(PCE) and using sustainable materials – which require further research until the technology can reach the industrial scale [16, 17]. The sustainability research is focusing on life-cycle assessment (LCA), eco-design and green chemistry [18]. Life-cycle assessments focus on the environmental impact of a technology, eco-design examines in detail the sustainability of components, and green chemistry tries to avoid waste and concentrates on degradability among other aspects [19–21]. Researchers note that recycling DSSC material can improve the environmental impact of the technology [20]. However, practical studies on recycling and remanufacturing of DSSC were non-existent [18, 22].

Goal of this thesis was to investigate the suitability of the DSSC technology and the used materials for the circular economy framework. Therefore, it was required to investigate the recycling and remanufacturing potential of DSSC material as well as circular design approaches.

In consequence, the following research hypothesis was formulated: The materials required for the production of DSSCs can be subjected to cyclic technological processes, so that the achieved stability of structural, optical and electrical parameters allows their reuse in photovoltaic devices.

In figure 1 an overview of the material cycle of DSSCs and the corresponding chapters in this thesis is given.

In chapter 2 “Theoretical Foundations”, the motivation for the investigation is made clear and the history of DSSC development, the state of the art as well as related works in the field of sustainability research in the DSSC context are pointed out.

In chapter 3 “Methodology”, the experimental setup and used materials and devices are discussed. First, the state of the art in recycling concepts was examined with a bibliographic study, using the VOSviewer tool [18].

Furthermore, for the recycling experiment, the DSSC glass substrates were analyzed using optical emission spectrometry with inductively coupled plasma (ICP-OES) and scanning electron microscopy energy dispersive X-ray (SEM-EDX). In a melting experiment, a mixture with DSSC cullet was melted in a furnace to simulate a standard glass recycling process. In a next step the remanufacturing potential was investigated. Therefore, old

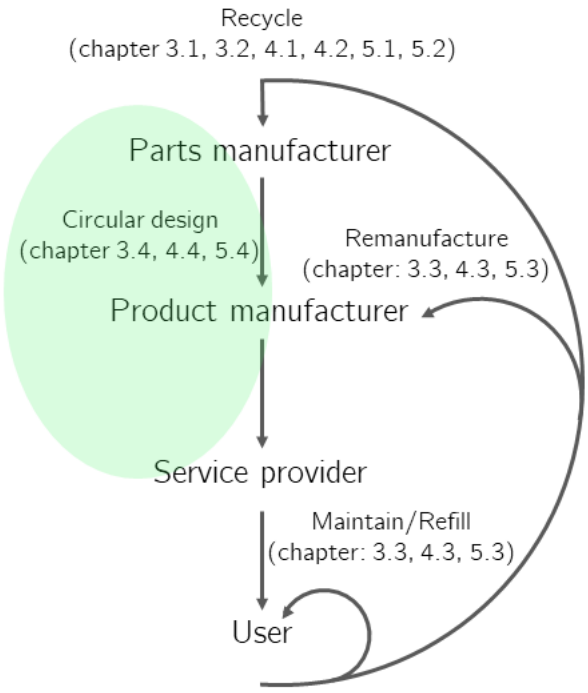

Figure 1: Overview of the material cycle of a DSSC and the corresponding chapters.

DSSCs were taken apart and the material, especially the conductive glass substrate, was used to build new DSSCs. Finally, the circular design of DSSC was investigated using the Circo method, which is usually used in companies to transform a linear product to one which can be circulated in material cycles.

In chapter 4 “Experimental Results”, all results as well as graphical evaluation of the data is provided.

Followed by chapter 5 “Discussion”, where the results are discussed and possible statements are derived from the collected data. In existing works, recycling materials were used to built DSSCs, for instance, conductive substrates from smartphones or flat-screen TVs [23]. Recycling experiments with used DSSCs were non-existent [18, 22]. Therefore, a melting experiment was performed to investigate the recycling potential of DSSC material for a conventional glass recycling process [24]. The recycled glass quality is promising, so that non-toxic DSSC can potentially be used for a conventional glass recycling process. Since melting glass is an energy-intensive process, the remanufacturing potential of DSSCs

was investigated in a further step. Old DSSCs were taken apart and the material, especially the conductive glass substrate, was used to build new DSSCs. The PCE proved to be stable and several generations of DSSCs could be produced from the same material [25]. For market entry, DSSC stability and PCE need to be further improved, but performance-contracting business models for recyclable and remanufacturable DSSCs could be identified as promising solutions.

Finally, in chapter 6 “Conclusion”, the main statements are given as well as an outlook for further investigations.

2 Theoretical foundations

After the motivation for this work, a swift overview of the history of DSSC is given in this chapter. The functioning principle and relevant materials for DSSC manufacturing are given as well as the state of the art of DSSC research with the focus on sustainability and materials. Finally, the idea for a circular DSSC is explained and lessons learned from c-Si PV technology for repair, recycling and remanufacturing processes are described.

2.1 Motivation

During the research of my own PhD project, it became clear that sustainable technologies for the use of renewable energies will be needed in the future. Material science plays an important role in making such technologies possible. With appropriate materials sustainable and circular DSSCs can be manufactured. Manufacturing c-Si PV is a very energy-intensive process, while DSSCs can be manufactured in a low-tech and low-energy approach [17]. Furthermore, DSSCs have not reached the industrial scale yet [14]. Consequently, any adjustments to the design for more circularity could be made in advance. On top of that, there is the chance to learn from mistakes made in the well-established c-Si PV industry, where modules are not made for recycling or remanufacturing processes yet – general results from this research can also be applied back to enable more sustainable c-Si PV modules as well [25].

Own research in this field has been published in the following papers:

A Schoden, Fabian, Dotter, Marius, Knefelkamp, Dörthe, Błachowicz, Tomasz, Schwenzfeier-Hellkamp, Eva; *Review of State of the Art Recycling Methods in the Context of Dye Sensitized Solar Cells*; Energies; 14; 3741; 2021.

B Schoden, Fabian, Schnatmann, Anna Katharina, Davies, Emma, Diederich, Dirk, Storck, Jan Lukas, Knefelkamp, Dörthe, Błachowicz, Tomasz, Schwenzfeier-Hellkamp, Eva; *Investigating the Recycling Potential of Glass Based Dye-Sensitized Solar Cells – Melting Experiment*; Materials; 14; 6622; 2021.

C Schoden, Fabian, Detzmeier, Joscha, Schnatmann, Anna Katharina, Błachowicz, Tomasz, Schwenzfeier-Hellkamp, Eva; *Investigating the Remanufacturing Potential of Dye-Sensitized Solar Cells*; Sustainability; 14; 5670; 2022.

D Schoden, Fabian, Schnatmann, Anna Katharina, Błachowicz, Tomasz, Manz-Schumacher, Hildegard, Schwenzfeier-Hellkamp, Eva;*Circular design principles applied on dye-sensitized solar cells*; Sustainability; 14(22); 15280; 2022.

The contents of these articles are partly included in this thesis.

2.2 History of DSSCs

The DSSC was invented by Michael Grätzel and Brian O'Regan in 1991 [26]. At that time, the production of c-Si PV was very expensive and the DSSC technology presented a low-cost alternative, because of a less energy consuming production process. That is why, from 2000 to 2010, many companies tried to push DSSCs to industrialization, especially in Asian countries – in that time, more than 50% of the submitted patents in DSSC context came from Japan [27]. Examples of Japanese companies working on DSSC technology of that time are Sony, Toyota, Hitachi Maxell or Fuji Film, to name a few [28]. At which point, almost all companies active in that field had the goal to develop technology to replace c-Si PV systems. Some examples of such products were investigated by Hagfeldt et al. in 2010 [29].

However, from 2005–2015 the manufacturing costs for c-Si PV could be drastically reduced – caused by China building up c-Si PV industry and subsidizing their products. Because of this decrease in c-Si PV prices, DSSCs were no longer competitive. It would have required a significant increase in the efficiency of DSSCs to change that. Therefore, there are no industrial DSSC applications that try to replace c-Si PV modules today [28].

After the approach of replacing c-Si PV, DSSC technology was further investigated for applications where this technology could supplement c-Si PV. For instance, in building integrated photovoltaic (BIPV) and aesthetic applications, such as colored facades or other aesthetic applications in architecture. Samsung, Aisin Sekie and Toyota are among the

companies which have worked on such applications [28]. A large-scale project that was realized and represents a milestone for this aesthetic DSSC applications is the conference center at "École polytechnique fédérale de Lausanne" (2014), with a see-through facade of DSSC modules, manufactured by the company Solaronix [30].

Another application of DSSCs are low-power devices such as watches – Swiss companies such as Asulab and Leclanché produced prototypes of such products in the mid-nineties [28]. Around 2000 flexible DSSCs were used by companies such as G24 Power and implemented in several products such as Logitech keyboards, solar backpacks, etc. [31]. A trend that could further increase the demand for DSSCs in low-power devices is the Internet of Things – which will increase the number of low-power devices. With millions of such low-power devices, integrated DSSCs could finally find their niche application and mature to industrial scale.

For DSSCs to be competitive, they need to have a life span of around 5 years for wearable and around 20 years for applications in the construction sector [20, 32]. The transparent conductive oxide (TCO) layer as well as the glass substrate are the most stable components. The electrolyte and the dye are the components most susceptible to degradation and thus to long-term stability problems. Michael Grätzel showed that the N3 dye is stable for 20 years by observing the redox cycles of the dye [33]. He also states that it is essential to regenerate the ruthenium dye fast, within nano- or microseconds, otherwise it could lead to failure of the cell [34]. Advantages of the DSSC technology are [28, 33]:

- insensitivity to temperature change – raising the temperature from 20 to 60 °C has no negative effect on the PCE. In contrast, c-Si PV have a high-temperature-dependent PCE;
- low-cost production and materials;
- easy to fabricate;
- potentially composed of non-toxic materials;
- colorful and aesthetic;
- transparent;
- efficient in low-light and high-temperature conditions.

Indoor applications for DSSCs seem to be most promising, which is confirmed by latest niche applications concerning low-power devices. Examples are a wireless multi-sensor by Fujikura Ltd. in Japan or medical and sports devices by 3GSolar Photovoltaics Ltd. in Israel. In addition to the low-light intensity advantage, other factors such as price, color and flexibility will play an important role in the success of DSSCs in these niche applications. The only company producing solid-state DSSCs so far is Ricoh Company, Ltd. in Japan with the RICOH EH DSSC. This product is used for internet-of-things devices [28]. The DSSC market is expected to grow by 12.4% from 2020 to 2027 [35]. That indicates the DSSC technology will become a more important part of green energy production but consequently will also cause DSSC waste – sustainable solutions are required.

2.3 DSSC materials and functioning principle

The first cell in 1991 was composed of a 10-μ-thick layer of TiO_2 on a conducting glass substrate. The rough TiO_2 surface was coated with a mono-layer of dye (tris(2,2'-bipyridyl-4,4'-carboxylate) ruthenium(II)) and the PCE was 7.1% respectively 12% in diffuse light. Today, PCEs over 13% were reached using the global standard spectrum (AM1.5g), which corresponds to 1.000 W/m^2 [36].

In laboratories, power conversion efficiencies (PCE) above 14% can be reached – in this case, toxic and scarce components are used, such as ruthenium dyes and platinum [17, 37, 38]. The advantage of DSSCs becomes visible in ambient light, where a PCE of 34% was achieved in experiments [36]. The DSSCs investigated in this work are based on natural dyes and graphite instead of platinum. These non-toxic DSSCs usually reach PCEs below 1% [39–41]. Besides the lower PCE, the long-term stability remains a problem of this technology – the electrolyte evaporates quickly. Experiments show that DSSCs can at least work for four month when refilled with electrolyte [42]. Research is being conducted on solid-state and gel-electrolytes to increase the long-term stability of DSSCs [43, 44]. Experiments with DSSCs filled with gel-electrolyte are stable for at least 140 days [45]. Further research is needed to improve the long-term stability and PCE of DSSCs.

The composition of the DSSC as well as the functional principle is explained in figure 2.

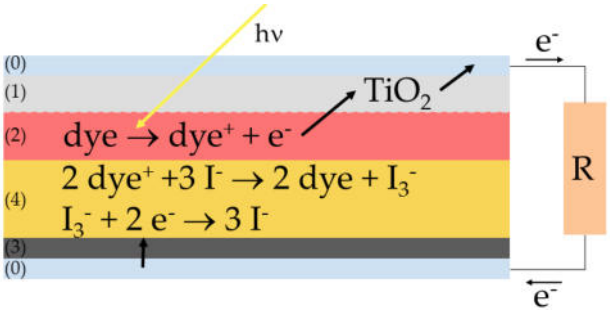

Figure 2: Functional principle of a DSSC, adapted from [18].

Two conductive substrates are required. A commonly used material is a glass substrate coated with fluorine-doped tin oxide (FTO) – number (0) in figure 2. The glass of the front electrode is additionally coated with semi-conductor material, most common is TiO_2 – number (1). Dye is then applied on the porous layer of TiO_2, which is the photo active component – number (2). The counter electrode consists of the second conductive glass element which is coated with a catalyst such as graphite or platinum – number (3). Both electrodes are put together and an electrolyte is filled in, often iodine/potassium iodide is used – number (4). When exposed to light, the electrons in the dye get excited and are injected into the conduction band of the the semi-conductor and finally reach the conductive glass. From there the current can be used, for instance, to charge a phone in an external circuit. At the counter electrode, the electrons can flow across the graphite or platinum layer. The catalyst layer reduces the electrolyte, which transports the electrons back to the dye molecules and regenerates the dye [26]. In following, the different components and materials of the DSSC technology are explained.

2.3.1 Semiconductor materials

In the conventional p-n junction, light absorption and charge carrier transport happens in the semi-conductor. In the DSSC, the light is absorbed by the dye and electrons get excited. These electrons enter the conduction band of the semiconductor via photo-induced electron

injection [33]. The most common semiconductor material in DSSC manufacturing is TiO_2 in its anatase form. It is applied in paste form on the glass-substrate via screen printing or in lab scale with the doctor blade method. Printable TiO_2 is already commercially available [28]. After sintering at 400 to 500 °C, the organic components of the TiO_2 paste are evaporated and electronic interconnection with the conductive substrate is enabled. The surface of the TiO_2 is a mesoporous layer and is composed of nanometer-sized particles. Mesoporosity describes the size of pores of the material – the diameter of the pores is larger than 2 nm and smaller than 50 nm. The TiO_2-layer is around 5-20 μ thick with a porosity of 50-65% and an average pore size of 15 nm [28]. The porosity is $1 - (\rho_{bulk}/\rho_{particle})$ with ρ_{bulk} bulk density (of a solid) and $\rho_{particle}$ density of the particle. The band gap of TiO_2 in anatase form is approximately 3.2 eV [28].

Besides TiO_2, zinc oxide (ZnO) and tin oxide (SnO_2) are used for DSSCs. ZnO has better electron mobility but lower chemical stability compared to TiO_2 [46–48]. SnO_2 is chemically stable but has a lower conduction band gap energy than TiO_2, which leads to a lower voltage in the DSSC [28]. TiO_2 is commonly used, abundant, non-toxic and a good compromise between sustainability and efficiency [49].

A disadvantage of TiO_2 is the photo-catalytic activity – when hit by UV-light, organic compounds can be oxidized, which leads to degradation of the DSSC [50]. A UV-filter might solve the problem, but that adds another component and makes the cell more expensive and probably recycling more difficult.

2.3.2 Sensitizers

In DSSCs, the function of the dye is to absorb the light and separate charge. The dye is applied on the mesoporous layer of TiO_2 [51]. In the pursuit of higher PCEs, especially the sensitizers are of interest. The dyes which reach highest efficiencies are usually ruthenium or metal-based dyes such as: N3 [33], N719 [52], CYC-B11 [53], and the Black Dye [54].

By choosing the sensitizer, it is also determined which wavelength of light can be used by the DSSC for charge separation. The ruthenium dye N3, for instance, has absorption

maxima at 518 and 380 nm [33].

Another category of dyes are organic dyes, which are synthetic dyes. With such synthetic dyes, absorption maxima, color, thermal stability or other properties of the dyes can be chemically designed [28]. DSSCs with organic dyes such as indoline dye (D205) delivered a PCE of 9.4% [55] and with YA422 a PCE of 10.7% was reached [56]. Since the properties can be designed, organic dyes can potentially be used for tandem cells or co-pigmentation to increase the yield from the solar spectrum [28]. Tandem cells are two photovoltaic cells combined and both mainly use different parts of the solar spectrum for charge separation and thus use the light more efficiently. Co-pigmentation of DSSCs means that two different dyes are applied on the TiO_2-layer to improve the PCE [57].

Metal-based and synthetic dyes pose environmental risks through toxicity or the use of toxic solvents. That is why they might be replaced by more sustainable solutions, which leads to the third category of dyes – natural dyes. Natural dyes are extracted from plants and contain dyes such as anthocyanin, chlorophyll, etc. [58]. Anthocyanin absorbs wavelengths between 450 and 580 nm with the absorption maximum at 520 nm [59]. Chlorophyl has an absorption maximum at 430 nm [60]. A disadvantage of non-toxic DSSCs with natural sensitizers are comparably low PCEs of below 1% [39–41]. The low PCEs are mostly caused by the limited range of light which can be absorbed by natural dyes. Organic and metal-based dyes, in contrast, have a broad absorption spectrum [61].

2.3.3 Counter electrode

The counter electrode usually consists of a conductive substrate coated with a catalytic layer and serves two main functions in the DSSC. First, receiving electrons from an external circuit and transmitting them into the DSSC (low electric resistance required) and second, support and speed up the reduction of the electrolyte (catalyst function). Platinum has high conductivity and high catalytic activity, and thus was the material of choice for the active layer of the counter electrode, resulting in PCEs above 12% [62]. Disadvantages of platinum are the price, rarity and degradation effects in the DSSC [63].

Cost-effective alternatives are carbon-based materials which are abundant, have high catalytic activity and high conductivity, just to name a few advantages [64]. However, carbon-based materials cannot reach the conductivity and catalytic properties of platinum. Thus, researchers are focusing on enhancing the carbon-based counter electrodes with metals and halogens to improve the PCEs [65].

2.3.4 Charge transport materials

The task of the charge transport material is to regenerate the dye and transport electrons from the counter electrode to the dye. Iodide/triiodide redox couple (I^-/I_3^-) is often used as liquid charge transport material [66]. The electrolyte is reduced at the counter electrode, transports electrons from the counter electrode to the front-electrode and regenerates the dye [28]. I^-/I_3^- was used for a long time as best option for liquid electrolyte. However, one disadvantage of I^-/I_3^- is that it has corrosive effects on the counter electrode material as well as on the sealing – which motivated researches to find alternatives [64]. One alternative is bromide/tribromide Br^-/Br_3^-, which delivers increased photovoltage at the cost of lower current density compared to I^-/I_3^- [28].

The electrolyte is critical for the long-term stability of the DSSC. However, liquid electrolytes evaporate quickly, making their use unfavorable when it comes to long-term stability. To improve long-term stability, gel-electrolytes and solid-state electrolytes were developed, which are explained in more detail in the next two chapters.

2.3.5 Gel-electrolyte

The basis of gel-electrolytes is a liquid electrolyte, such as I^-/I_3^-, which is encapsulated in polymers. This way, gel-electrolytes are combining the properties of a liquid and a solid charge transport material. They have high thermal and long-term stability as well as good filling properties, which means that they can get in contact with the dye molecules and enable fast regeneration of the dye [67]. Common materials for gel-electrolytes are polyethylene oxide (PEO) or polyacrylonitrile (PAN) [28, 68]. PEO with lithium salts and

N3 ruthenium dye, for instance, reached a PCE of 4.2% [69]. Possible applications are flexible and wearable electronics [70].

2.3.6 Solid-state electrolyte

Solid-state electrolytes are homogenous polymers, organic or inorganic hole transport materials – which means that charge moves through the material and no ions are transported [71]. The liquid redox couple is replaced with a p-type hole transport material [72, 73]. Solid-state DSSCs main advantage is the long-term stability. However, they have lower efficiencies compared to liquid-electrolyte or gel-electrolyte DSSCs. This is due to poorer connectivity between the charge transport material and the dye molecules, resulting in less charge transfer and thus slower dye regeneration.

Solvents are used in the manufacturing process to make the hole transport material liquid. Then it is possible to spin-coat the solution on the surface of the porous TiO_2 layer [33]. The problem is that when the solvent evaporates, bubbles can form which then reduce conductivity. If the melting temperature of the hole transport material is lower than that of the glass substrate, without solvent, the material can be melted directly on the surface [74]. Burschka et al. manufactured a solid-state DSSC based on a polymer (spiro-OMeTAD) and reached a PCE of 7.2% [75]. An example for inorganic material was delivered by Chung et al., who used a tin-based material ($CsSnI_3$) as solid-state electrolyte and reached a PCE of 10.2% [76]. Other technologies of the third generation of photovoltaic are perovskite and organic solar cells, which are briefly touched upon below.

2.3.7 Perovskite and organic solar cells

Also in the focus of researchers are perovskite solar cells [77]. The advantages of perovskite solar cells are the high PCEs, around 25.5%, and low production costs [78]. Wang et al. even reached a PCE of 35.2% [79]. Their disadvantage is that lead is an important compound. Lead can potentially harm the environment, it makes a recycling process more difficult and even causes constraints for commercialization. Without lead, the PCEs are

considerably lower as well as the long-term stability [80].

Organic solar cells are the third technology, besides DSSCs and perovskite solar cells, research is focusing on [81]. Organic solar cells can be produced with low costs and reach PCEs of around 18% – Lee et al. even confirmed a PCE of 28.1% at 1000 lux [82, 83]. However, long-term stability remains a problem for this technology.

2.4 Idea for future circular DSSCs

In the future, sustainable technologies for energy generation must be designed in such a way that the materials they are made of can flow in material cycles. Previous research approaches that focused on sustainable DSSCs range from life-cycle assessment to eco-design and green chemistry [14, 20, 84]. In the following, these terms will be explained, the experience with recycling c-Si photovoltaic will be summarized, and the research gap will be identified.

2.4.1 Life-cycle assessment

With LCA studies, the environmental impact of a product can be investigated. Important figures that are estimated in an LCA are:

- The energy payback time (EPBT): It explains how long it takes for the DSSC to generate enough energy to compensate for the energy that was required to produce it.
- The cumulative energy demand (CED): It explains how much energy the DSSC requires over the observed lifetime – depending on system boundaries. For a cradle-to-grave investigation, for instance, energy for resource extraction, transport, manufacturing, use-phase and disposal is taken into account.
- The greenhouse gas (GHG) emission rate: It shows how much CO_2-equivalents are emitted per kWh generated by the DSSC – GHG in CO_2-equivalents/kWh.

An important piece of information for the LCA is the system boundary, which provides information about which phases of the product's life are included in the analysis.

The conducted studies set the system boundaries to a cradle-to-grave approach [20,85,86]. That means that the entire life-cycle of the product is taken into account. From mining resources, manufacturing, use-phase and disposal. Due to the lack of information about DSSC recycling, disposal of the materials was the only option for the LCA [87]. Only Parisi et al. made an assumption and used recycling data available for c-Si PV and applied those to their DSSC LCA investigation – 90% of metals and 68.8% of glass can be recycled, the rest of the material is declared as hazardous waste and is disposed of [20]. The glass however, is downcycled and cannot be used for photovoltaic, container or flat glass applications in its second life.

LCA investigations of DSSC technology confirm that the production of the conductive glass substrate is the most energy-intensive part, having a very high environmental impact [20,85,86]. That is why, with a recycling process, especially for energy-intensive TCO glass substrate production, the environmental impact of DSSCs could be reduced – a cradle-to-cradle approach could be enabled [18].

Parisi et al. suggest to switch from the energy-intensive glass substrate to a polymeric substrate, which would reduce the energy consumption for producing a DSSC by about 35% [85] – cradle-to-grave approach. They also point out that in their comparison of well-established thin-film technologies, such as amorphous silicon (a-Si), copper indium diselenide (CIS) and cadmium telluride (CdTe), DSSC technology is on the same level regarding CED, GHG emission rate and EPBT. Furthermore, the DSSC technology has high potential energy savings in the production when it reaches mass production on industrial scale [85].

To conclude, the environmental impact of DSSCs could be reduced if the glass substrate were to be recycled. Glass recycling is a well known process, however, till this thesis no real recycling experiments with DSSCs have been conducted.

2.4.2 Green chemistry

The twelve principles of green chemistry focus on preventing waste and toxicity, improving energy efficiency in the production process as well as using regenerative raw materials and design for degradation, just to name a few principles [19]. It is important to note that solvents, which are required in the production process of DSSCs, make an evaluation of the environmental impact more difficult [88]. Mariotti et al. emphasize to apply the twelve principles of green chemistry on DSSC technology and use non-toxic and abundant materials [14].

With the twelve principles of green chemistry, each material is evaluated in its toxicity, however, an holistic approach for recycling or remanufacturing is not possible with this investigation [21].

2.4.3 Eco-design

Eco-design is a concept for designing products with a holistic approach, so to speak, minimizing environmental impacts and also considering costs, and thus economical aspects [84]. Miettunen et al. used the eco-design approach for DSSCs and concluded that for recycling concepts for DSSCs it is mandatory to look at the entire system and not focus on the material level – as does green chemistry [21]. This is because the amount of material and its value determine whether the product or materials can be recycled in an economically viable manner. Miettunen et al. focused on the silver in DSSC and pointed out that for thin glass substrates the silver proportion is high enough so that a recycling process would be economically viable [21].

Eco-design usually focuses on a holistic approach along the entire life-cycle of a product. To the author's knowledge, only Miettunen et al. took an eco-design approach for DSSCs and focused on recovering silver in a pyrometallurgic process [21, 89]. They pointed out that the recycling of glass substrate is important, but challenges are labor intense cleaning of substrates and toxic materials.

Using existing recycling structures, such as glass recycling, would enable a recycling

process without the necessity for enormous quantities of old DSSCs or investment in expensive machines and equipment. That is why designing and manufacturing DSSCs that are suitable, as they are, for a conventional glass recycling process can be advantageous.

2.4.4 Lessons learned from c-Si PV

Since c-Si PV is a well-established technology and already old modules are entering a recycling process, one can learn from design mistakes or problems with this technology. That knowledge can be used to improve DSSC design even before the technology enters the industrial scale.

So far, except for the aluminum frame, no high-quality materials can be recovered from conventional recycling of c-Si PV modules [4]. In a conventional recycling process the entire module is shredded and then the mixture of materials runs through a sorting plant. The ethylene-vinyl acetate (EVA) foil is a problem, because materials, such as plastics, glass and metal components, are laminated together by the foil and they cannot be separated in the conventional sorting plant. One alternative to EVA could be to use polyvinyl butyral (PVB) foil for encapsulation. This material is used in safety glass, degrades when the glass is shredded and exposed to sunlight, and thus can be separated from other materials [90,91]. A patented method describes how to separate PVB from windshields – which could also be adapted to c-Si PV modules or DSSCs with sealing [92]. A company that is already using PVB foil in their c-Si PV module is Trosifol Solar [93].

So there is at least one alternative for an encapsulation material, which enables higher quality recycling. Other alternative encapsulation materials are, for instance, thermoplastic polyolefin, polyolefin elastomer or thermoplastic polyurethane [94].

Due to the shredding of the module, metal parts contaminate the glass [4]. This material mix cannot be used for conventional glass recycling because metal parts become inclusions in the glass which cause weaknesses, and thus make the glass fragile.

Research projects like EOL-Cycle found that the quality of the glass can be improved with more cleaning and sorting steps. However, even in the EOL-Cyle project the glass

quality was not high enough for flat glass production [3]. When more complex sorting and cleaning processes are used, there is a risk that the recycling process will no longer be economically viable. Another issue that EOL-Cycle has uncovered is a fluctuation in the materials used in PV modules – different polymers are used and the glass composition varies [3]. A material passport for each module batch could help to enable a better recycling process.

A totally different approach is investigated by NPC Incorporated, a Japanese company. They do not shred the module but separate the glass from the EVA foil with a highly heated knife [95]. With such a less destructive method, material could be recovered with higher quality. The ReProSolar project is working on a non-destructive delamination method with high-intensity light pulses. This way, layer by layer could be separated from the compound and it would be possible to reuse module parts or increase the value of the recycling [96].

In the CIRCUSOL research project they found that defects in the first four years of a PV module cause 80% of PV waste and between 45% and 65% of these modules could be repaired [4]. This indicates that a repair process is technically possible. However, those processes have not yet been scaled to the industrial level.

For giving c-Si PV modules a second life, building up fault detection and testing of the modules is essential. Glatthaar et al. developed the PV-Rec recycling concept. The current-voltage of the old or defect c-Si PV module is tested under standard test conditions followed by an electroluminescence investigation, infrared imaging and visual evaluation of defects. After the repair or remanufacturing process, the current-voltage is tested again to evaluate the new characteristics [97].

Some companies, such as Solar-pur GmbH, pvXchange, Rinovasol or Second Sol, already offer repair services for c-Si PV modules with defective junction boxes, bypass diodes, module frames, module cables and module back sheets [98–101]. Defective solar cells, broken glass or lose foil defects cannot be repaired with the methods used so far [99].

Thin-film modules are closer to the DSSC technology and for cadmium telluride (CdTe) modules First Solar has developed a reverse logistic and recycling solution [102]. Within their process, it is possible to recover 90% of the glass and semiconductor material with

high quality – it can be reused for thin-film modules [103, 104]. High effort is required to recover the high-quality material. Since CdTe modules are toxic, it is important to have a defined end-of-life process for these modules. A repair or remanufacturing process, however, is not possible with the First Solar approach – their recycling process consists of mechanical shredding and wet chemical processes.

Finally, Apollon Solar is approaching the problem from a design perspective and is using an alternative encapsulation method using neutral gas instead of plastic in the module. This "New Industrial Solar Cell Encapsulation" (NICE) technology would enable a higher quality recycling and is also promising for repair and remanufacturing approaches [105].

This information should be used to design DSSCs in a way that a recycling and remanufacturing approach becomes possible.

2.4.5 Unexplored research area

With the existing LCAs, only ideas for different conductive substrates have been mentioned, because the environmental impact in the LCA could be reduced this way [20, 85, 86].

With a green chemistry approach, each individual material as well as the solvents are evaluated concerning toxicity [88].

The existing eco-design approach focuses on recycling silver in a pyrometallurgical process [21].

Missing elements in the research field of sustainable DSSCs are:

- recycling experiments;
- remanufacturing experiments;
- circular concepts and business models for DSSCs.

These will be topics of this dissertation and enable circular DSSC technology. Circular design aims to develop a product that is durable, is designed for circularity and is connected to a business model. This way, industrialization of DSSC technology can be realized. End-of-life scenarios like remanufacturing, reusing components of the DSSCs as well as a recycling process are required for circularity, and are thus the foundation of a circular

business model. A circular DSSC would be made from non-toxic, abundant material, have a long life expectancy, can be remanufactured or recycled, and is a viable product in a circular business model.

3 Methodology

The methodology chapter includes four approaches to test the research hypothesis. In the first chapter 3.1, the general meaning of sustainability in context of DSSC research is analyzed and visualized with a bibliographic analysis with the VOSviewer tool. In the second part, chapter 3.2, the methodology of a recycling experiment with standard DSSCs and gel-electrolyte DSSCs is described. In chapter 3.3, the methodology of a remanufacturing experiment with old DSSCs is pointed out. The DSSCs were remanufactured several times and the PCEs are observed over time. In the final part, chapter 3.4, the Circo method is described, which is a tool to develop a circular business model for a product.

3.1 State-of-the-art recycling methods in the context of DSSCs – bibliographic analysis

In the theoretical part of the experiments, a bibliographic analysis was conducted to investigate the relevance of sustainability research in the field of DSSCs. Therefore, the VOSviewer tool (VOSviewer version 1.6.16) from the Leiden University was used. The tool was developed by Nees van Eck and Ludo Waltman [106]. This software can be used for bibliographic studies to create visualizations of publications and terms. The number of appearances and the co-occurrences of words can be visualized in a term map. Co-occurrence means that words appear together in the same publication. To perform the bibliographic analysis information about the publications have to be downloaded from the Web of Science. Therefore, the database was searched with the term “dye sensitized solar cell”. All information from the publications had to be downloaded and were saved in a bibliographic database file. In figure 3 the export options that have been chosen in the Web of Science are shown.

The information from the Web of Science could only be downloaded for 500 search results at once. Therefore, this exporting process had to be repeated until all information from the search results was downloaded. This database file then had to be analyzed. In

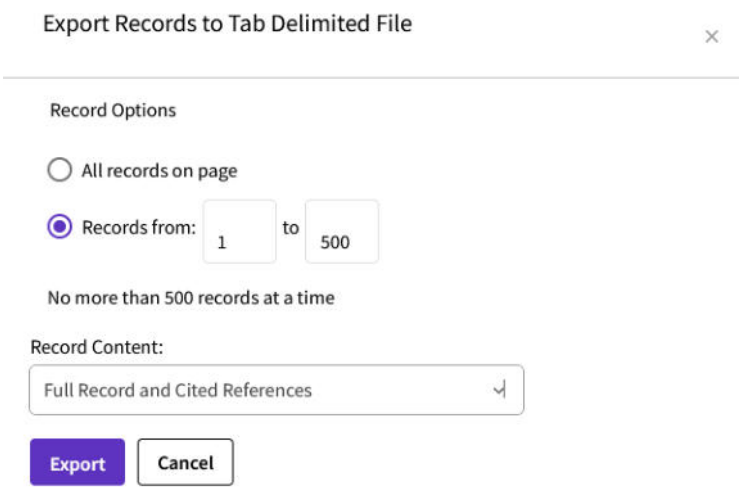

Figure 3: Export options in the Web of Science.

figure 4 it is shown step by step which settings have been chosen to analyze the data.

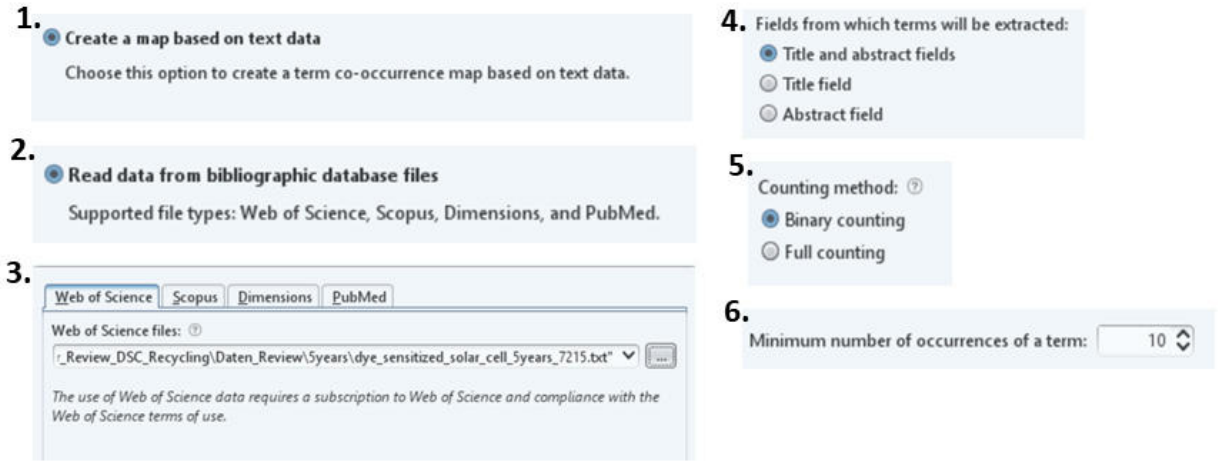

Figure 4: Explanation of the VosViewer Tool.

1. The option “Create a map based on text data” was chosen, since the downloaded information from the Web of Science is in text format.
2. “Read data from bibliographic database file” – the information downloaded from the Web of Science.
3. Data from the bibliographic database files was loaded in the VOSviewer tool.
4. Terms from title and abstract should be used for the investigation.

5. “Binary counting” was chosen, which means that not the total appearance of a term was counted but just the existence or non-existence of a term in one publication. Otherwise, a term that appears more than once in a publication could distort the overall picture.
6. The minimum number of occurrences was set to 10, so that terms that appear less then 10 times do not appear on the resulting graph.

The result of this investigation is a list of terms and the number of appearances as well as a term map, which can be found in chapter 4.1. The following chapter describes the methodology for the recycling experiment performed.

3.2 Recycling of DSSCs – melting experiment

The results of the recycling experiment were published in the following publication [24]. The required devices are not available in the Bielefeld University of Applied Sciences, which is why the experiments were performed at the Institute for Glass and Raw Materials Technology (IGR) in Göttingen. For the melting experiment, old DSSCs from 2018 and 2020 were used [68]. First, the glass substrate was investigated. The glass substrate were bought from Man Solar B. V. (Petten, The Netherlands). The glass substrates from 2018 were 2 mm thick and weighed 4 g. The glass substrates from 2020 were 3 mm thick and weighed 6 g. Both types of glass were rectangular with dimensions of 40 mm by 20 mm. The following equipment was used to investigate the glass substrate and to perform the melting experiment:

- Carl Zeiss EVO MA10 from Carl Zeiss AG [107];
- SmartEDX from Carl Zeiss AG [107];
- ICP-OES Thermo Scientific iCAP 6300 Duo from Thermo Fischer Scientific Inc. [108];
- Mixer Mill MM 400 from Retsch GmbH [109];
- Universal oven UF260 from Memmert GmbH and Co. KG [110];

- Microwave MARS 6 from CEM GmbH [111];
- Laboratory chamber furnace-CWF from Carbolite Gero GmbH & Co. KG [112];
- SteREO Discovery.V20 from Carl Zeiss AG [113].

3.2.1 SEM-EDX

Scanning electron microscopy energy dispersive X-ray (SEM-EDX) with Carl Zeiss EVO MA10 from Carl Zeiss AG (Oberkochen, Germany) was used to examine the surface of the glass substrates. The microscope can be seen in figure 5.

Figure 5: Carl Zeiss EVO MA10 from Carl Zeiss AG [107].

The Carl Zeiss EVO MA10 can create a high vacuum, a pressure in the order of 10-5 mbar, and has the capability to generate an acceleration voltage of up to 30 kV [107]. High vacuum prevents scattering of the primary electron beam and high acceleration voltage enables to investigate a variety of different materials. Further details of the Carl Zeiss EVO MA10 can be found in the Appendix in figures 55 and 56.

In figure 6, the functioning principle of SEM-EDX is depicted.

This method is a non-destructive way to examine the composition of the material. In SEM-EDX, an electron beam, in this case with an accelerating voltage of 20 keV, is used to knock electrons out of the atoms of the surface of the material under investigation. The knocked off electrons leave a hole, which is then filled by an electron from a higher sphere. In this process, the electron emits X-rays that are material specific. With the EDX, this radiation can be evaluated and the investigated material can be identified [115].

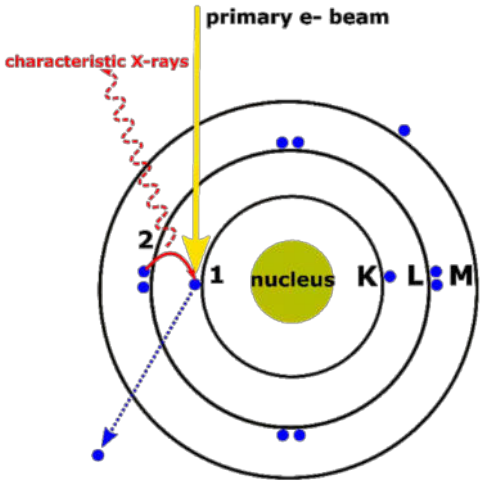

Figure 6: SEM-EDX principle [114].

In figure 7, the ZEISS SmartEDX from Carl Zeiss AG sensor is shown.

Figure 7: SmartEDX from Carl Zeiss AG [107].

The used SmartEDX has an energy resolution of 129 eV, uses a silicon nitride (Si_3N_4) detector, has an active area of 30 mm^2, an input count rate (ICR) of 1,000,000 counts per second (cps) and an output count rate (OCR) of between 40,000 cps and 300,000 cps. Counts per second is an index for the intensity, and thus indicates how many impulses per time were detected. The intensity also correlates with the concentration of the detected element in the sample – higher intensity indicates higher concentration of the element. The ICR gives the total number of X-rays which hit the detector, while OCR is the number of X-rays that can be processed by the SmartEDX. The $deadtime = (1 - (OCR/ICR) \times 100)$ gives the percentage of X-rays that have not been processed. This number should not be larger than 20-30% [116]. More details about the SmartEDX can be found in the Appendix in figure 57.

The preparation of the samples and the execution of the SEM-EDX measurements were performed according to ISO 22309:2011 “Microbeam analysis – Quantitative analysis using energy-dispersive spectrometry (EDS) for elements with an atomic number of 11 (Na) or above” [116]. The glass substrates were cleaned and then cut in two equal large pieces. One half was examined unchanged with SEM-EDX, while the other half was etched with concentrated sulfuric acid and concentrated hydrofluoric acid in a 1:1 ratio for 10 minutes prior to SEM-EDX examination. One half of the 2020 substrate was additionally etched with concentrated hydrofluoric acid for one minute. Always both sides of the glass substrates were analyzed with SEM-EDX. The etching process was used to investigate which parts of the coatings could be removed and which elements remained on the surface. The total pulse rate detected by the SmartEDX had to be at least 2,000 to 3,000 cps. The accelerating voltage of 20 keV was chosen and the samples were measured for 120 s each.

3.2.2 ICP-OES

Inductively coupled plasma optical emission spectrometry (ICP-OES) makes it possible to determine the composition of the material. The ICP-OES Thermo Scientific iCAP 6300 Duo from Thermo Fischer Scientific Inc. (Waltham, USA) was used for the ICP-OES investigation and is depicted in figure 8.

Figure 8: ICP-OES Thermo Scientific iCAP 6300 Duo from Thermo Fischer Scientific Inc. [108].

The Thermo Scientific iCAP 6300 Duo can simultaneously analyze 66 elements with the detection limit of less than 1 part per billion. Only liquid samples can be analyzed. The advanced charge injection camera technology enables the analysis of over 50,000 analytical wavelengths. The Thermo Scientific iTEVA software is used to process the results and manage the system [108, 117]. More details of the Thermo Scientific iCAP 6300 Duo can be found in the Appendix in figure 58.

The experiments were performed according to DIN 51086-2 "Testing of oxidic raw materials and materials for ceramics, glass and glazes Part 2: Determination of Ag, As, B, Ba, Be, Bi, Ca, Cd, Ce, Co, Cr, Cu, Er, Eu, Fe, La, Mg, Mn, Mo, Nd, Ni, P, Pb, Pr, S, Sb, Se, Sn, Sr, Ti, V, W, Y, Yb, Zn, Zr by optical emission spectrometry with inductively coupled plasma (ICP OES)" [118].

Therefore, the glass was crushed with a Mixer Mill MM 400 from Retsch GmbH (Haan, Germany). In figure 9, the mill is depicted. The cullet diameter of the crushed glass was 8.0 mm. Detailed information about the Mixer Mill MM 400 can be found in the Appendix

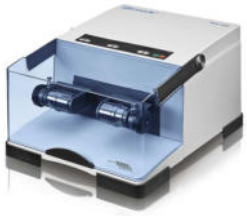

Figure 9: Mixer Mill MM 400 from Retsch GmbH [109].

in figure 59.

After crushing the samples, the cullet was dried with the Universal oven UF260 from Memmert GmbH and Co. KG (Schwabach, Germany) at 115 °C for 20 minutes – which is depicted in figure 10.

Technical details about the Universal oven UF260 can be found in the Appendix in figures 60 and 61.

To proceed, 1 g of the cullet was put into a plastic container together with 2 ml of nitric acid (15 mol/l), 1 ml hydrochloric acid (12 mol/l) and 3 ml hydrofluoric acid (23 mol/l).

Figure 10: Universal oven UF260 from Memmert GmbH and Co. KG [110].

This mixture was put into the Microwave MARS 6 from CEM GmbH (Kamp-Lintfort, Germany) – figure 11. Details about the microwave MARS 6 can be found in the Appendix in figures 62 and 63.

Figure 11: Microwave MARS 6 from CEM GmbH [111].

The mixture was heated up to 200 °C within 15 minutes (900-1800 W), the temperature was kept for another 15 minutes. No stirring was applied. The mixture was then cooled down to room temperature before further processing.

The mixture was put into a plastic measuring flask with a nominal volume of 100 ml. Water was added until the 100 ml mark was reached and the sample was analyzed. The ICP-OES process is depicted in figure 12 and explained below the figure.

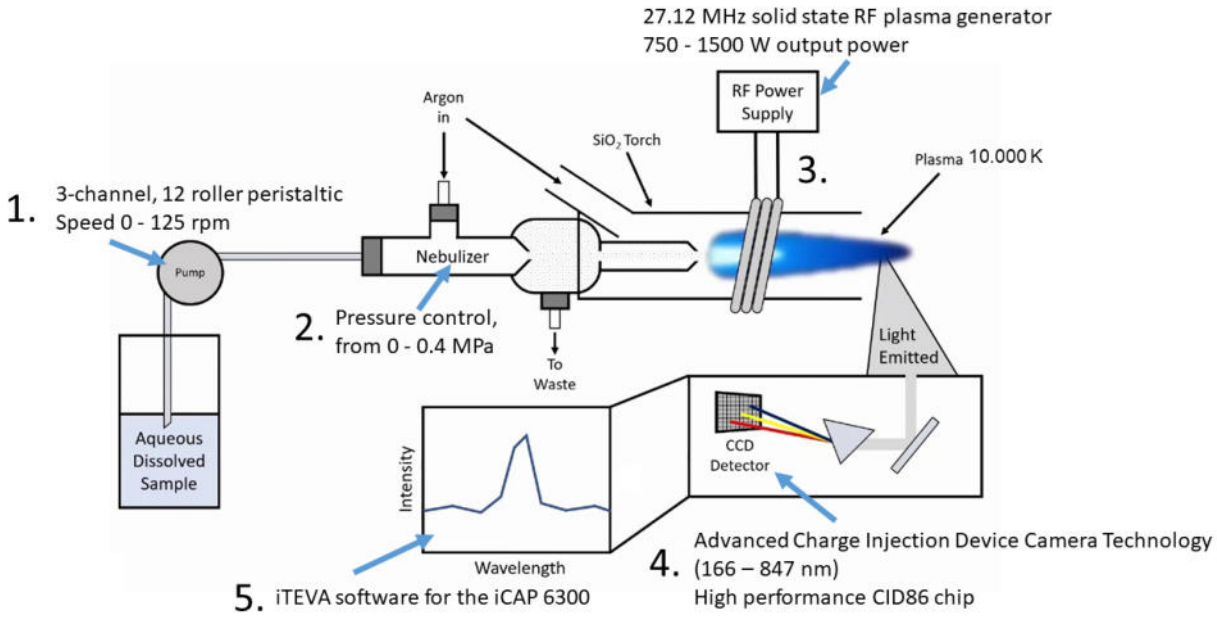

Figure 12: Schematic illustration of the ICP-OES – adapted from [119].

The following list explains the steps 1. to 5. in figure 12 [120]:

1. The dissolved sample gets pumped into a nebulizer. A peristaltic pump is used to create a continuous flow.
2. In the nebulizer, the sample is mixed with argon gas and is turned into an aerosol.
3. The vaporized sample is heated up to 10,000 K with an argon plasma torch. The radio frequency (RF) power supply generates a frequency of up to 27.12 MHz and has an output power between 750 W and 1,500 W. The heat causes the excited atoms to emit electromagnetic radiation.
4. This radiation is material specific, gets split up with a prism and can be analyzed with a spectrometer. An advanced charge injection device camera technology was used, which can detect light with wavelengths from 166 nm up to 847 nm.
5. For processing and evaluating the results, the iTEVA software for the iCAP 6300 was used.

3.2.3 Melting experiment

In total, four different melts were used in the melting experiment to investigate if standard DSSCs and DSSCs with gel-electrolyte can be used in a recycling process.

Melt A: 60 wt% white cullet and 40 wt% raw material (reference sample).

Melt B: 60 wt% DSSC cullet with gel-electrolyte (17 wt% PEO with 600 kg/mol molecular weight (MW) PEO and 38 wt% glycerol) and 40 wt% raw material.

Melt C: 60 wt% DSSC cullet with gel-electrolyte (8 wt% PEO with 600 kg/mol PEO and 47 wt% glycerol) and 40 wt% raw material.

Melt D: 60 wt% DSSC cullet with iodine/potassium iodide electrolyte and 40 wt% raw material.

Melt A is a standard glass recycling mixture and serves as a reference sample. The white cullet was white container glass from a processing plant in Germany. The 40 wt% raw material composition is shown in the following list and is given in weight percentages [24]:

- 59.2 wt% sand;
- 17.2 wt% soda;
- 12.4 wt% dolomite;
- 5.0 wt% nepheline;
- 2.5 wt% calumite (calcium aluminum silicate);
- 2.5 wt% lime;
- 1.2 wt% sodium sulfate.

This raw material composition was used in all melts.

Melt B, additionally to the 40 wt% raw material, consisted of 60 wt% DSSC cullet with gel-electrolyte (17 wt% PEO with 600 kg/mol MW PEO and 38 wt% glycerol). These DSSC were used in a previous publication from 2020 as sample 1 [68]. Melt C also contained a gel-electrolyte (8 wt% PEO with 600 kg/mol MW PEO and 47 wt% glycerol) and was referred to as sample 2 in reference [68]. Melt D consisted of standard DSSCs without gel-electrolyte from 2018 – there were no results published from these DSSCs.

The following list gives an overview of the estimated weight percentage of the composition of the DSSCs [24]:

- 97.7 wt% FTO glass;
- 0.7 wt% TiO_2;
- 1.5 wt% electrolyte;
- 0.1 wt% graphite.

DSSCs in melt B, C and D consisted of FTO coated glass substrate from Man Solar. Forest fruit tea from Mayfair was used as dye extraction. In melt D, graphite from a pencil, grade 6B from J. S. Staedtler, was used as catalyst layer. In melt B and C, graphite spray from CP-Graphitprodukte GmbH was used.

To prepare the DSSCs for the melting experiment, the adhesive tape holding the DSSC parts together was removed. The DSSCs for melt B were going through a simulated weathering process. In a real recycling facility, glass cullet is piled up and sunlight and rain have a cleansing effect on the glass cullet. To simulate that the DSSCs from melt B were washed with tap water and dried in the Universal oven UF260 from Memmert GmbH and Co. KG at 115 °C (figure 10). DSSCs in melt C and D were not going through such a weathering process. All DSSCs were crushed with a Mixer Mill MM 400 from Retsch GmbH (figure 9). The diameter of the DSSC cullet was 0.8 mm. The melts were heated with the laboratory chamber furnace-CWF from Carbolite Gero GmbH & Co. KG (Neuhausen, Germany) to a temperature of up to 1,300 °C – figure 13. The laboratory chamber furnace-

Figure 13: Laboratory chamber furnace-CWF from Carbolite Gero GmbH & Co. KG [112].

CWF can heat up to 1,300 °C and needs 47 minutes heat-up time to reach this maximum

temperature. Further technical information of the laboratory chamber furnace-CWF are provided in the Appendix in figure 64 [112].

After 5 minutes, three lab spatulas of each batch, melt A to D, were added to the specific melt. After 20 minutes and 50 minutes, this procedure was repeated. During this time, the melts were visually evaluated. The melting experiment continued for 24 h and the melts were cooled down slowly. Finally, the melts were investigated with a SteREO Discovery.V20 from Carl Zeiss AG – figure 14. The microscope has excellent depth perception and a

Figure 14: SteREO Discovery.V20 from Carl Zeiss AG [113].

magnification of up to 345x is possible [113]. For this investigation, 10x magnification was used. More technical details of the SteREO Discovery.V20 can be found in the Appendix in figure 65. The experiments were performed with standard DSSCs and DSSCs with gel-electrolyte. Table 1 gives an overview of the experimental setup.

Table 1: Summary of the experimental setup.

melt	electrolyte	graphite source	weathering process
Melt A[a]	non	non	no
Melt B	17 wt% PEO with 600 kg/mol PEO and 38 wt% glycerol	graphite spray	yes
Melt C	8 wt% PEO with 600 kg/mol PEO and 47 wt% glycerol	graphite spray	no
Melt D	iodine/potassium iodide	pencil 6B	no

[a] reference sample

3.3 Remanufacturing of DSSCs

The experimental results have been published in the following paper [25].

The equipment that was used to perform the remanufacturing experiments is listed below:

- Nabertherm L5/11 from Nabertherm GmbH [121];
- Keithley 2450 source meter from Tektronix Inc. [122];
- LS0500 solar simulator from LOT-Quantum Design GmbH [123];
- Axio Observer 7 materials microscope from Carl Zeiss GmbH [124];
- Ultraviolet–visible (UV-Vis) spectrophotometer Genesys 10S from Fisher Scientific GmbH [125];
- FlexAFM from Nanosurf AG [126].

The remanufacturing process for DSSCs is based on preparing the electrodes, applying TiO_2, dye and graphite, putting together the electrodes and adding the electrolyte. Similar to the recycling experiment, FTO coated glass substrate from Man Solar was used. Graphite from a pencil (9B) from Faber-Castell was used as a catalyst layer on the counter electrodes.

In figure 15 an overview of the remanufacturing procedure in this experiment is given.

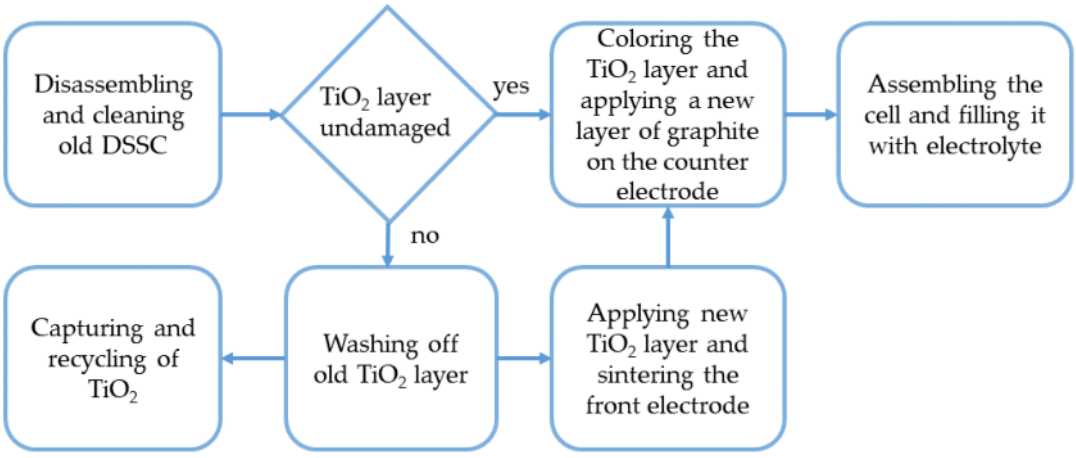

Figure 15: Remanufacturing procedure [25].

At the beginning, old DSSCs were disassembled and cleaned. For cleaning, ethanol and desalinated water was used. When the TiO_2 layer was damaged, it was rubbed off under running water with a rubber glove. The water and TiO_2 could be captured for recycling purposes. A new TiO_2 layer was applied by using TiO_2-paste from Man Solar. A thin homogenous layer (thickness approximately 30 μm) of TiO_2-paste was applied by using the doctor blade method. The front electrode was sintered in a Nabertherm L5/11 oven from Nabertherm GmbH (Lilienthal, Germany) at 500 °C for 2 h. The Nabertherm L5/11 has a maximum temperature of 1,100 °C and is depicted in figure 16. More technical details of the Nabertherm L5/11 can be found in the Appendix in figure 66.

Figure 16: Nabertherm L5/11 from Nabertherm GmbH [121].

For dye extraction, 2.5 g hibiscus flowers were mixed with 7.5 g ethanol and 22.5 g distilled water. Everything was mixed at room temperature for 20 minutes. The TiO_2 coated front electrode was then placed in the filtrate for 20 minutes, cleaned with ethanol and dried at room temperature. In the final step, front electrode and counter electrode were assembled with adhesive tape from Tesa SE (Norderstedt, Germany) and two drops of iodine potassium iodide electrolyte, from Man Solar, were dropped in the DSSC.

To measure the current-voltage curves of the DSSCs, they were contacted with alligator clips with a Keithley 2450 source meter from Tektronix Inc. (Beaverton, USA). The 6 cm^2 active area of the DSSCs was illuminated with an LS0500 solar simulator from LOT-Quantum Design GmbH (Darmstadt, Germany). This light source illuminated the DSSCs with 100 mW/cm^2 with a 1.5 G spectrum – this spectrum is commonly used for flat plate modules and stands for the annual average solar irradiance at mid-latitudes considering 1.5 times the thickness of the atmosphere of the earth. Technical details for the Keithley

2450 source meter and the LS0500 solar simulator can be found in the Appendix in figures 67 and 68. In figure 17, an overview of the experimental setup is shown, with the Keithley 2450 source meter on the left and the LS0500 solar simulator on the right.

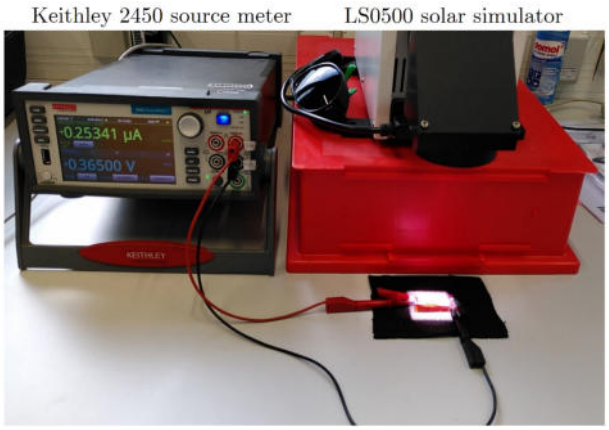

Figure 17: Experimental setup with the Keithley 2450 source meter on the left and the LS0500 solar simulator on the right.

To measure the current-voltage curves of the DSSCs, the following settings for the Keithley 2450 source meter were chosen:

- Voltage sweep (dual sweep);
- Start voltage 0 V;
- Stop voltage 0.6 V;
- Voltage step 0.005 V;
- Current limit 0.005 A;
- Delay 0.1 s.

The Keithley 2450 source meter was used as electronic load to measure the current-voltage curves. Therefore, a dual sweep was applied. Starting at 0 V, the voltage was increased up to 0.6 V and then reduced to 0 V in 0.005 V steps. There was a delay of 0.1 s between each 0.005 V step. For the measurement of PCE, only the sweep back from 0.6 V to 0 V was used, since a smaller number of fluctuations occurred in this sweep. In figure 18 an example what a typical current-voltage curve looked like is given.

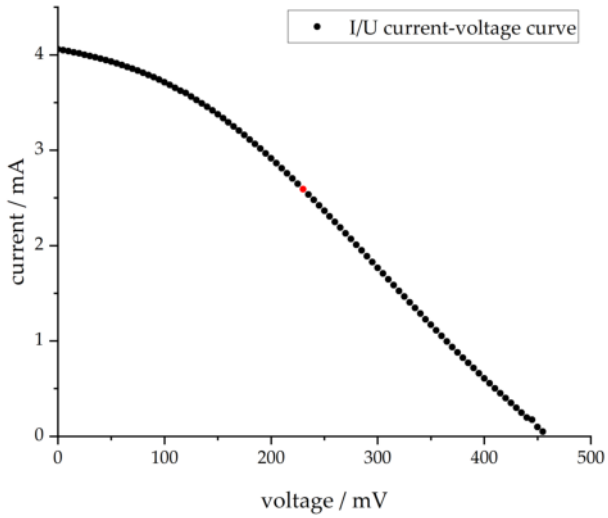

Figure 18: Typical current-voltage curve.

With the measured current and voltage, the power generation of the DSSC could be measured ($P = U \times I$). With the active DSSC area of 0.6 cm^2 and an illumination power of 100 mW/cm^2, the PCE of the DSSC could be calculated. The maximum power point can be seen as red dot in figure 18. After the DSSCs had degraded, they were either remanufactured as described above or rehydrated with liquid electrolyte.

In addition to the current-voltage measurements, the recovered glass substrates were investigated visually with the Axio Observer 7 materials microscope from Carl Zeiss Microscopy GmbH. In figure 19, the Axio Observer 7 materials microscope can be seen.

Figure 19: Axio Observer 7 materials microscope from Carl Zeiss GmbH [124].

To investigate the glass substrate, 1.25x and 10x magnification was used – further technical details of the Axio Observer 7 materials microscope can be found in the Appendix in figures 69 and 70. Three different remanufacturing experiments were performed.

3.3.1 DSSCs with commercially applied TiO_2 layers – four generations

New glass substrate was used for this experiment. They were bought from Man Solar and the front electrodes already had a commercially applied TiO_2 layer. The six samples in this series of experiments got the abbreviation G1.1 to G1.6. After assembling the six DSSCs (G1.1 to G1.6), they were measured with the Keithley 2450 source meter. After their PCEs dropped, they were remanufactured. The new generation of DSSCs got the abbreviation G2.1 to G2.6. This process was repeated till a fourth generation (G4.1 to G4.6) was measured until the PCEs dropped.

3.3.2 DSSCs with manually applied TiO_2 layers – two generations

The glass substrate for the samples in this experiment were recovered from old DSSCs. The twelve samples got the abbreviation T1.1 to T1.12. After the PCEs of the samples dropped, they were rehydrated with electrolyte and measured again until their PCEs dropped below 0.01% – samples called T1.1rehy to T1.12rehy. Then, six samples were rehydrated again (T1.1rehyII to T1.6rehyII). The other six samples were used for remanufacturing a new generation (T2.1 to T2.6). This experiment was performed to measure differences between simple rehydrating and remanufacturing of the cells.

3.3.3 DSSCs from 2015 – remanufactured

In a third experimental setup, 18 DSSCs from 2015 were used. Six DSSCs were rehydrated with electrolyte to investigate if the DSSCs could simply be revived by rehydrating after several years (Reviv1 to Reviv6). The next six DSSCs from 2015 were used for remanufacturing, while, after cleaning, the old TiO_2 layer was kept in place and an additional new layer of TiO_2 was sintered on top of the old layer – sample abbreviation Over1 to Over6.

The last six DSSCs were used for a remanufacturing process and the old TiO_2 layer was washed off before a new layer was applied – sample abbreviation New1–New6. These 18 DSSCs were measured as mentioned above and compared to differentiate between different remanufacturing approaches and potential advantages and drawbacks.

3.3.4 Atomic force microscopy

To investigate the surface of the glass, the atomic force microscope FlexAFM from Nanosurf AG (Liestal, Switzerland) was used – figure 20.

Figure 20: FlexAFM from nanosurf AG [126].

The FlexAFM is a versatile microscope and complex materials can be characterized in combination with a powerful C3000i controller [126]. More technical details can be found in the Appendix in figures 72 and 73.

New, unused glass substrates from Man Solar from 2021 and glass substrates from the remanufacturing experiments from chapter 3.3.1, 3.3.2 and 3.3.3 have been investigated with atomic force microscopy (AFM). From the remanufactured glass substrates each time the DSSCs with the highest and lowest PCE have been chosen for the investigation. The DSSCs were disassembled and the glass substrates were cleaned with desalinated water and ethanol. The TiO_2 layer was partly removed with a rubber glove to investigate the FTO layer beneath it.

The goal was to investigate if the roughness of the glass is influenced by the reman-

ufacturing process and if the PCE of the DSSC and the roughness of the glass surface is connected. In figure 21, the functioning principle of AFM is depicted.

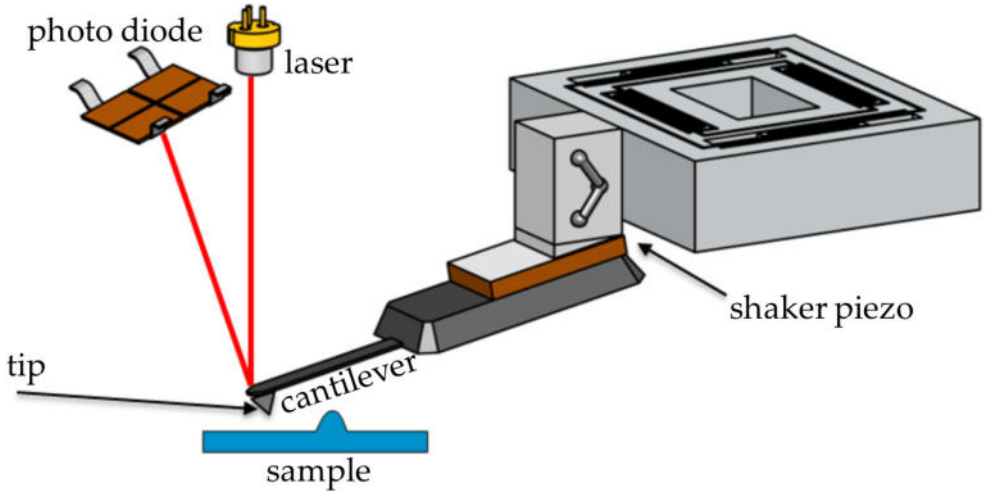

Figure 21: Functioning principle of AFM – adapted from [126].

In AFM, a cantilever with a very sharp tip is used to scan a defined grid on the surface of the sample. A cantilever, Tap190Al-G from Innovative Solutions Bulgaria Ltd. (Sofia, Bulgaria), was used in this experiment [127]. The tip has a radius of 10 nm and the detector side of the cantilever is coated with aluminum for better reflection properties [127]. Further technical details of the cantilever Tap190Al-G can be found in the Appendix in figure 74. In this case, the non-contact mode was used, which means that the tip oscillates over the sample but does not touch it. The advantage of this method is less wear on the sample and the tip. The tip is attached to a flexible cantilever. A shaker piezo element vibrates the cantilever.

As the tip approaches the surface of the sample, the resonant frequency of the cantilever is changed by the van der Waals interaction and the Coulomb force. These forces can be indicated by deformation of the cantilever. To measure the deformation of the cantilever, a laser beam and a photo diode are used. Correspondingly, a topographic image of the surface can be created. The resolving power is determined by the quality of the tip [128]. The Software Nanosurf C3000 Version 3.8.5.10 was used. The following settings were used for the AFM measurements:

- Image size: 6.25 μm;
- Scan rate / time per line: 1.4 s;
- Points per line: 512;
- Setpoint: 55% (The setpoint represents the remaining vibration amplitude when the tip gets close to the surface of the sample. The smaller the setpoint the larger the reduction of the vibration frequency becomes. To avoid tip and sample wear, the set point should be set as high as necessary.);
- Vibration frequency: 167,075 Hz;
- P-Gain: 550 (The P-Gain represents the Z-Controller reaction to the error signal, which is proportional to the error signal.);
- I-Gain: 1000 (The I-Gain represents the Z-Controller reaction, which is proportional to the integral of the error signal.);
- D-Gain: 0 (The D-Gain represents the Z-Controller reaction, which is proportional to the derivative of the error signal.);
- Free vibration amplitude 1.5 V;
- Non-contact mode.

To evaluate the roughness of the substrates, Gwyddion 2.62 was used [129]. To measure the average particle size, the software ImageJ 1.53t was used [130]. To investigate possible connections between DSSC properties and the sample roughness, the fill factor (FF) of the measured DSSC samples was calculated [48].

$FF = P_M/(J_{sc} \times V_{oc})$

The FF equals the power at the maximum power point (P_M) divided by the short circuit current J_{sc} times the open circuit voltage V_{oc}.

Since at first glance no clear correlations between the parameters shown can be identified, a linear correlation calculation was performed with the table data. The "virgin glass" sample was excluded from the calculations. In this approach, successive rows of the table are treated as 7-component vectors and columns as situation-dependent signals.

The linear correlation between any two signals x and y was calculated using the standard formula:

$$r_{xy} = \frac{\overline{x \cdot y} - \overline{x} \cdot \overline{y}}{sd(x) \cdot sd(y)},$$

where sd(x) and sd(y) denote the standard deviation of signal x and y. The variables $\overline{x \cdot y}$, $\overline{x}$ and $\overline{y}$ represent the corresponding mean values.

3.3.5 Potential recovering process for TiO_2

During the remanufacturing process of DSSCs, the TiO_2 layer is usually washed off. The washed off TiO_2 could be recovered. For this purpose, the old DSSCs are disassembled and residual electrolyte and dye were washed off with desalinated water. The TiO_2 layer was then rubbed off carefully while rinsing the surface with desalinated water. The water was captured in a plastic vessel. The desalinated water then evaporated over time and TiO_2 settled at the ground of the vessel.

To evaluate the optical properties of used TiO_2 layers, an old DSSC front electrode was cleaned and analyzed with a UV-Vis spectrophotometer Genesys 10S from Fisher Scientific GmbH (Schwerte, Germany). The UV-Vis is depicted in figure 22.

Figure 22: UV-Vis spectrophotometer Genesys 10S from Fisher Scientific GmbH [125].

The UV-Vis can generate wavelengths between 190-1100 nm and the absorbance and transmittance of materials can be investigated. Further technical details of the Genesys 10S can be found in the Appendix in figure 71. The results were compared to the same TiO_2 layer after a sintering process and a new TiO_2 layer.

3.4 Circular design of DSSCs

This chapter is based on the following publication [89]. For a technology to reach industrial scale, an essential part is a suitable business model and thus the ability for a company to make a profit with the technology. That is why in this chapter the Circo method is explained. The Circo method is a tool and a scientific framework developed at the University of Delft by C. Bakker et al [131]. This framework usually is used by companies to make a product service shift – transforming from simply selling products to service oriented business models [132].

The following steps are part of the Circo method – adapted from [89]:

1. Identify challenges and opportunities along the value chain.
2. Investigate design and business model changes.
3. Elaborate a circular business model and determine required changes.
4. Structure the required actions and plan their implementation.

3.4.1 Identify challenges and opportunities along the value chain

During the first step of the Circo method, value losses along the supply chain and the life-cycle of the product are identified. In figure 23 a picture of the value pyramid to illustrate which processes add value to a product and which lead to value losses is shown.

Value is added to the product during the cradle-to-consumer phase. Resources are extracted, parts are manufactured, products are assembled and marketing increases the value of a product.

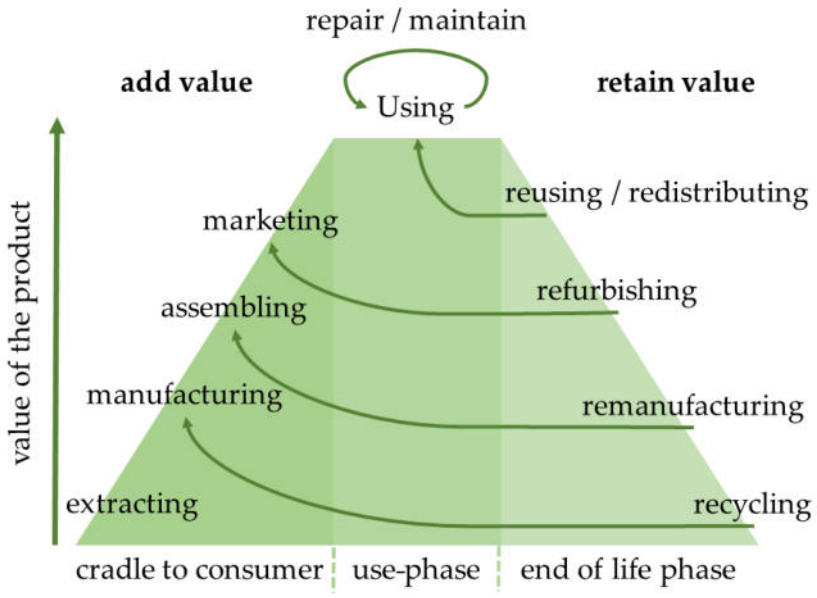

Figure 23: Value pyramid [89].

During the cradle-to-consumer phase the value is continually increased – figure 23. However, value losses due to transportation or storage can appear in this phase too. During the use-phase the product might get damaged or malfunctions appear, representing possible value losses. After the use-phase, the value of the product usually decreases. To retain value the processes known from the circular economy: repair, reuse, refurbish, remanufacture and recycle can be applied. In figure 24 the life-cycle of a product and several investigation steps is shown. In the center, all key actors are mentioned. From raw material manufacturer to the user and a potential recycling company. In a second layer, the transactions in the system are displayed. Usually, materials and products flow from left to right through the system and money transactions flow from right to left. On the third layer, value losses and opportunities are given. First, the value losses are identified and opportunities can usually be derived from them. From the last given value loss in figure 24 “Downcycling”, for instance, the opportunity of upcycling or remanufacturing the product could be derived. This way, a higher value could be retained.

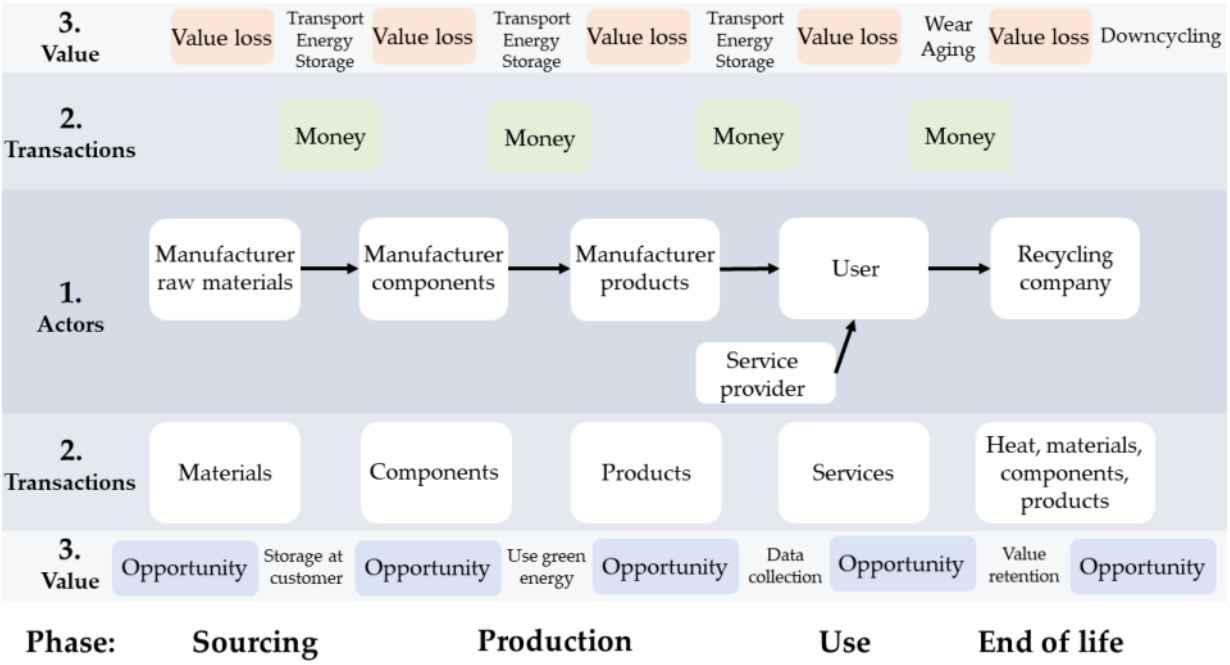

Figure 24: Identify challenges and opportunities along the value chain [89].

3.4.2 Investigate design and business model changes

Possible design and business model changes are described by Bakker and den Hollander in the book "Products that last" [131]. The five described business models are:

1. Classic long-life: A company sells a high-quality product, often a high-priced product. A service, such as repair or maintenance, may be attached to the product.
2. Hybrid model: This involves a combination of a durable product, such as a printer or coffee machine, and a consumable item, such as printer cartridges or coffee pads. This model generates continuous revenue through the regular sale of consumables.
3. Gap exploiter: This model has three forms. The first is the regular repair service – a bike repair shop, for instance. The second form is the secondhand market – ebay for example. The third form is the recovering of resources or product parts and selling them.
4. Access model: A consumer gets access to a product or service. A classic example is car sharing, were the customer pays for using the car.

5. Performance model: This model is optimal from a circular-economy perspective. The company and the customer agree on a specific goal – clean laundry or a warm apartment, for instance. How the company delivers the service or achieves the goal is up to the company.

Theses business models can be of help when looking for adaptions or complete transformation of the company's strategy. The following are possible modifications to a product that would allow for a more circular design [131]:

1. Design for product attachment and trust: This principle is aiming for creating an emotional connection between customer and product. This way, the consumer wants to use the product longer and does not discard it easily. Possible examples are self-designed shoes, inherited items or a photo.
2. Design for durability: The products are designed in a way which ensures that they have a long lifetime. Most often, high-quality material and components are used and tested. Examples are taxis, some washing machines or quality craftsmen tools.
3. Design for standardization and compatibility: Products and parts are designed in a way that they are compatible with other products. Charging cables of smartphones, for instance, are standardized.
4. Design for ease of maintenance and repair: The product is designed in a way which ensures it can be repaired easily. Only a few tools are required to change modules or parts.
5. Design for upgradability and adaptability: This design principle is required when customer demands are changing or technology advances can be expected. The product can be improved over time, software products are usually upgradable.
6. Design for disassembly and reassembly: For remanufacturing or repair, this design principle delivers advantages, because the product can be taken apart easily and parts can be reused or exchanged.

In a creative process, the identified opportunities in the life-cycle of the product are combined with business models and design strategies to create possible combinations of

value. The economic and environmental benefits or disadvantages of the business model should be evaluated. Since this is only a fictitious case to show the framework and possible business models, the experimental results for the economic and ecological values are only qualitative assessments. The created business models are assessed and the most promising one is chosen for further investigation.

3.4.3 Elaborate a circular business model and determine required changes

One business model is developed in further detail. Core questions such as income streams, customer interaction and all actors in the value chain have to be clarified. The consequences for the company have to be pointed out on three different levels [89]:

1. Core: The core elements are product design and the service. These elements can be adapted or changed directly by the company.
2. Internal: In this category, more external influences intervene. Examples in this category are logistics, marketing, purchasing and finances.
3. External: These elements are not within the control of the company and are therefore difficult to influence. Examples are new knowledge, politics or the supply chain.

At this point, all information is gathered, summarized and evaluated. A business model canvas for the case is created to clarify all facets of the business model.

3.4.4 Structure the required actions and plan their implementation

The changes that have to be made for the transformation to the new business model and design principles have to be visualized in a road map.

The road map has two dimensions, time on the x-axis and significance on the y-axis. The road map is a tool for pitching the ideas in front of colleagues or the chief executive officer of the company. As well as the evaluation in chapter 3.4.3 this part of the Circo framework is not applied in detail because only a fictitious case is investigated.

4 Experimental results

This chapter shows the results of the described experiments in the previous chapter. First, chapter 4.1, the bibliographic analysis with the VOSviewer tool is shown – including a term map and lists of most frequently appearing terms. The results of the melting experiment includes the SEM-EDX graphs, a list of the composition of the glass substrates (ICP-OES), the melting process and the evaluation of the resulting melts A to D – chapter 4.2. In chapter 4.3, the results of the remanufacturing, AFM investigation and TiO_2-recovery experiments are shown. Finally, in chapter 4.4, the results of the Circo method are displayed.

4.1 State-of-the-art recycling methods in the context of DSSCs – bibliographic analysis

This chapter is based on the authors own publication from 2021 [18]. The investigation was repeated to visualize the state of the art and to be able to show changes over time.

The Web of Science was searched for the term "dye sensitized solar cell" – 27,014 search results were found on the 6^{th} December 2022. In comparison the same search request delivered 24,441 results on the 15^{th} March 2021 [18]. That shows that 2,573 publications concerning DSSCs have been added in the Web of Science in a time window of around one year and 9 months. When the search results are filtered by publication year, there are 1,315 publications in 2021 and 1,025 in 2022 for the search "dye sensitized solar cell". The titles and abstracts of these 27,014 publications were downloaded from the Web of Science. In figure 25 the resulting term map can be seen.

The size of the words and circles in the map, figure 25, is an indicator for the number of appearances – the bigger the word, the higher the number of appearance of the specific word. The location of each word on the term map depends on the co-occurrences of the terms. The words that co-occurred are located closer to each other.

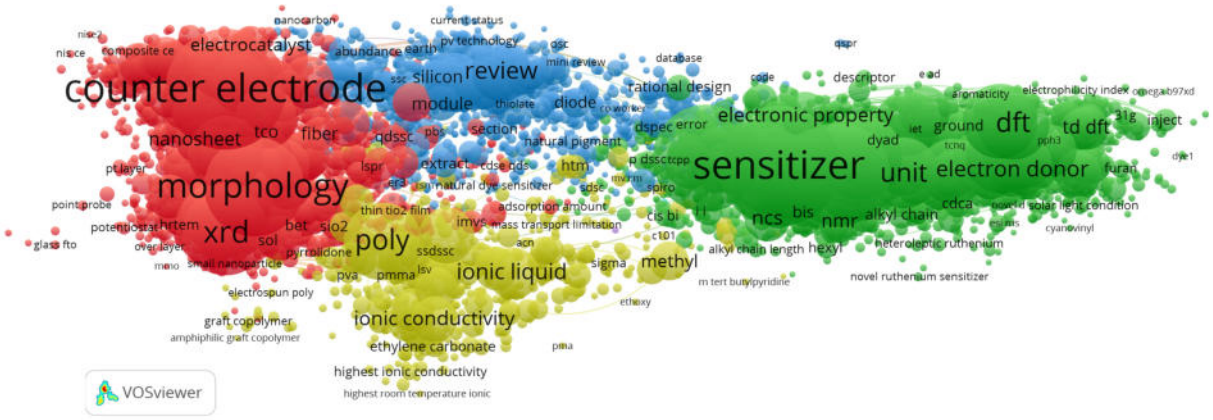

Figure 25: Term map of dye-sensitized solar cell publications from the Web of Science 6th December 2022.

On the right part, green circles can be seen, which show terms connected with the dye and sensitizers of DSSCs. The red area on the left side has a focus on the "counter electrode". The yellow area on the bottom shows terms connected to "solid state DSSCs" and the "electrolyte". The blue area shows a more general topic, terms like "review" or "photovoltaic technology" are given. In this blue field, the terms concerning "sustainability", "life-cycle assessment", "natural pigments" or "abundance" appear as well. Table 2 shows the terms which appear most often during the two investigations.

Table 2: Important words and their number of appearances.

	6^{th} December 2022		15^{th} March 2021	
Position	Term	Number of appearances	Term	Number of appearances
1	counter electrode	3048	sensitizer	2810
2	sensitizer	3043	counter electrode	2769
3	molecule	2389	molecule	2086
4	group	2273	group	2263
5	morphology	2087	morphology	1899
6	xrd (x ray diffraction)	1574	organic dye	1396
7	series	1527	series	1357
8	organic dye	1517	substrate	1474
9	complex	1513	xrd (x ray diffraction)	1316

It can be seen that the term “counter electrode” appears more frequently and moves to the top of the table – the term “sensitizer” has moved down one position. The term “x ray diffraction” rose from ninth to sixth place. The term “organic dye” dropped from the sixth to the eighth position. The term “substrate” cannot be found on its own in the new investigation, but in connection with other words, resulting in terms like “glass substrate” or “flexible substrate”. For the term “complex”, 1297 occurrences were registered in 2021.

In figure 26 the same terms as in figure 25 are shown, but the circles are colored from blue to yellow, while blue indicates that the paper is older and yellow indicates more recent papers or developments. Terms like “ionic conductivity” or “methyl” are blue, which indicates that the average publication date or all publications in which this term appeared are, on average, from 2013. Terms such as “rational design” or “composite” appear in yellow, which indicates a recent average publication date – in this case 2017. In figure 27,

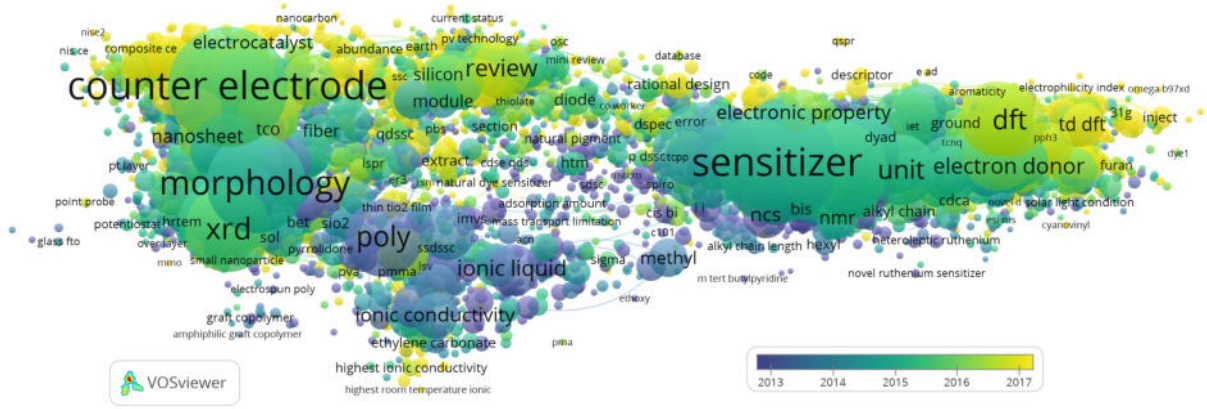

Figure 26: Important words and their graphical representation related to the number of appearances.

an enlarged section of figure 26, in the area of the term “review”, can be seen. Terms like “life-cycle assessment”, “lca” and “sustainability” have a yellow color. Which indicates that these terms appeared in recent studies. The term “life-cycle assessment” appeared 12 times in 2021 and 15 times in 2022. The term “lca”, which stands for life-cycle assessment, did not reach the 10 occurrences count in 2021 (in 2022, 11 times). The term “sustainability” appeared 35 times in 2021 and occurs 49 times in 2022. The term “sustainable” does not occur alone, but in combinations with other words such as “sustainable material” (10

times), “sustainable energy” (16 times) and “sustainable development” (19 times).

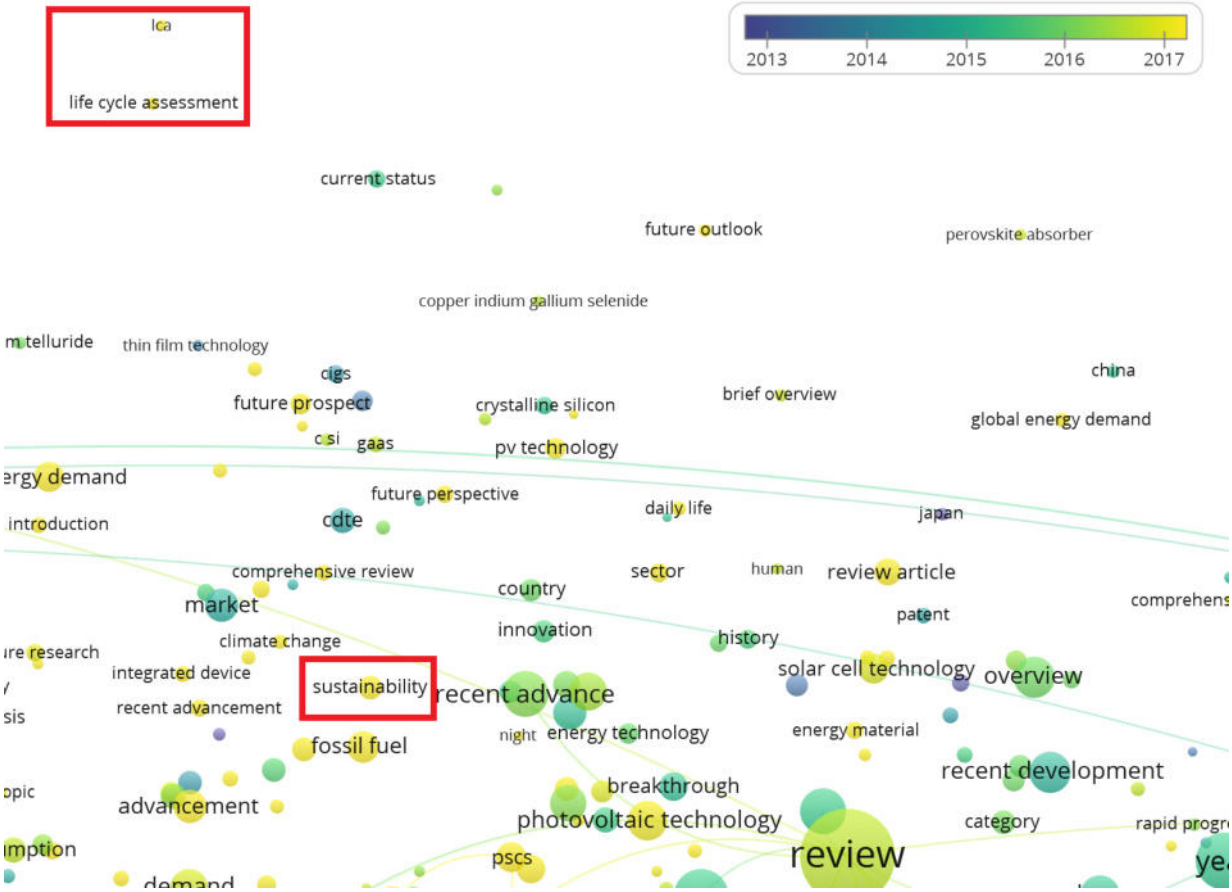

Figure 27: Zoom of the term map showing sustainability terms.

4.2 Recycling of DSSCs – melting experiment

This chapter shows the results of the SEM-EDX and ICP-OES analysis of DSSC glass substrates from 2018 and 2020 bought from Man Solar. Furthermore, the results of the melting experiment are given in chapter 4.2.3.

4.2.1 SEM-EDX

As described in chapter 3.2.1 the SEM-EDX investigation was performed according to ISO 22309:2011. The entire DSSC electrodes, front and counter electrode, were etched and

always both sides were investigated with SEM-EDX before and after the process. In figure 28 the SEM-EDX results of the front electrode from 2018 before etching are shown.

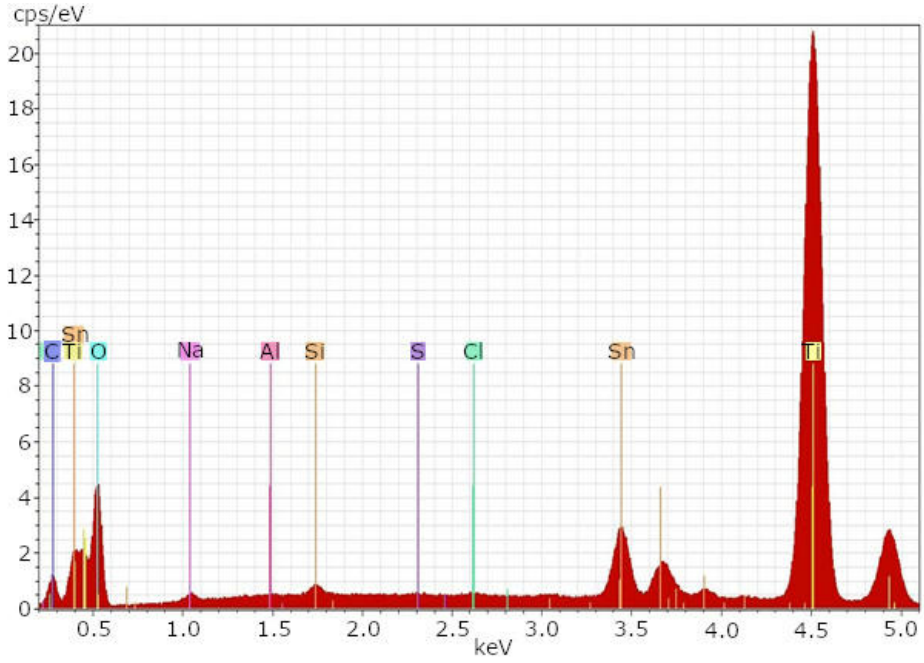

Figure 28: Result of SEM-EDX investigation of a DSSC front electrode from 2018 – before etching [24].

On the x-axis of figure 28, the energy of the detected radiation is given in keV. The y-axis shows the counts per second (cps) divided by the energy (in this case given in electron volts) – which indicates the number of photons detected per second. The two peaks on the right side, Ti (titanium) and Sn (tin), indicating the TiO_2 layer and the FTO layer on the surface of the front electrode. High concentrations of these two elements have been detected. The elements to the left of Sn are typical glass elements such as: Si (silicon), Al (aluminum), Na (sodium), O (oxygen), Sn (tin), Ti and C (carbon). Those glass elements are shown in lower concentrations.

In figure 29 the SEM-EDX result of a DSSC front electrode after the etching process with concentrated sulfuric acid and concentrated hydrofluoric acid in a 1:1 ratio for 10 minutes are shown. The titanium peak is considerably lower after the described etching process. The tin layer can still be detected and shows higher concentrations than before

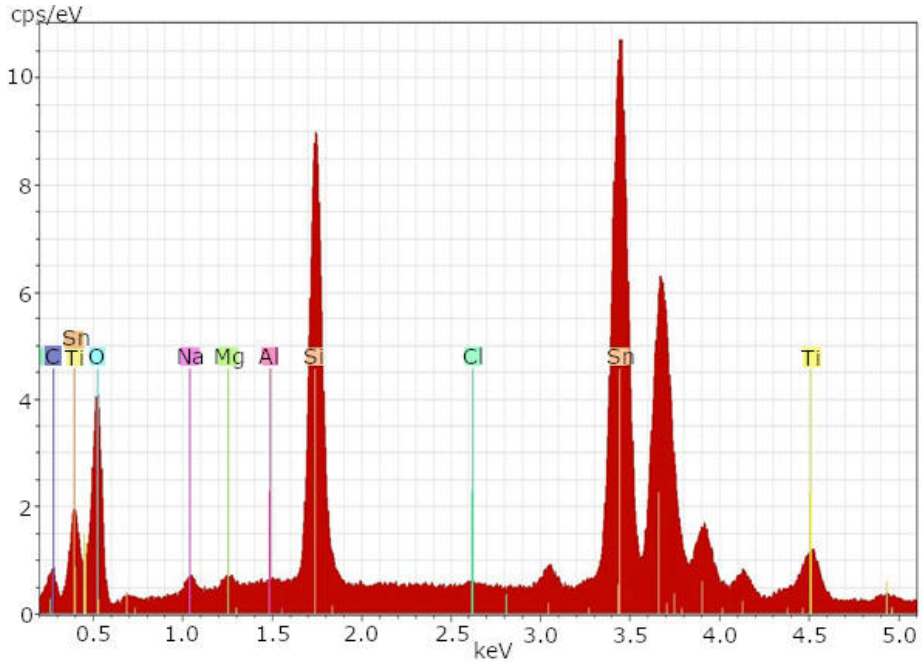

Figure 29: Result of SEM-EDX investigation of a DSSC front electrode from 2018 – after etching [24].

the etching process. The typical glass elements can be detected and show higher concentrations compared to figure 28. In figure 30, the result of the SEM-EDX investigation of a DSSC counter electrode from 2020 before the etching process is shown. The Ti peak is very low. Typically the counter electrode has no TiO_2 layer. The tin peak has a high concentration and indicates the FTO layer. Typical glass elements can be detected. In figure 31, the SEM-EDX result of the same counter electrode from 2020 after the etching process with concentrated sulfuric acid and concentrated hydrofluoric acid in a 1:1 ratio for 10 minutes and additionally etched with concentrated hydrofluoric acid for one minute can be seen. After the first etching process, the sample showed no differences to figure 30. That is why the additional etching process with concentrated hydrofluoric acid for one minute was performed. After the two etching processes, the results are still similar. High concentrations of tin and typical glass elements were detected for the counter electrode before and after etching.

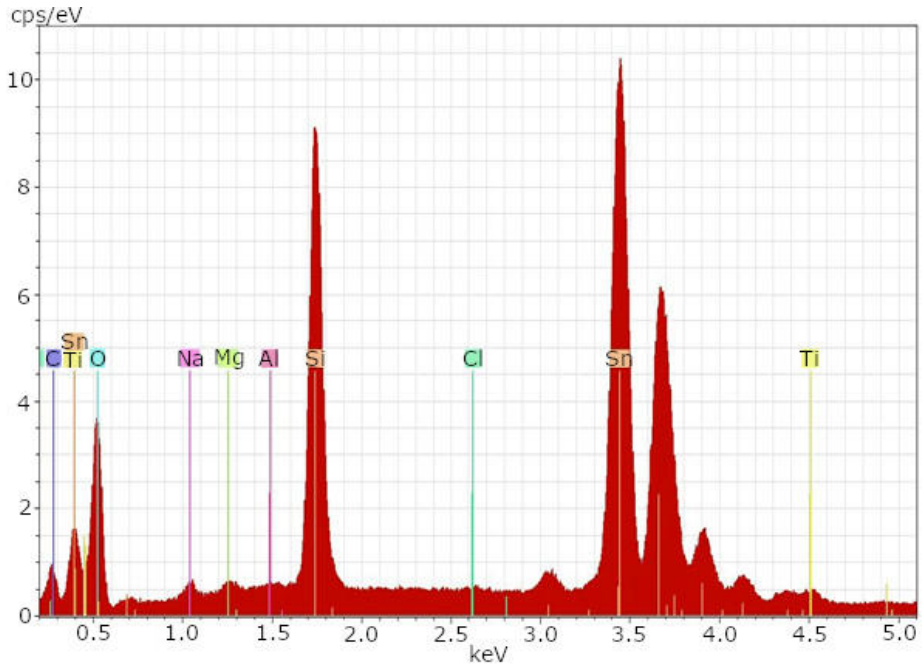

Figure 30: Result of SEM-EDX investigation of a DSSC counter electrode from 2020 – before etching [24].

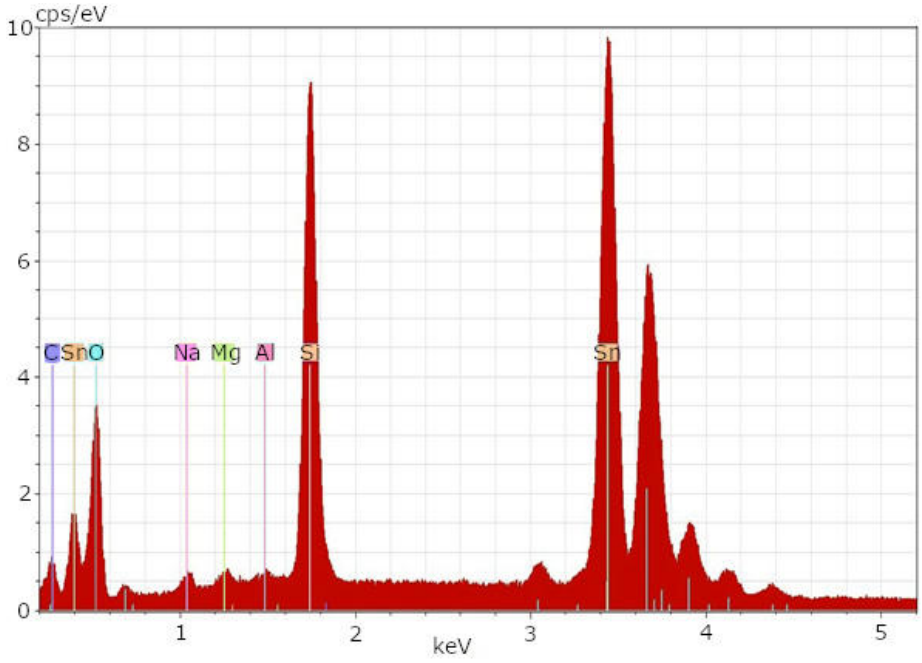

Figure 31: Result of SEM-EDX investigation of a DSSC counter electrode from 2020 – after etching [24].

In figure 32 the backside of DSSC front electrode from 2018 is shown. No differences before and after the etching process were identified.

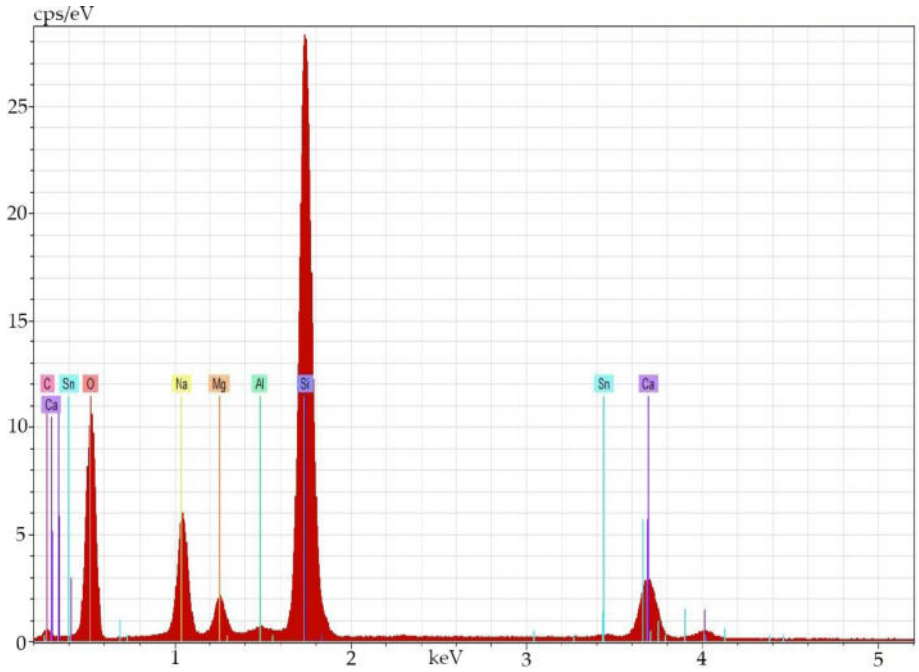

Figure 32: Result of SEM-EDX investigation of a the backside of DSSC front electrode from 2018 – before and after etching [24].

In figure 33 the backside of DSSC counter electrode from 2020 is shown. No differences before and after the etching process were identified.

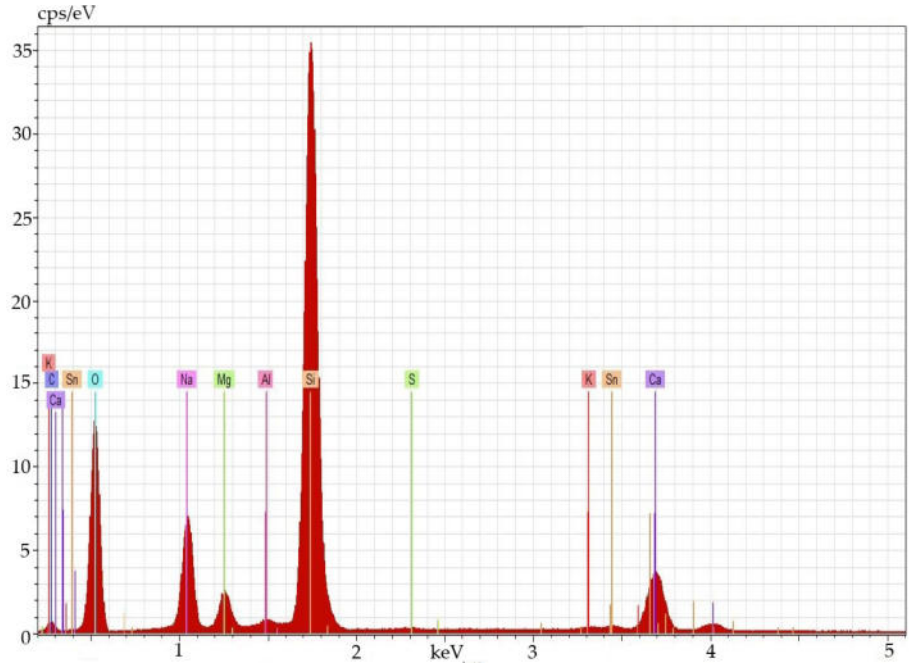

Figure 33: Result of SEM-EDX investigation of a the backside of DSSC counter electrode from 2020 – before and after etching [24].

4.2.2 ICP-OES

Table 3 shows the result of the ICP-OES investigation adapted from [24]. The left column shows the detected elements. Columns two and three show the results of the ICP-OES analysis for the investigated glasses from 2018 and 2020. The fourth column shows the elements of a patented glass mixture for photovoltaic applications from Schott AG [133]. For Al_2O_3, the patent glass emphasizes considerably higher values in comparison to the DSSC glass substrates from Man Solar.

Table 3: Results of the ICP-OES investigation adapted from [24] in weight percentage.

Element	DSSC glass from 2018 (wt%)	DSSC glass from 2020 (wt%)	Patent glass (wt%) [133]
Al_2O_3	0.540	0.070	4.7-19
Fe_2O_3	0.009	0.100	0-0.5
CaO	8.950	8.880	0-5
MgO	4.260	3.960	0-6
SrO	0.005	0.006	0-7
Na_2O	13.800	13.640	10-18
K_2O	0.050	0.040	0-8
Li_2O	0.003	0.002	0-4
BaO	0.001	0.001	0-10
PbO	0.000	0.000	-
TiO_2	0.005	0.010	0-6
Cr_2O_3	0.000	0.001	-
Mn_2O_3	0.001	0.006	-
NiO	0.001	0.000	-
SnO_2	0.013	0.024	-
ZnO	0.002	0.003	0-0.3
ZrO_2	0.000	0.010	0-0.5
SO_3	0.220	0.218	-
SiO_2	72.140	73.030	49-69

The glass substrates from 2018 have higher Al_2O_3 values compared to glass substrates from 2020. However, both DSSC glass substrates have higher CaO values than emphasized in the patent. The Fe_2O_3 concentration in the glass substrates from 2020 is higher than in the glass substrates from 2018. However, the Fe_2O_3 values from both glass substrates are in the emphasized range of the patent. Most of the other values are within the range of the patent values.

4.2.3 Melting experiment

In figure 34 melt A to D after 5, 20 and 50 minutes in the furnace are shown – adapted from [24].

Melts A and B were in the center of the oven and the material is already melted after 5 minutes.

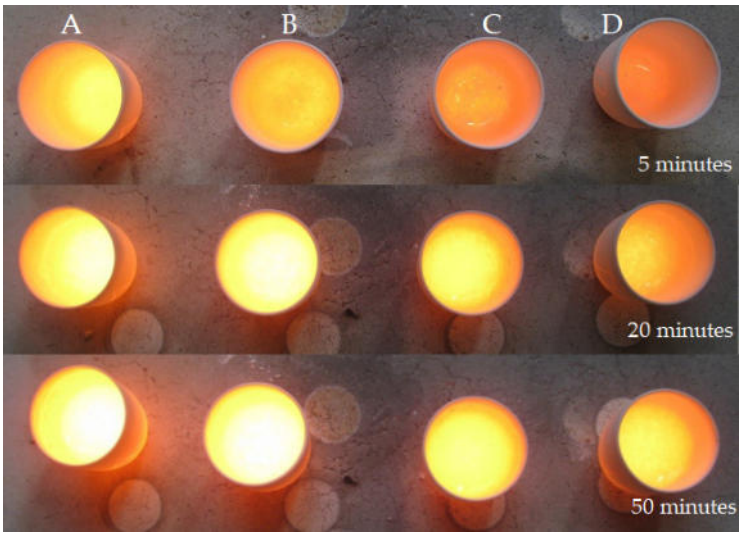

Figure 34: Melts A to D after 5, 20 and 50 minutes in the furnace [24].

However, seeds (air inclusions < 1 mm) and bubbles (air inclusions > 1 mm) can be seen. Melts C and D were closer to the door of the furnace and thus were inserted last and pulled out first. Melt C and D show more unmelted material after 5 minutes and larger bubbles. After a melting time of 20 minutes, seeds and unmelted material could still be identified. Melt A had the most seeds and melt D the most unmelted material after 20 minutes in the furnace. No unmelted components could be detected after the melts had been in the furnace for 50 minutes. Melt A and B had bigger bubbles compared to melt C and D. In figure 35 melts A to D are displayed after the melts had been cooled down slowly to room temperature. Pinkish streaks can be seen at the bottom of all four melts. The melts show slight differences in color. Melt C was marginally greenish and melt D was marginally pinkish. Melt B was clear and no coloration could be identified. The reference sample melt A, was marginally bluish. In figure 36 melts A to D are shown under the microscope. No ceramic or metal pieces can be seen. No huge visual differences between the melts can be detected. Most streaks and seeds could be found in melt C. Melt D had fewer streaks than melt C, but the seeds in melt D were slightly bigger compared to melt C. The seeds in melt A were marginally larger compared to melt D. In melt B, the fewest streaks but the most seeds could be found.

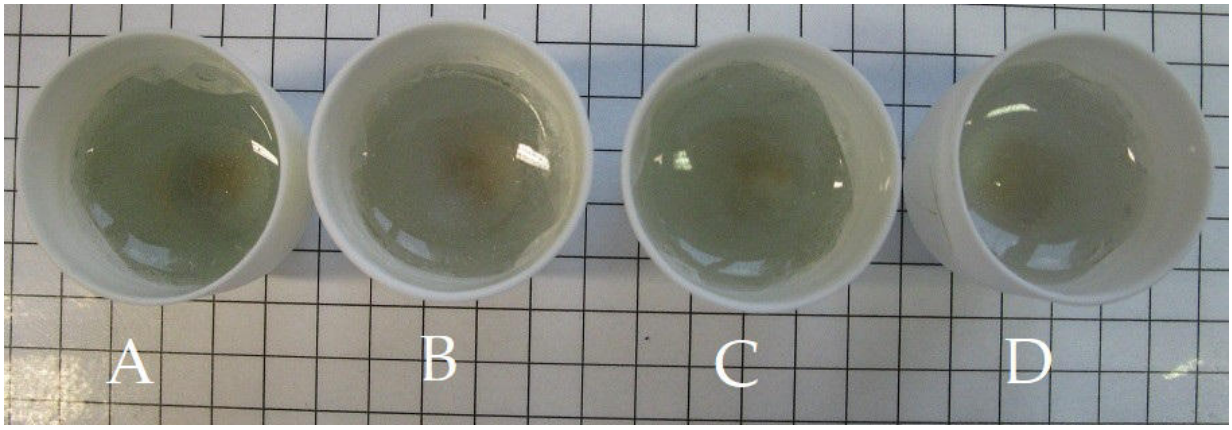

Figure 35: Melts after the melting process at room temperature [24].

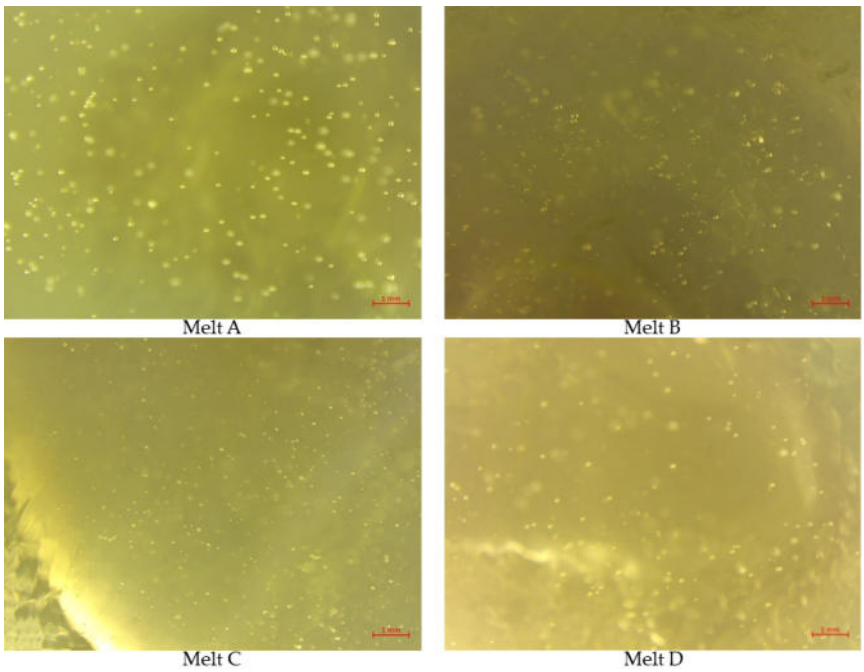

Figure 36: Melting experiment results – melts A to D under the microscope 10 times magnified (adapted from [24]).

4.3 Remanufacturing of DSSCs

This chapter shows the results of all remanufacturing experiments as well as the recovering possibilities for TiO_2 and the quality investigation with the UV-VIS. The results have been published in [25].

4.3.1 DSSCs with commercially applied TiO_2 layers – four generations

In figure 37 the average PCE of the different DSSC generations with commercially applied TiO_2 layers over time are shown.

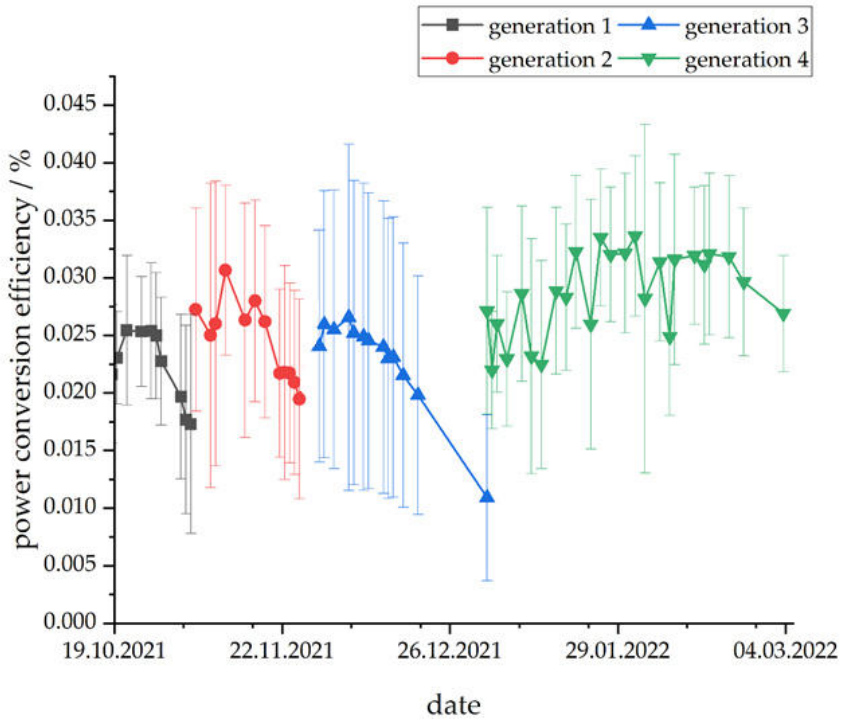

Figure 37: Average PCE of DSSCs with commercially applied TiO_2 – four generations [25].

When the color of the graph changes, this indicates that a new generation of DSSCs was remanufactured. After the remanufacturing processes, the PCE is similar or even higher than the PCE of the first generation. Furthermore, the PCEs stay on a higher level for a longer time period. In figure 38, the average short circuit current (J_{sc}) and circuit voltage (V_{oc}) are shown over time.

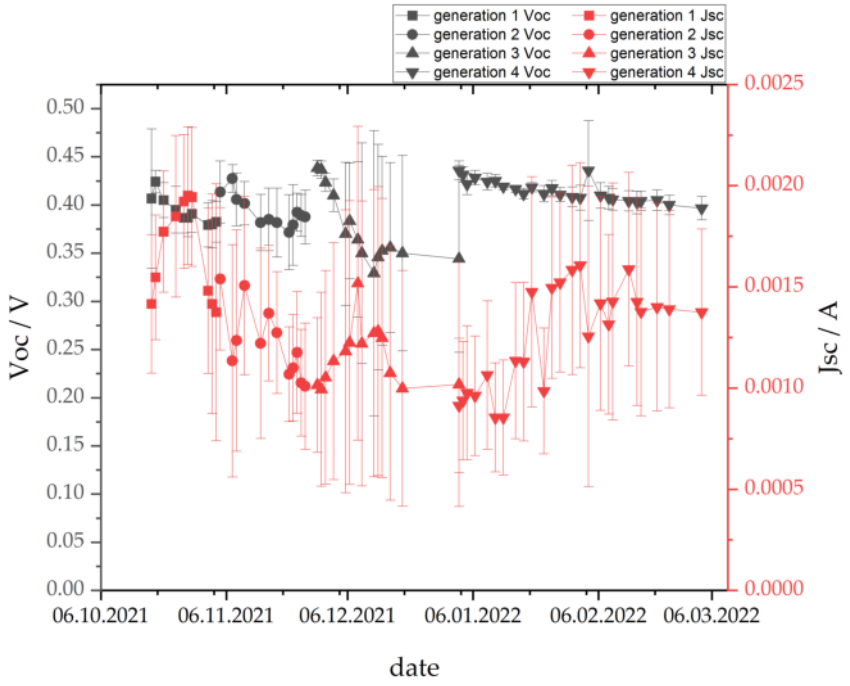

Figure 38: Average J_{sc} and V_{oc} of DSSCs with commercially applied TiO_2 – four generations [25].

It can be observed that after the remanufacturing procedures the values for J_{sc} and V_{oc} are rising. The standard deviation of J_{sc} is fluctuating more compared to the standard deviation of V_{oc}. That behavior relates to the bigger fluctuations in the fourth generation of DSSCs in figure 37.

In figure 39 the damaged glass substrate under the microscope is shown. The damage was dealt to the glass by connecting it with the alligator clips several times. The damage got worse with each generation due to a growing amount of measurements, which included connecting and disconnecting the DSSCs.

4.3.2 DSSCs with manually applied TiO_2 layers – two generations

In figure 40 the result of the PCE measurement of 12 DSSCs with manually applied TiO_2 layers is shown. After the 6^{th} December, 2021, all 12 DSSCs have been rehydrated with electrolyte. The PCE went up almost as high as at the beginning of the first remanufacturing process.

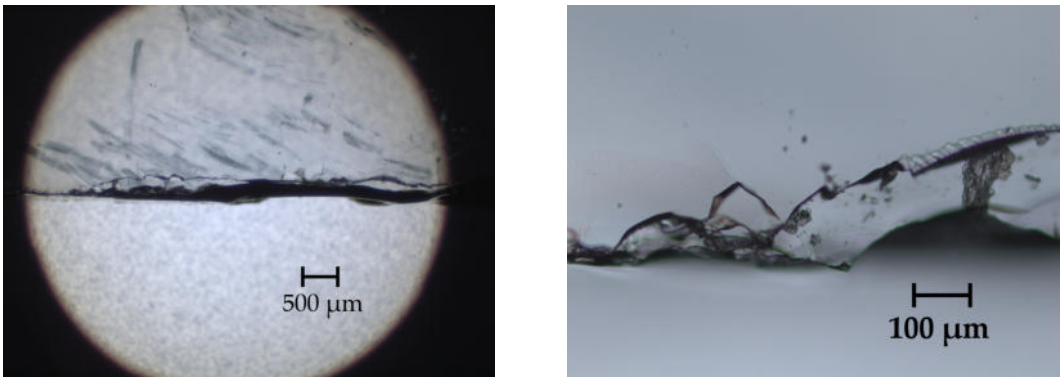

(a) (b)

Figure 39: Damaged glass substrate: (a) 1.25 times magnified; (b) 10 times magnified [25].

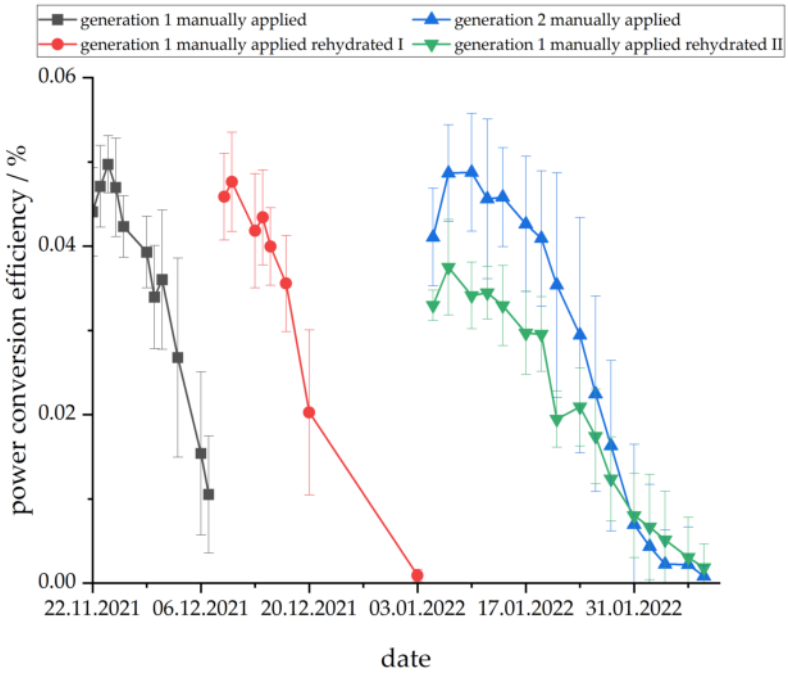

Figure 40: Average PCE of DSSCs with manually applied TiO_2 – two generations [25].

After the 3^{rd} January 2022 six DSSCs have been rehydrated and the other six DSSCs have been remanufactured. It can be seen that the remanufactured DSSCs reach higher PCEs compared to the rehydrated DSSCs.

In figure 41 the J_{sc} and V_{oc} of the 12 DSSCs are shown. The J_{sc} of the second generation

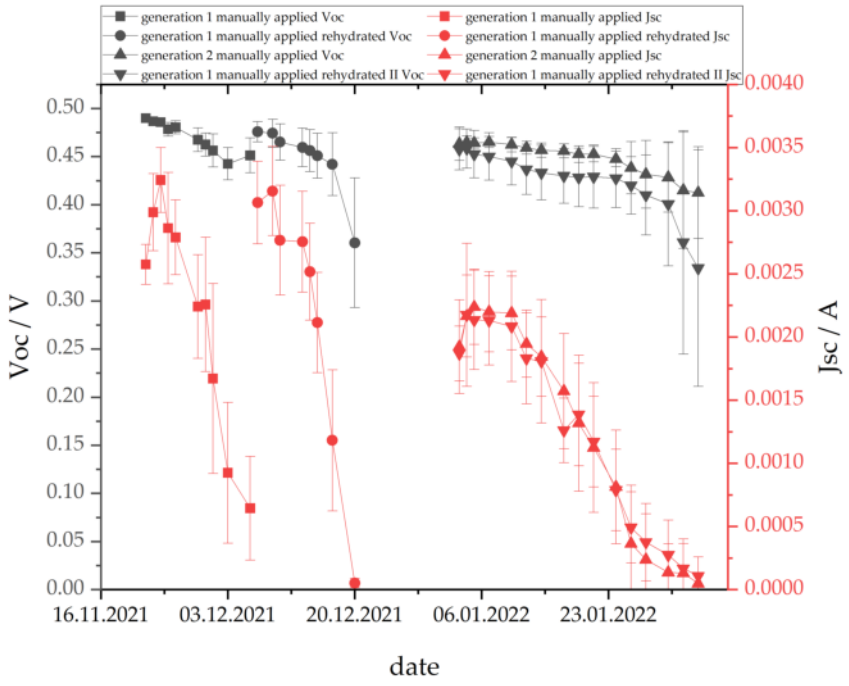

Figure 41: Average J_{sc} and V_{oc} of DSSCs with manually applied TiO_2 – two generations [25].

of DSSCs and the DSSCs that have been refilled with electrolyte twice is considerable lower compared to the first generation. The V_{oc} of the second generation equals the average V_{oc} of the first generation. The V_{oc} of the twice rehydrated samples is lower than that of the second generation.

4.3.3 DSSCs from 2015 – remanufactured

In figure 42 the result of rehydrating and remanufacturing DSSCs from 2015 is shown. The DSSCs from 2015 cannot be revived by rehydrating them with electrolyte – only in one out of six DSSCs a PCE can be measured (0.002%).

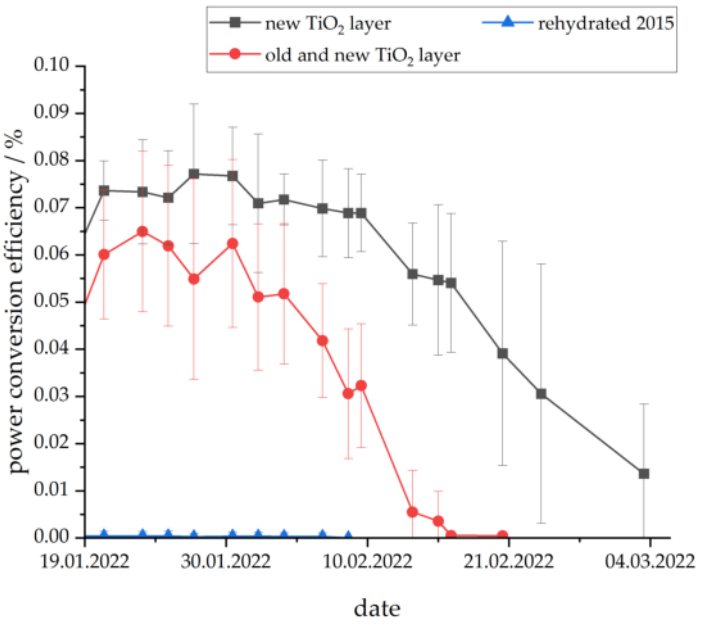

Figure 42: Average PCE of DSSCs from 2015 with manually applied TiO_2 – in gray: DSSCs with a new TiO_2 layer, in red: DSSCs with an additional TiO_2 layer above the old one and in blue: DSSCs that were rehydrated with electrolyte [25].

The blue line shows the average PCE of the rehydrated DSSCs. The typical lilac color of the DSSCs with fruit tea dye faded away, the DSSCs had a whitish color. The red line shows the average PCE of six DSSCs which have been opened and carefully cleaned, ensuring that the TiO_2 layer was kept unharmed. After that, an additional TiO_2 layer was applied and new DSSCs were manufactured from them. The gray line shows the average PCE of six DSSCs from 2015 that have been remanufactured similarly, only the old TiO_2 layer was washed off during the cleaning process. The DSSCs which have been cleaned off the old TiO_2 layer achieve the highest PCEs and have a higher stability compared to the DSSCs with an old TiO_2. The standard deviations of the average PCEs are high and overlap in the first 17 days.

In figure 43 the J_{sc} and V_{oc} of the 18 DSSCs from 2015 are shown. The V_{oc} of the remanufactured DSSCs is similar and decreases slightly over the observed time.

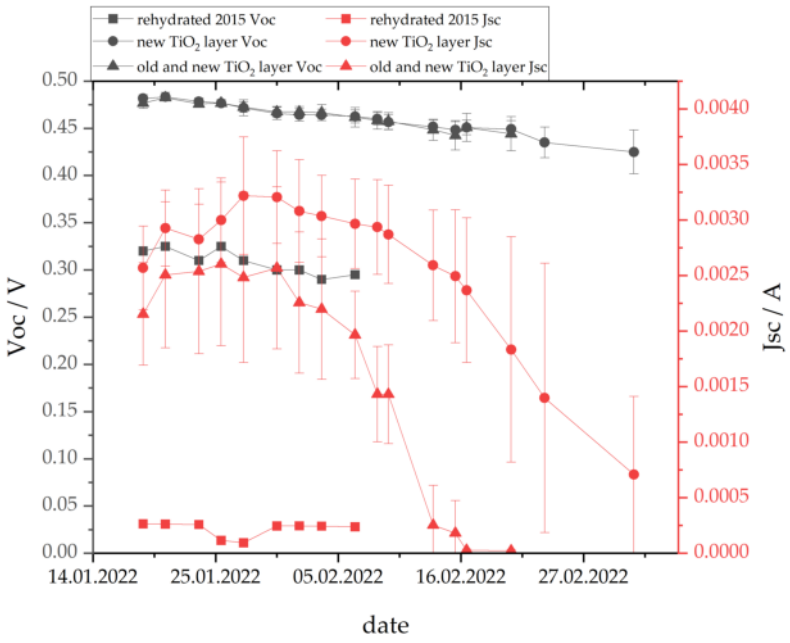

Figure 43: Average J_{sc} and V_{oc} of 18 DSSCs with manually applied TiO_2 – squares indicate J_{sc} and V_{oc} from the rehydrated DSSCs, dots show the J_{sc} and V_{oc} of DSSCs with a new TiO_2 layer and triangles show J_{sc} and V_{oc} of DSSCs with an additional TiO_2 layer [25].

The average J_{sc} of the DSSCs with a new TiO_2 layer is higher compared to the DSSCs with an additional TiO_2 layer. The standard deviation grows over time. The J_{sc} of the DSSCs with an additional TiO_2 decreases faster and reaches zero before the end of the experiment.

4.3.4 Atomic force microscopy

In table 4, the investigated sample names, electrical properties and root mean square roughness (R_q) of the substrates, on which the cells were fabricated, can be seen. The table shows selected samples, their designations and, among other things, information about sample generations.

"T1.1rehyII" has a large FTO roughness and a low FF, but "G4.3", with the highest FF, does not have a particularly low FTO roughness. The TiO_2 roughness of "T1.1rehyII" and "New1" is similar. The two DSSCs, however, are electrically similar only in terms of V_{oc}.

Table 4: Electrical properties of DSSC samples and root mean square roughness investigated with the AFM. Designations: J_{sc} – short-circuit current, V_{oc} – open-circuit voltage, PCE – power conversion efficiency, FF – fill factor (the ratio of the maximum power obtained from the cell to the product of the short-circuit current and open-circuit voltage, R_q FTO – root mean square roughness of the FTO substrate, R_q TiO_2 – root mean square roughness of the TiO_2 layer, R_q C - root mean square roughness of the graphite catalyst layer.

Sample name	J_{sc} (mA)	V_{oc} (mV)	PCE (%)	FF (%)	R_q FTO (nm)	R_q TiO_2 (nm)	R_q C (nm)
G4.2	2.26	400	0.05	29.79	6.48	10.59	4.37
G4.3	1.00	415	0.03	38.51	6.63	10.26	2.23
T2.5	3.64	490	0.06	19.69	7.09	16.01	1.62
T1.1rehyII	3.06	450	0.04	17.95	10.10	18.28	3.04
New1	4.06	455	0.10	32.28	6.75	17.26	6.67
Over3	3.31	480	0.05	18.41	6.55	9.43	4.69
Virgin glass	–	–	–	–	7.54	12.02	–

The R_q of the TiO_2 of "G4.2", "G4.3", and "Over3" are similar, but the V_{oc}, FF and J_{sc} values differ significantly. The graphite shows the greatest differences in roughness, but again no correlation between R_q and electrical properties of DSSCs can be seen. The manually applied TiO_2 layers have a higher R_q compared to the commercially applied TiO_2 layers. The sample "Over3" is an exception. After applying a second TiO_2 layer above the old one, the roughness is the lowest of all measured samples. The control sample "Virgin glass", with commercially applied TiO_2 layer, has a higher R_q value compared to the other samples with commercially applied TiO_2 layers. To evaluate the differences in roughness of one sample, the sample "New1" was measured at two more positions and the R_q was evaluated – with following results: $R_{q1} = 17.26\ nm$, $R_{q2} = 18.96\ nm$ and $R_{q3} = 14.65\ nm$.

To visually evaluate any correlations, different graphs are derived from table 4 and are depicted in figure 44. Generally, the graphite layer has the lowest R_q values (1.62 nm up to 6.67 nm). The FTO layer has higher R_q values (6.48 nm up to 10.10 nm) than the graphite layer but lower values than the TiO_2 layer (9.43 nm up to 18.28 nm). No correlation between R_q and the electrical properties of the DSSCs is visible.

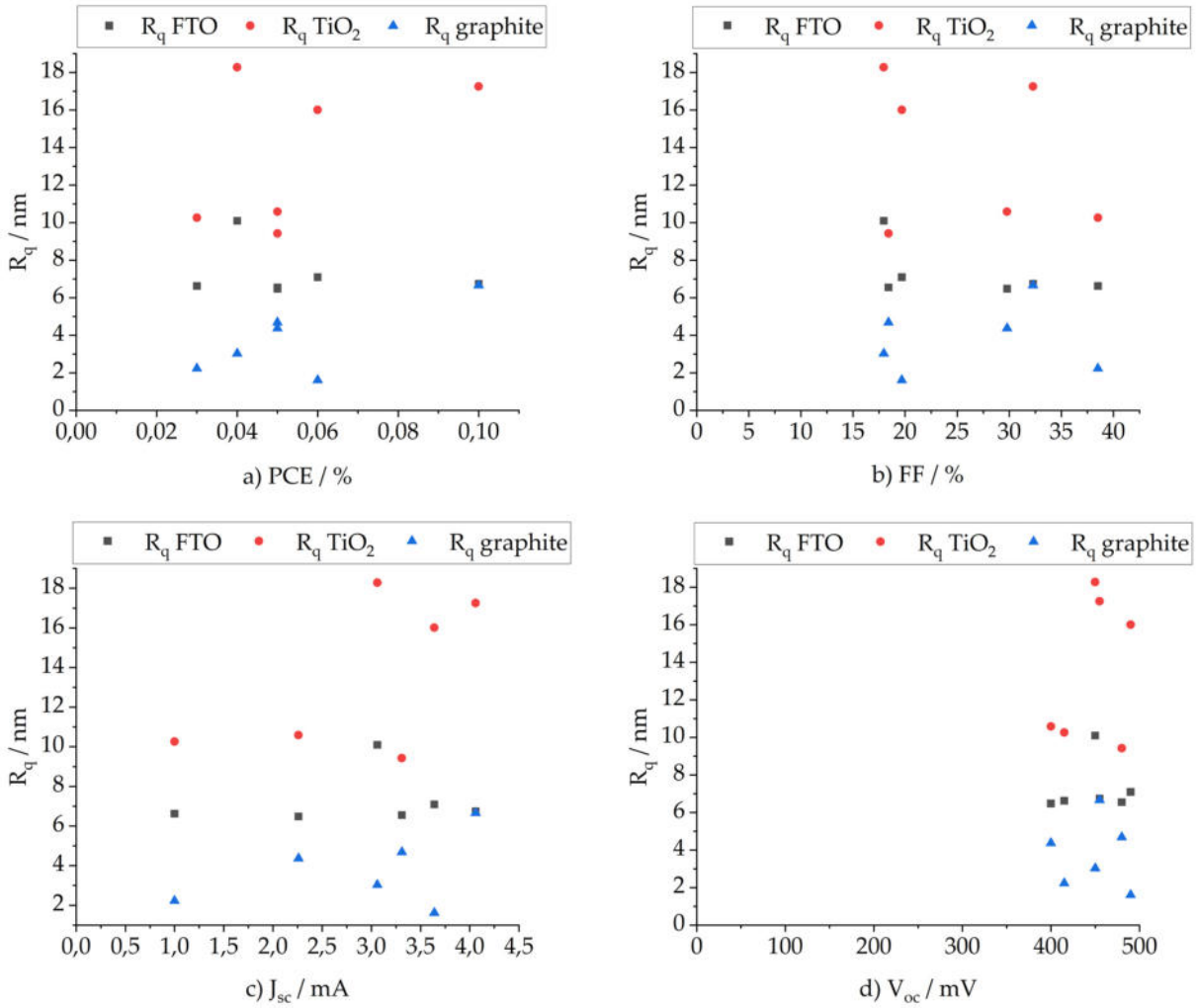

Figure 44: R_q and a) PCE, b) FF, c) J_{sc} and d) V_{oc} of the samples from table 4.

In figure 45, the result of the AFM investigation of the surface of the counter electrode of sample "G4.2" as well as a statistical evaluation of the particle size can be seen. The bin size for all histograms is set to 10 nm and the begin and end values are set to 0 nm and 280 nm respectively.

The graphite layer is visible and holes can be seen. The average particle size of the graphite layer is 91 nm ±27 nm.

In figure 46, the result of the AFM investigation of the surface of a front electrode with TiO_2 as well as a statistical evaluation of the particle size can be seen – sample "Over3". The porous surface of the TiO_2 can be seen.

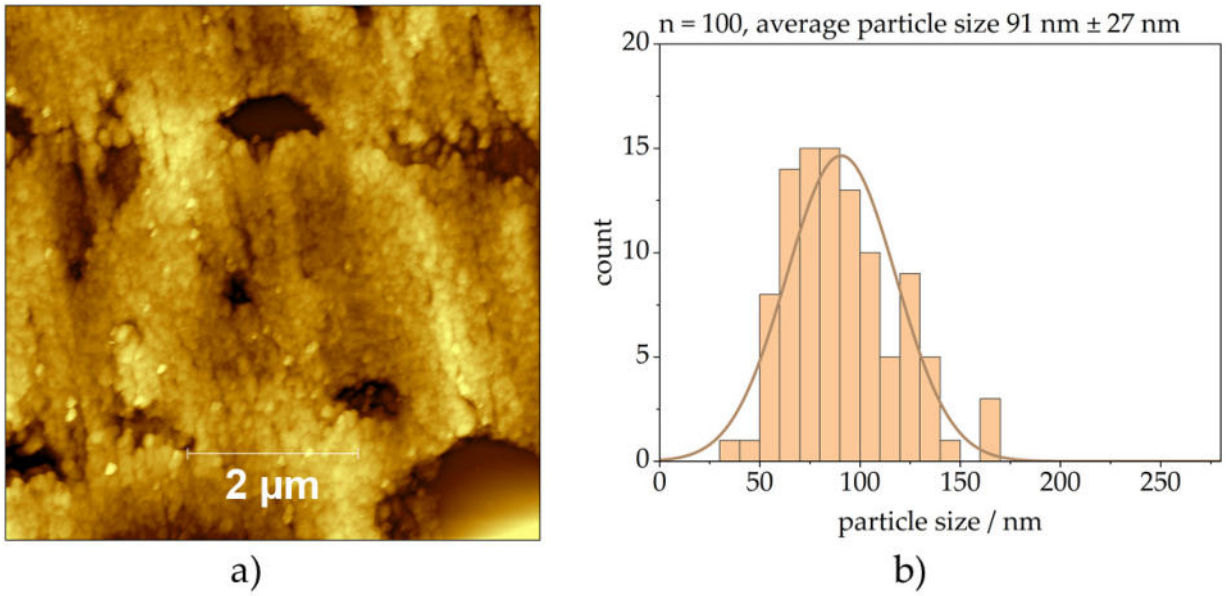

Figure 45: a) AFM image of a counter electrode with graphite and b) statistical evaluation of the particle size.

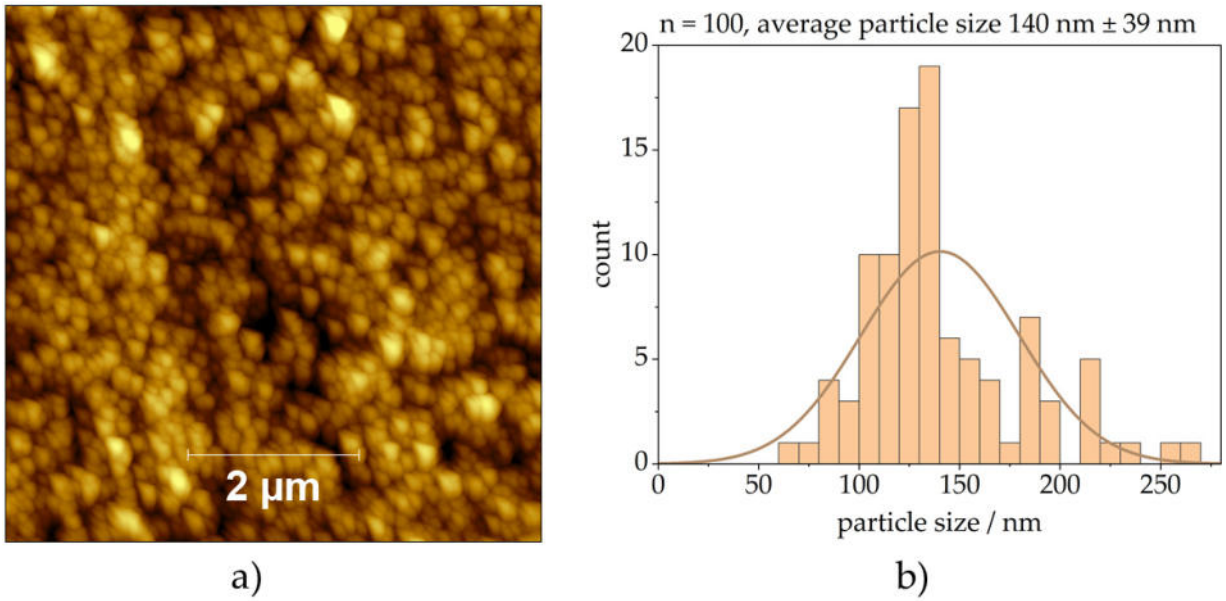

Figure 46: a) AFM image of a front electrode with TiO_2 and b) statistical evaluation of the particle size.

The average particle size of the TiO_2 layer is 140 nm ±39 nm. In figure 47, the result of the AFM investigation of the surface of a front electrode with FTO as well as a statistical evaluation of the particle size can be seen – sample "New1". The average particle size of

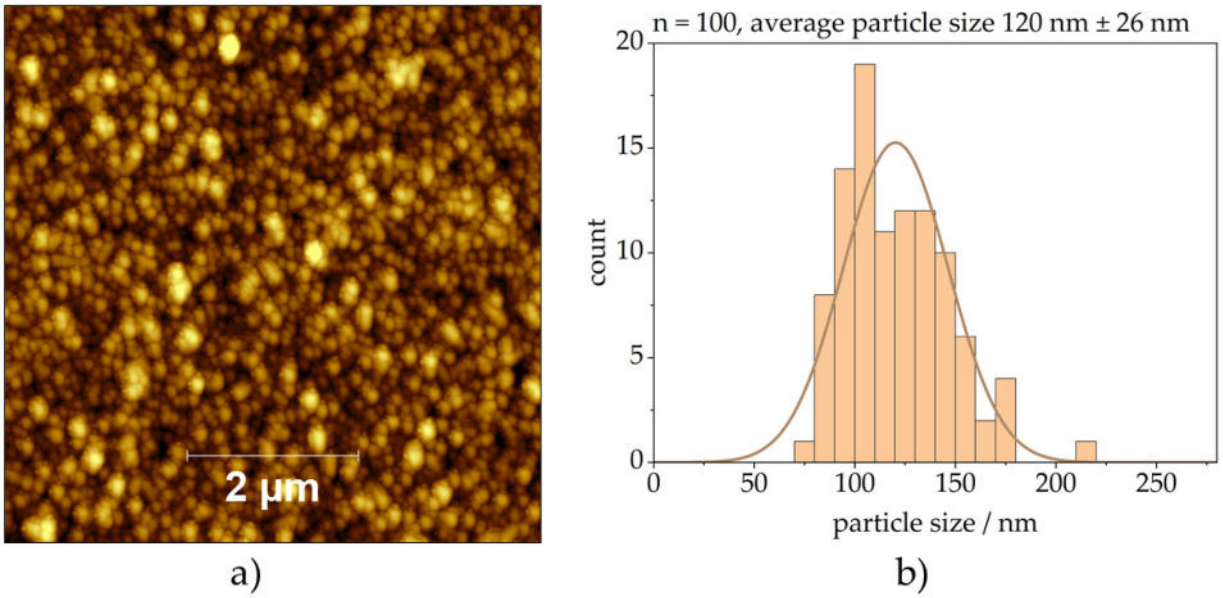

Figure 47: a) AFM image of a front electrode with FTO and b) statistical evaluation of the particle size.

the FTO layer is 120 nm ±26 nm. In addition, since no clear relationships are discernible between the parameters presented, a linear correlation calculation was performed with the data. The correlations are shown in Table 5.

In table 5 a significant positive correlation between the roughness of the graphite layer and the PCE can be seen. A moderate (0.5-0.6), positive correlations between the roughness of the graphite layer and TiO_2 and the short-circuit current is noticeable. Similar observation can be made for the roughness of the TiO_2 layer and the PCE. There is also a noticeable anti-correlation between the roughness of the FTO layer and the FF.

4.3.5 Potential recovering process for TiO_2

The TiO_2 layer washed off during the remanufacturing process was recovered together with desalinated water. After the water evaporated, the TiO_2 could be reused.

Table 5: Correlations of electrical parameters and surface roughness from the respective DSSC layers. Area designations: electrical parameters (blue), roughness (green), correlation between graphite layer roughness and PCE (red), correlations between graphite layer roughness, TiO_2 layer roughness and short circuit current (yellow), correlation between TiO_2 layer roughness and PCE (yellow), anti-correlation between FTO layer roughness and fill factor (gray).

	J_{sc}	V_{oc}	PCE	FF	R_q FTO	R_q TiO_2	R_q C
J_{sc}	1.00	0.79	0.77	-0.56	0.08	0.57	0.52
V_{oc}	0.79	1.00	0.35	-0.78	-0.09	0.17	0.06
PCE	0.77	0.35	1.00	0.10	-0.29	0.47	0.75
FF	-0.56	-0.78	0.10	1.00	-0.47	-0.24	0.14
R_q FTO	0.08	-0.09	-0.29	-0.47	1.00	0.63	-0.22
R_q TiO_2	0.57	0.17	0.47	-0.24	0.63	1.00	0.11
R_q C	0.52	0.06	0.75	0.14	-0.22	0.11	1.00

To evaluate the quality of the TiO_2, a measurement in the UV-Vis was performed. In figure 48 the UV-Vis spectra of a new TiO_2 layer, an old TiO_2 layer and the same old TiO_2 layer after a sintering process are shown.

The spectrum of the used TiO_2 differes significantly from the spectrum of the pure TiO_2 layer. Even after the sintering process the original spectrum of pure TiO_2 cannot be restored.

4.4 Circular design of DSSCs

The results of the Circo method are displayed in this chapter. Since the method is usually used by a company, in this case, the method was used from the point of view of a fictitious DSSC module manufacturer. The DSSC modules of concern are used as building integrated systems – such as facades or windows. The results have been published in the following paper [89].

4.4.1 Identify challenges and opportunities along the value chain

In figure 49 the value chain of a DSSC module, which is derived from several publications is displayed [20, 87, 134].

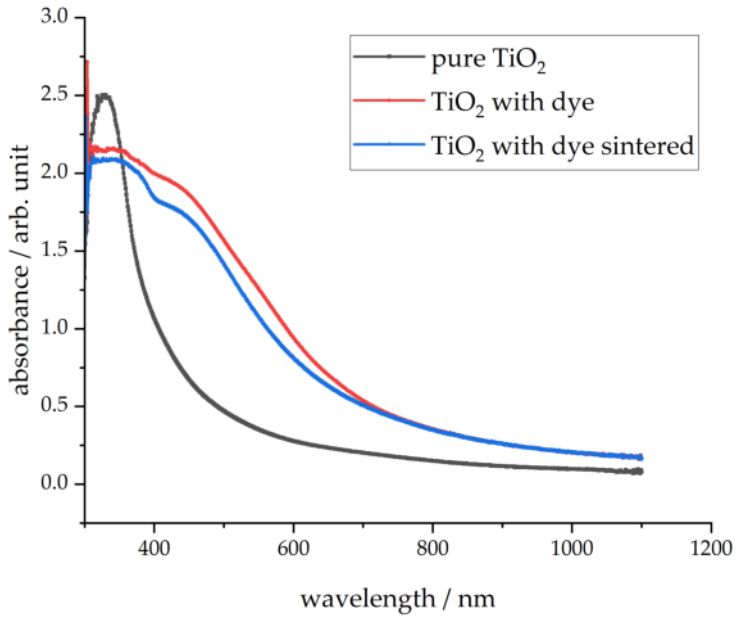

Figure 48: UV-Vis spectra of a new TiO_2 layer (black), an old TiO_2 layer including dye (red) and the same old TiO_2 layer after a sintering process (blue) [25].

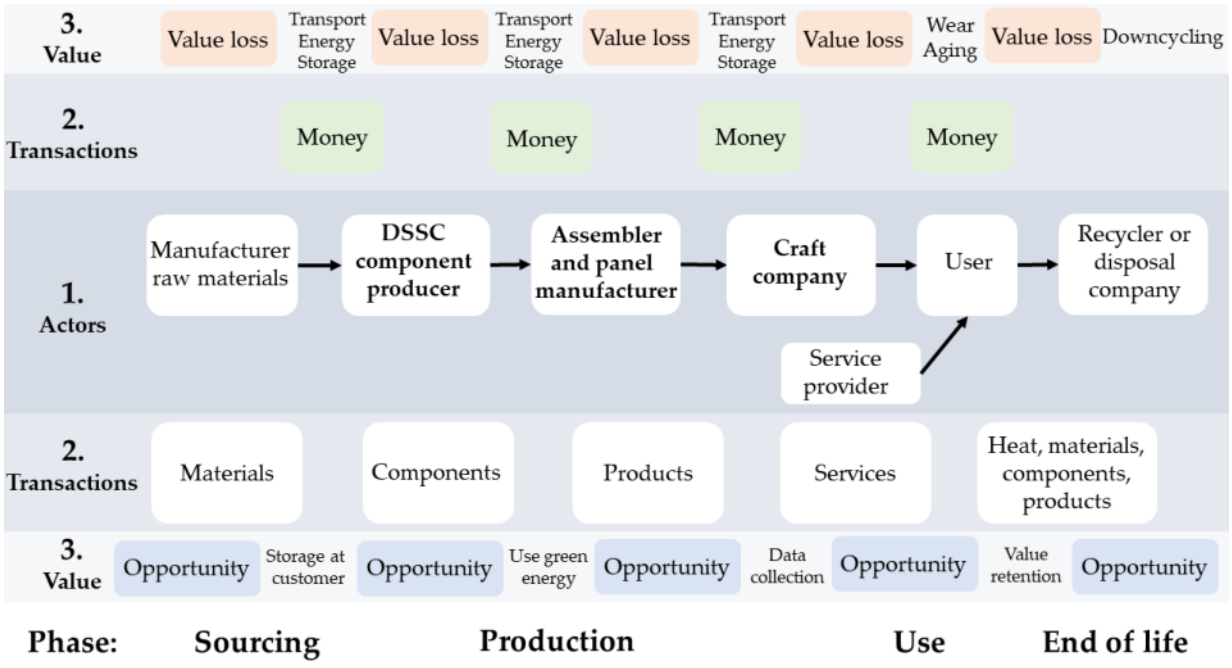

Figure 49: Value chain of a DSSC module [89].

All changes compared to figure 24 can be identified by bold letters. The actors in the center of figure 24 are specific for DSSC manufacturing. Resources are mined, the DSSC components are manufactured and assembled by the component producer and the panel manufacturer. Next, the system is installed at the users building by a craftsmen company. A service provider maintains or repairs the system if required. The service provider also has the opportunity to collect data about the usage of the product and use them, together with the module manufacturer, to improve the product. Finally, a recycling or disposal company can retrieve the material. In the cited publications, a downcycling process is mentioned at the end of the useful life of a DSSC module. Greater value retention could be achieved with a remanufacturing or recycling process. The following list gives an overview of the materials used for DSSC manufacturing [89]:

- Conductive glass or plastic – substrate;
- TiO_2 – semiconductor material;
- Ruthenium (N719 [87] or Z907 [20]), organic [81], natural [135] – dyes;
- Graphite or platinum – catalyst layer;
- Iodine potassium iodide – electrolyte;
- Silver [87] or carbon solutions [136] – improved conductivity;
- Ethylene vinyl acetate copolymer [87], polyethylene, low density resin [87] – sealing of the module;
- Deionized water, soap, ethanol [87], organic solvents [20] – other chemicals required in the process.

To manufacture a DSSC module on an industrial level, the following steps have to be applied [85, 89]:

- Preparation of the glass substrate – laser-scribing and cleaning;
- Applying silver paste – printing and drying;
- Applying TiO_2 – screen printing;
- Sintering TiO_2 layer – 500 °C;
- Applying platinum or graphite on the counter electrode – printing;

- Sintering platinum – 450 °C;
- Applying dye – printing or dipping;
- Assembling and sealing – commonly PE is used as sealing;
- Curing the components – drying in an oven;
- Injecting electrolyte;
- Patching the sealing;
- Joining assemblies – ultrasonic soldering;
- Assembling the panel.

Solaronix SA is a Swiss company that is already manufacturing DSSC modules on a pre-industrial level similar to the above mentioned process [30]. The process is less energy intensive compared to c-Si module manufacturing [85]. However, more than 90% of the energy required is used for the production of the glass substrate and the metal components [87]. Researchers emphasize to use different substrates, plastics for instance, to reduce the embodied energy [22].

After the DSSC module was assembled, it can be mounted as a building-integrated system. Therefore, the craftsman company has to add cables, a charge controller, an inverter and possibly a battery to the system. The energy payback time for a DSSC module ranges from 0.6 up to 3.28 years [20].

In the performed LCAs, a recycling process for DSSC material was investigated only in one case. Parisi et al. used data from c-Si PV recycling, in which 68.8% of glass and 90% of metals can be recycled [20]. Other studies did not include a recycling process in their analysis due to a lack of data [22, 85]. Table 6 gives an overview of the mentioned value losses and opportunities derived from them [89].

Table 6: Value losses and opportunities along the value chain [89].

Value loss	Opportunity
energy demanding production of glass	using recycled material, use green energy or reuse the material
high toxicity of ruthenium	use natural non-toxic solutions
scarce and precious metals (silver and platinum)	use carbon as catalyst and to improve conductivity
recycling and remanufacturing strategies are non existent	apply the circular economy concept at product design
after the point of sale no information gets to the company	apply service oriented business models to enable information flow during the use-phase
low PCE and lifetime of DSSCs	gel-electrolytes or solid-state electrolytes are technologies that might solve the long-term stability problem [44, 137]
market is dominated by c-Si PV, which is a well-established technology	use DSSCs as supplements in niche applications – indoors or ambient light applications

4.4.2 Investigate design and business model changes

With the derived opportunities from table 6, a matching process was performed. Suitable business models and design principles were combined to form potential matches. Table 7 shows the results of the matching process.

Table 7: Results of the matching process – opportunities, design strategies and business models (adapted from [89]).

opportunities	design strategies	business models	References
1. Refillable DSSCs	ease of maintenance and repair and upgradability	hybrid	[42, 138]
2. Design element applications	durability and attachment and trust	gap exploiter and classic long life	[30]
3. Durable DSSCs	durability	classic long life	[20, 32]
4. Recyclable DSSCs	design for recycling	gap exploiter	[24]
5. Remanufacturable DSSCs	standardization and compatibility	gap exploiter	[25]
6. DSSCs from recycled material	dis- and reassembly	gap exploiter	[139, 140]
7. Performance-contracting	upgradability, adaptability, ease of maintenance and repair	performance	[141]

The list below provides more details for each match as well as an economic and ecologic evaluation.

1. Refillable DSSCs: DSSCs have a short lifetime compared to c-Si PV. With refillable DSSCs and the hybrid business model, a high-quality DSSC can be sold with a subscription for refill packs. This way, the lifetime of the DSSCs could be prolonged. In addition, the customer could change the color or adapt the transparency for different seasons. This could motivate customers to buy refill packs. That represents an economic value for the company. From the ecological side, regular refill packs will cause a lot of packaging. In the future, refilling might be realized by humidity in the air or rain [42, 138].
2. Design element applications: Architects can use DSSCs as shades, facades, or windows, and artfully design buildings. Such products can be sold for a higher price – economic value. Since the customer will be attached to the design, it is in the interest of the customer to use the product as long as possible – ecological value. An example where building integrated DSSCs are used as design elements is the SwissTech Convention Center [142].
3. Durable DSSCs: The advancing solid-state or gel-electrolyte technology enables more stable DSSCs. The aim is to achieve a service life of at least 20 years in order to compete against c-Si PV on the market [20,32] – ecological value. High-quality DSSCs could be sold for a higher price. However, c-Si PV technology is well-established and will set a price limit. At the moment, the price for commercially available c-Si PV modules is below EUR 0.35 Watt peak [143]. This leads to a limited economic value for DSSCs.
4. Recyclable DSSCs: First experiments indicate that non-toxic DSSCs could be used in existing glass recycling processes [24]. Recycling the material enables both economic and ecologic benefits.

5. Remanufacturable DSSCs: Especially the conductive glass substrate has a high environmental impact and a high potential for being reused [25]. Compared to recycling, a higher value can be preserved and less energy is required in the process. No raw materials have to be mined and purified, and the energy for melting can also be saved. The reverse logistic system, however, is more difficult to establish and reduces the economic benefit.
6. DSSCs from recycled material: To reduce the environmental impact, conductive substrates from other technologies, such as flat screens or smartphones, could be reused for DSSC manufacturing [139,140]. This way, ecologic value can be generated. Economic risks are the quality of the product and the reverse logistic system.
7. Performance-contracting: Instead of selling DSSC modules, the company keeps ownership of the modules, mounts them on the roof of the customer's building and provides green energy. The public utility company in Aachen already uses a performance-contracting business model with c-Si PV technology [141]. The disadvantages of a performance model is the high investment for the company at the beginning – the products are not sold but a monthly fees represent the revenue. Since the company keeps ownership of the product, it is in the interest of the company to design long-lasting and repairable products – which represents the ecologic value. Within the concept of the circular economy, service oriented business models are the best option, because they deliver economic and ecologic value [7].

In figure 50 the evaluation of the economic and ecologic benefits of the described matches are shown. The evaluation of economic and ecologic values in the Circo method is performed by experts and is only a qualitative assessment. To proceed with the Circo method, further evaluation steps are required. In the publication [89], the procedure is explained in detail. The fictitious company has to evaluate what effort would be required to realize each match. Furthermore, the number of matches is reduced by fusing them together. At the end of this process, the company has to decide which business model will be experimented with first.

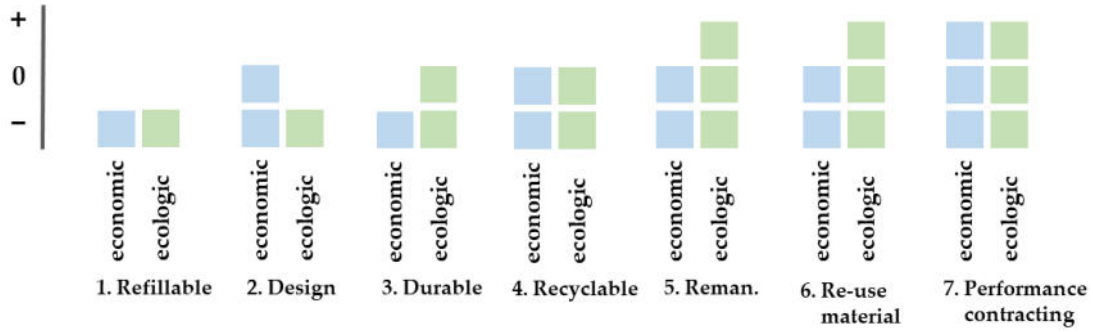

Figure 50: Circo method evaluation of economic and ecologic benefits (adapted from [89]).

In this case, the performance-contracting model was fused with recycling and remanufacturing DSSCs. This combined business model was further investigated.

4.4.3 Elaborate a circular business model and determine required changes

In figure 51 the fused performance business model in which the DSSC can potentially be recycled and remanufactured is shown.

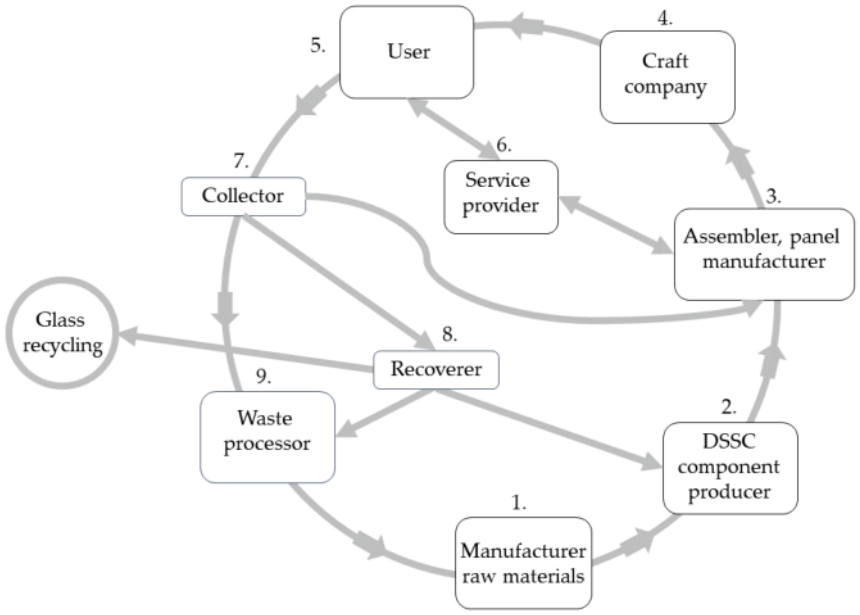

Figure 51: Circular business model, adapted from [89].

More details about the actors in the model are provided in the list below, adapted from [89]:

1. Raw material manufacturer: This stakeholder supplies raw materials for the component manufacturer.
2. DSSC component producer: This stakeholder manufactures DSSC components from raw materials and supplies them.
3. DSSC panel manufacturer (fictitious company in this investigation): This stakeholder assembles the DSSC module from the components. The service of repair, maintenance and upgrade is also part of this company. Close contact to the company that dismounts old systems is established and used modules run through a reverse logistic system back to the panel manufacturer. There, the modules are remanufactured and parts are used to built new DSSC modules.
4. Craft company: This stakeholder mounts the system on or in the building of the customer. It is also possible that these companies are part of the repair and maintenance service of the system.
5. User: Instead of buying a product, the user signs a contract and is provided with energy from the DSSC system.
6. Service provider: Since it is beneficial for the panel manufacturer (the fictitious company), they would prefer to have the service provider in their own company. The service provider collects data and is responsible for repair and maintenance services.
7. Collector: This stakeholder is responsible for collecting old DSSC modules. The systems need to be dismantled and transported to the recoverer or the panel manufacturer.
8. Recoverer: Old DSSCs are evaluated and sorted by the recoverer. Here, usable parts are delivered back to the component producer or put into a glass recycling process.
9. Waste processor: At the end of the cycle is the waste processor who deals with all parts that cannot be kept in the cycle. The material usually is burned to reduce the volume and eliminate any germs. The heat of this process can be used to generate electrical energy or directly heat houses or industry complexes.

In figure 52 the business model canvas of the performance-contracting model is shown. In the center of the business model canvas is the value proposition.

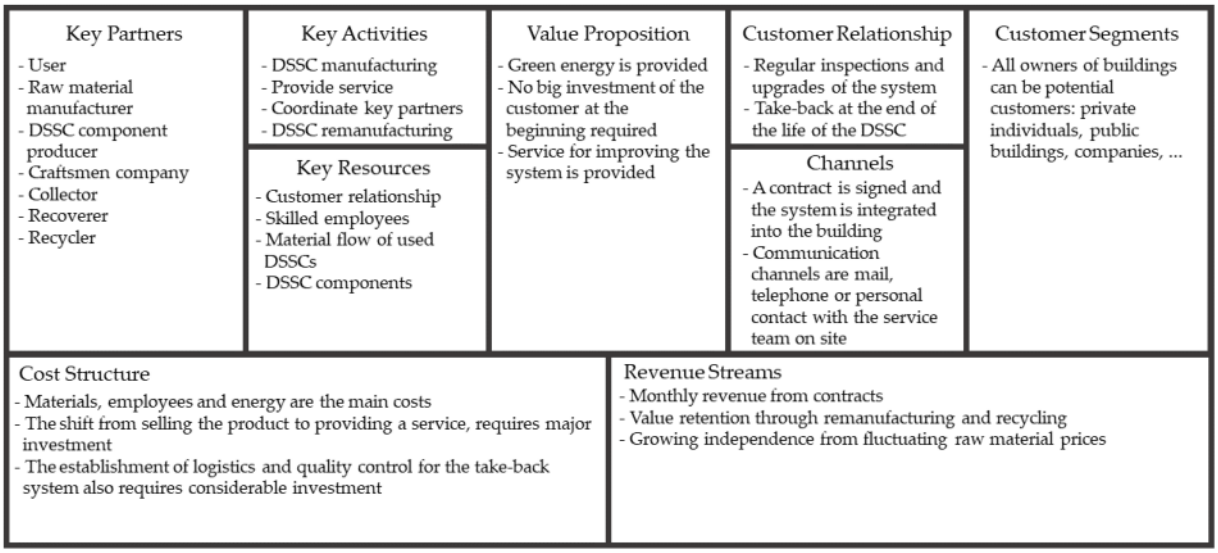

Figure 52: Performance-contracting DSSC business model [89].

It describes what value is offered to the customer. In this case, it is green energy supply with low initial investment costs and a service for maintaining and improving the system. The customer relationship is improved thanks to the contract and regular inspections. Individual wishes of the customers, such as a different color of the system or any upgrades, could be realized as well.

Revenue is generated through monthly payments from customers or costs for upgrades. By taking back old products, the material can be reused and the value is retained. Information from the use-phase can be utilized to improve product quality.

The required changes in the design and service area need to be described next. Table 8 shows which design changes are required.

Table 9 shows the changes which are required in the service field. The core elements, product design and the service changes have been described. Internal and external factors, such as marketing, politics etc., are not further discussed in this work. The entire investigation can be found in [89].

Table 8: Changes to the product design and possible solutions (adapted from [89]).

new activity	design changes	solutions
upgrade and repair	easy to clean, modular construction, availability of spare parts	upgrade or prolong lifetime with refilling, improved electrolyte
remanufacturing	easy to disassemble, no toxic components, compatibility over the evolution of a product	reuse the glass substrate, use non-toxic materials
recycling	easy to disassemble, no toxic components, material composites that are separable	use non-toxic materials and feet the material stream into the glass recycling process

Table 9: Changes to the service and possible solutions (adapted from [89]).

new activity	design changes	solutions
contracting	transform from selling a product to a service business model	A building integrated DSSC system is installed at the customer's building. Green energy is provided. Based on a contract, the energy costs are payed monthly.
Upgrading and retaining value	repair, upgrade, collecting data and implement predictive maintenance	During the use-phase, data is accumulated and evaluated. This way, the service and performance can be optimized.

4.4.4 Structure the required actions and plan their implementation

To complete the Circo method, it is necessary to create a road map. In figure 53, an example for a potential road map is given. It is used to plan further steps and implement the ideas. In this example, the next steps are “discussing the ideas with colleagues”, “use

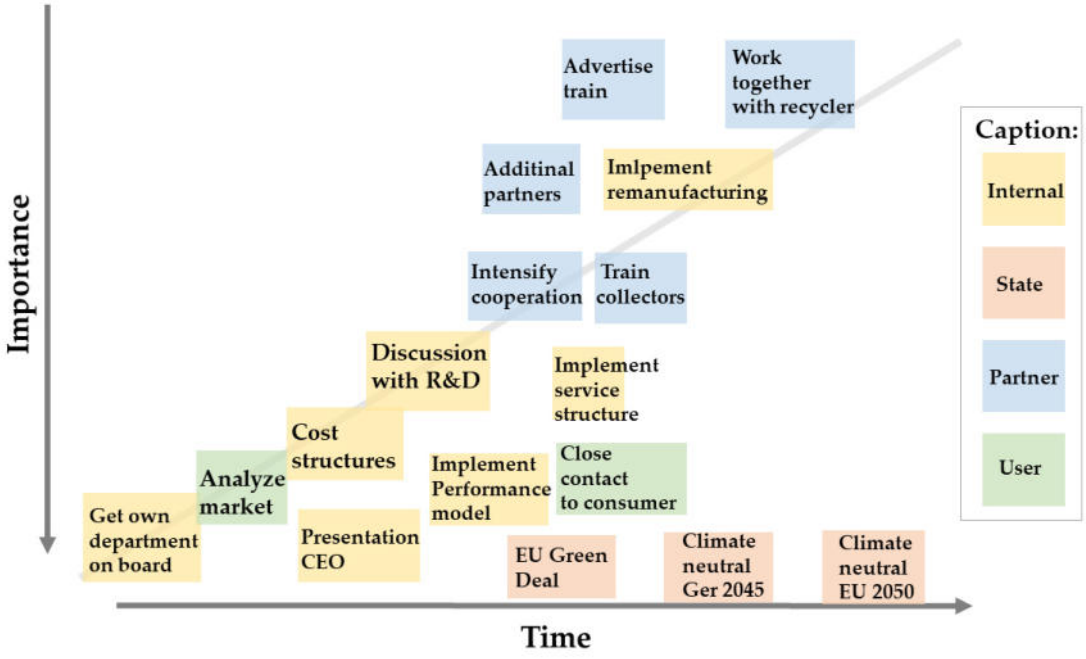

Figure 53: Circo method road map of next steps [89].

further tools to analyze the market and the feasibility of the idea” and “pitch the idea to the CEO”. External factors, such as the EU Green Deal, will influence the company. If the CEO decides to approach this idea, further implementation steps can be realized.

5 Discussion

This chapter discusses the results and relates them to the research question. First, the review of recycling is discussed and the research gap is highlighted. After that, the recycling and remanufacturing experiment results are discussed. Finally, the results of the Circo method are investigated further.

5.1 Recycling review

The experimental results of the bibliographic analysis have shown that sustainability plays a minor role in DSSC research. That was also the conclusion in the similar investigation in 2021 [16]. However, "sustainability" and "life-cycle assessment" appear more often in the last two years, which indicates that the importance of sustainability research is increasing. Table 11 shows the growth rate of all DSSC publications, the term "sustainability" and the term "counter electrode", which occurs most often.

Table 10: Growth rate of terms.

term	occurrences 15th March 2021	occurrences 6th December 2022	growth rate
all DSSC publications	24,441	27,014	1,11
"counter electrode"	2,810	3,048	1,08
"sustainability"	35	49	1,40

The growth rate in this case is the number of occurrences in 2022 divided by those from 2021. This indicates that the term "sustainability" is growing faster compared to the term "counter electrode". For total numbers, however, "counter electrode" grew by 238 and "sustainability" by 14.

5.1.1 Use of recycling material for DSSC manufacturing

Papers about DSSCs and recycling so far focus on using recycled material to built DSSCs [16]. Graphite from recycled batteries or from almost used up pencils is one option to

use recycled materials to built DSSCs. Nair et al. compared theses two sources and concluded that a higher efficiency could be reached with carbon, which was recycled from batteries [144]. Daut et al. also used recycled carbon from batteries and built the counter electrode with the recycled materials [145]. Carbon powder, however, is not expensive and the source of recycled carbon should be economically viable compared to virgin carbon powder. Graphene could become an important component of sustainable DSSC manufacturing because of the material properties, such as mechanical, chemical, thermal or optoelectronic properties [146].

Besides the recycled graphite, old thin-film transistor liquid crystal displays (TFT-LCD) or smartphone displays could be used as conductive substrate for DSSC manufacturing [16]. The TFT-LCD experiment showed that the conductivity of the displays, which are coated with indium tin oxide, had to be improved with copper nano wires – performed by Chen et al. [139]. Another option for producing counter electrodes for DSSCs is using smartphone displays. Ayaz et al. cleaned the smartphone display and applied carbon as catalytic material from the flame of a candle [140]. Zhu et al. used perovskite cells and reused the conductive glass together with the TiO_2-layer to built a new perovskite cell and reached a PCE of 9.12% [147]. In table 11, an overview of the collected resources about using recycling material for DSSC construction is given – adapted from own publication [16].

Table 11: Approaches of using recycled materials for DSSC / perovskite applications – overview [16].

Resource	Application	Material	Efficiency
[145]	Counter electrode	Carbon from batteries	No information
[144]	Counter electrode	Carbon from batteries	8.2%
[144]	Counter electrode	Carbon from pencils	7.23%
[140]	Conductive glass	Smartphone screens	0.0244%
[139]	Conductive glass	TFT-LCD	3.94%
[147]	Conductive glass with TiO_2	Perovskite cells	9.12%

Applying the recycling concept is sustainable, because it is often possible to save energy in the production process this way. An example for that is aluminum recycling, where energy savings up to 95% can be achieved – comparing energy investment for producing

raw aluminum compared to recycled aluminum [148]. The same is true for glass recycling, where using recycled cullet will lead to indirect and direct energy savings. Indirect savings are achieved because no resources have to be mined or transported long distances. Direct energy savings can be achieved because the cullet has a lower melting temperature compared to the raw material, and thus the furnace can work at lower temperatures. Around 1.9-2.35 MJ can be saved for each kg of cullet replacing raw material [149]. In addition, about EUR 84 and 0.13 tCO_2 can be saved per ton of DSSC cullet replacing the raw material [89]. The problem with using recycled material is unknown quality and possible price challenges. Carbon powder, for instance, is comparably cheap and recycled carbon from batteries could be more expensive than the new product.

5.1.2 Expending lifetime of DSSCs

Besides recycling, there are approaches in research to expand the lifetime of DSSCs. A critical point of DSSC technology is the long-term stability, which strongly depends on the electrolyte. A liquid electrolyte can evaporate fast [88]. One approach to solve this issue is to use solid-state or gel-electrolytes [150]. Biopolymer gel-electrolytes based on carrageenan, cellulose, chitosan or starch could be more sustainable solutions compared to crude-oil-based electrolytes [151, 152]. Encapsulation of the DSSC is another approach to prevent the DSSC from drying out. Usually, plastic components are used for encapsulation – which means adding different materials to the DSSC, making a recycling process more complicated [16]. If a liquid electrolyte is used, it may be possible to rehydrate it, as Juhász Junger et al. showed [42]. In textile applications, DSSCs integrated in tents, for instance, morning dew or air humidity could rehydrate DSSCs in the future [138].

5.2 Recycling experiment

In the following chapter, the SEM-EDX, ICP-OES and melting experiment results are discussed.

5.2.1 SEM-EDX

The findings confirm the elements expected in the DSSC glass substrate. Since Man Solar did not provide any detailed information about the composition of the glass substrate, further investigations prior to the melting experiment were required. The TiO_2 layer can be removed with the described etching process. After etching, the typical glass elements can be detected with higher concentrations because the TiO_2 layer was removed. However, the FTO layer cannot be removed with the described etching process. When it is required to remove the FTO layer, for a recycling or remanufacturing approach of the glass substrate, for instance, hydroiodic acid or sulfuric acid is required [153, 154].

5.2.2 ICP-OES

Most of the weight percentages of the elements of the DSSCs from 2018 and 2020 are within the recommended values of the patent. However, the range of weight percentages in the patent is large. This is common in patents to protect the idea or, in this case, the recipe of the ideal glass for photovoltaic applications. The Al_2O_3 values of the DSSC glass substrates are below the emphasized range of the patent but CaO is considerably above the range. Both elements are used to increase the viscosity and chemical resistance of the glass [155, 156]. Since both elements have similar effects on the properties of the glass, it is possible that the price of the material might influence which material is used in glass production.

Usually, glass for photovoltaic applications has very low Fe_2O_3 values because iron compounds reduce the transmission, and thus the photovoltaic efficiency [133]. In the DSSC glass substrates from 2018, the Fe_2O_3 weight percentage is low (0.009 wt%). The Fe_2O_3 weight percentage of the glass substrates from 2020 is considerably higher (0.1 wt%).

However, both are within the range given by the patent (0-0.5 wt%). Fe_2O_3 in the glass especially absorbs photons in the UV spectrum (300 nm and below) [157]. As an example, 1‰ of Fe_2O_3 in the front glass reduces the c-Si PV module efficiency by 9.8% for a glass thickness of 3.2 mm [133, 157]. For 2-mm-thick glass substrates, the decline of efficiency for the same amount of Fe_2O_3 in the glass (1‰) is only 6.4% [157]. That means thinner glass and very low Fe_2O_3 values in the glass improve the transmission. The different glass composition could also be a cause for the varying PCE results in the remanufacturing experiments (chapter 4.3) – since old DSSCs were used with varying material composition.

A side effect of maximizing efficiency, however, are drawbacks on the long-term stability of the photovoltaic system. The UV light is responsible for aging processes in the module, especially the EVA foil and semiconductor material in c-Si PV [158]. DSSCs could also degrade when exposed to UV radiation or thermal stress [159]. The sealing of DSSCs is often realized with plastic components which are prone to UV radiation. Gel-electrolyte DSSCs are more robust compared to liquid electrolyte DSSCs, and thus are less sensitive to thermal stress or UV radiation [160]. However, just reducing Fe_2O_3 to a minimum to achieve optimal PCEs is counter productive and it needs to be further investigated which glass composition is optimal for DSSC applications. Especially, because TiO_2 is photo-active. When TiO_2 is hit by UV-light, organic compounds in the DSSC can be oxidized, which leads to degradation of the DSSC [50].

Finally, the different glass composition of the different batches, for instance, glass substrates from 2018 and 2020, is a potential problem for a future recycling process. This problem is already occurring in the recycling of c-Si PV modules. A constant substrate composition is required for high-quality recycling. To make this possible, photovoltaic glass would have to be standardized, or at least each photovoltaic module should be given a material passport or some kind of declaration showing the composition of all components for the recycling company.

5.2.3 Melting experiment

No anomalies, such as foam or big bubbles, could be identified during the melting experiment. The DSSC melts have no big differences compared to the reference sample. This indicates that the used DSSC material is suitable for glass recycling. All melts exhibit pinkish streaks, indicating that these are caused by impurities from other sources and are not DSSC specific. The light blue color of melt A could be caused by higher Fe_2O_3 weight percentage in the glass composition [156]. Melt B was clear and had no recognizable coloration. That indicates that the weathering process could reduce organic compounds, dust, fingerprints and so on. These impurities could explain the coloration of melt C and D, which did not go through a simulated weathering process. This indicates that the quality of the melt can be improved by a weathering process.

A possible recycling application for the described DSSCs is promising, however, further experiments are required to investigate more material properties, such as chemical resistance, transparency or viscosity. Another point is the gases which could emerge during the melting process. They were not monitored or evaluated in this experiment. The used plastic components, in this case PEO for the gel-electrolyte, are decomposed at temperatures from 324 °C to 363 °C [161]. On top of that, in this experiment, comparably simple DSSCs have been used. When more metal elements are used, such as platinum or silver, glass recycling becomes much more difficult. That is why alternatives, such as carbon nanotubes, should be investigated further as options for improved conductivity without metal components [162].

5.3 Remanufacturing

In figure 54 the average PCEs of all remanufactured DSSCs is shown. Explanations for the differences in the PCEs are the differences in batch quality of the glass substrate, the conductivity (FTO-layer) and the method for applying the TiO_2 layer. The DSSCs with a manually applied TiO_2 layer have higher PCEs but shorter lifetime compared to the industrial applied TiO_2 layer DSSCs.

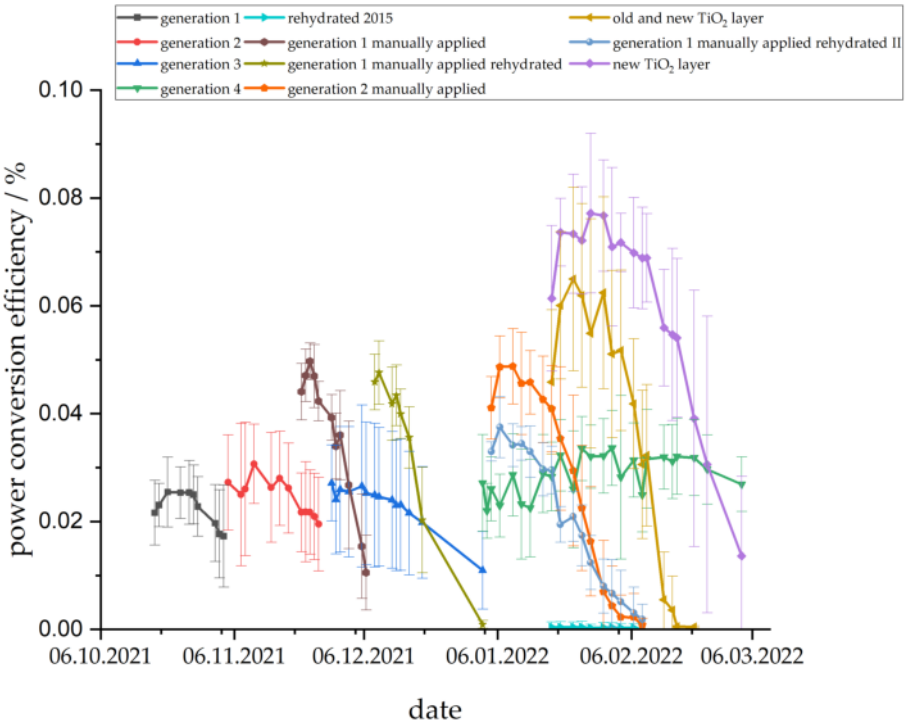

Figure 54: Average PCEs of all remanufacturing experiments [25].

The fluctuations of the PCE in the later generations of DSSC are increasing. One explanation for that could be the method of measuring. In figure 39 the damaged glass substrate is shown. The alligator clips caused damage with every measurement. This damage could have lead to a decrease in conductivity and PCE of the DSSCs. The FTO layer, which is about 10 nm thick and increases the conductivity, is not visible in figure 39. Thus, it cannot be evaluated if the scratches on the glass substrate also indicate a damaged FTO-layer. Some explanations for the standard deviation are:

- the PCE of sample "G3.1" drops to zero after the third measurement.
- the PCE of sample "G4.2" fluctuates between values of 0.04% and 0% due to bad connectivity – possible cause is the damaged glass substrate.

Reviving old DSSCs from 2015 with electrolyte was not successful. The whitish color of the DSSCs indicates that the dye degraded over time and simply refilling electrolyte is not sufficient to revive the DSSC.

The highest PCE that could be achieved was 0.09% with a glass substrate from 2015. The experimental results indicate that a remanufacturing for DSSCs is possible and that the long-term stability and even the PCEs are on the same level or even higher after the second, third or fourth remanufacturing iteration. One explanation for the increased PCE of older generations could be that the dye density on the TiO_2 layer gets more dense after several dying processes [163]. A big standard deviation indicates that the PCEs of the DSSCs varies. This shows that proper evaluation key performance indicators are required to evaluate which DSSC materials can be reused and which materials should better be recycled since the predicted PCEs of the DSSCs might be to low. It should also be possible to apply a similar remanufacturing procedure to DSSCs which are using ruthenium dyes. In this case, however, the dismantling and cleaning process of the old DSSCs has to be handled with care because of the toxic components.

The FF of different photovoltaic technologies ranges from 20% to 85%. For c-Si PV, a typical FF is about 80% and for a-Si about 67% [164]. DSSCs with ruthenium dyes, such as N719, reach FF of about 70% [164, 165]. The FF of DSSCs using natural dyes is considerably lower, ranging between 20% for spinach oleracea and 60% for rosella (anthocyanin) [166–168]. The FFs of the DSSC samples studied in this work, which were examined by AFM, ranged from 17.95% to 38.51% – table 4.

In table 4 and figure 44, no correlation between R_q and PCE, FF, J_{sc} and V_{oc} is visible. In addition, the AFM investigation showed that the roughness of the glass surface is not significantly influenced by the remanufacturing process. The control sample "Virgin glass", with commercially applied TiO_2 layer, has a higher R_q value compared to the other samples with commercially applied TiO_2 layers. This indicates that the roughness might be reduced through the cleaning and remanufacturing process. The linear correlation calculation, however, revealed that there are correlations between the surface roughness of the TiO_2 and graphite layer and the current J_{sc} and PCE.

Since the semiconductor material TiO_2 shows correlations between PCE and J_{sc} in table 5, it can be assumed that the morphology of the surface state of this layer can have a major impact on the efficiency of the conversion of light energy into electrical energy.

From an atomic point of view, the surface and volume morphology of a semiconductor material affects the nature of the energy gap between the valence and conduction bands – The width and fuzziness of this width depend on whether the material is amorphous or crystalline with a very well defined, long-range structural order.

The TiO_2 material studied is undoubtedly in a disordered phase. Processes, especially remanufacturing, change the degree of this disorder. The presence of a certain positive correlation between the morphology of the TiO_2 layer and the PCE can be associated with a change in the properties of the mentioned energy gap. Namely, in amorphous semiconductors, so-called diffusion tail states appear at the edges of the energy gap. Due to foreign inclusions and impurities in the TiO_2 layer additional states, located in the energy gap, are enabled. These states can be a source for additional charge carriers in the conduction band [169]. This conclusion should be considered preliminary and requires further research. However, the investigation of the energy structure of the TiO_2 semiconductor material was not the main concern of the current PhD thesis.

The remanufacturing experiments show that it might be beneficial to remove old TiO_2 layers before applying new ones. This way, PCE and long-term stability could be improved. The goal in the remanufacturing process is to reuse as many components as possible. A new TiO_2 layer only needs to be applied if the old one is damaged. Nonetheless, the washed-off TiO_2 can be recovered and reused. Dye residues colored the old TiO_2 layer lilac. In figure 48, it is visible that the absorption spectra of used TiO_2 is considerably different compared to pure TiO_2. However, the remanufactured DSSCs have similar or higher PCEs even with used TiO_2. This indicates that the TiO_2 can be reused for DSSC purposes. If the recovered TiO_2 is to be used for other purposes, a purification process may be required to improve the quality.

5.4 Circular design

The Circo method was introduced to present an instrument, which can help to transform a linear product into a service oriented business model. Especially for DSSCs, which have not yet reached industrial scale, this approach can help to generate ideas and solutions to directly develop business models that are suitable for a circular economy and help to solve the described resource and climate crises. Limitations of the Circo method are, however, that most of the evaluation tools are qualitative. For quantifiable numbers and costs additional tools, such as prototyping, cost-utility analysis or a feasibility study have to be used.

5.4.1 Identify challenges and opportunities along the value chain

The value chain of the fictitious DSSC module manufacturer was derived from several LCA studies and other publications. Value losses that generally appear in most value chains are intensive energy use and exploitation of humans and pollution of the environment. During the process of mining the raw materials, harm to the environment and exploitation of humans cannot be excluded.

Most environmental impact and human toxicity can be traced back to silver, ruthenium, platinum and electricity use [20]. Both issues are in focus of the European Union. The aim of the European Green Deal is a carbon neutral Europe till 2050 [170]. This implies that emissions from energy usage will be zero. Within the EU supply chain law, "Corporate sustainability due diligence", exploitation along the value chain should be reduced [171].

The value losses through exploitation and pollution are therefore the subject of state laws and objectives. A large loss of value occurs at the end of a DSSC's useful life when it is disposed of instead of being recycled or remanufactured. With circular design principles and business models, it is possible to retain large parts of the value of a product.

5.4.2 Investigate design and business model changes

The chosen fictitious DSSC module manufacturer has no reverse logistic, maintenance or remanufacturing processes. The DSSC technology has not yet reached industrial scale. That is why it can be expected that fast changes with new product generations will appear. Consequently, the product should be designed for upgradability. Well-established components are the conductive glass substrate and the TiO_2 layer. These parts can potentially be remanufactured and will probably be used in advanced DSSCs in the future as well [89]. Potential components for an upgrade are the dye and the electrolyte. Toxic substances make a circulation of materials more difficult, which is why in this work it is suggested to use non-toxic materials. However, with suitable cleaning processes, toxic components could be removed and a remanufacturing and recycling process could be made possible.

5.4.3 Elaborate a circular business model and determine required changes

The business model described in figure 51 cannot be realized instantly – time for the transformation and construction is required. The infrastructure for recycling or remanufacturing need to be put in place later. In the beginning, there is not sufficient DSSC scrap material for a recycling or remanufacturing process.

For that reason, the focus is on establishing a service branch in the company, so that a repair, maintenance, data collection and finally the performance contracting can be realized. The performance contracting will challenge the company because many new tasks, such as law requirements, pre-financing or the service infrastructure, will have to be implemented. In the beginning, certain tasks could also be outsourced until a functioning infrastructure is built within the company. The repair and maintenance service, for instance, could be outsourced to the crafts company. When old DSSCs come back through the reverse logistic system, one challenge will be to determine the quality of the product and to evaluate if it should be remanufactured or recycled. One quality check could be to measure the conductivity of the glass substrate and evaluate if its high enough, so that

the material can be used in a remanufacturing process. Since the Circo method mainly uses qualitative tools to evaluate the business model ideas, additional methods that could improve the validity of the results should be used in further steps. To investigate certain barriers or obstacles, a feasibility study and the political, economic, social, technological, environmental and legal (Pestel) analysis could be used. The feasibility analysis can be used to investigate if the idea can be realized on a technical and economical level. Furthermore, the main difficulties can be identified. With the Pestel analysis, the external factors are described and obstacles are identified.

5.4.4 Structure the required actions and plan their implementation

In the Circo method, the road map visualizes which steps have to be taken in which order, sorting the tasks by significance. To improve this road map, a bar chart could be used, which indicates how long a task takes, thus giving more detailed information. If the CEO supports the idea and the project is to be implemented, a more detailed work breakdown structure (WBS) should be created. With this method, dependencies in the project flow are visualized – step three cannot be done before step two. Furthermore, the WBS is part of the network planning technique, which also clusters tasks into working packages. With these tools, more structure in the project flow could be realized.

6 Summary and Conclusion

With a growing DSSC market, the possible applications and ecological benefits of DSSCs are becoming more diverse, especially when compared to other photovoltaic technologies, thus making DSSCs a promising technology. Despite this, sustainability plays only a minor role in DSSC research – the term "sustainability" appears only in 49 out of 27,014 publications. PCE improvements and long-term stability are necessary and should be realized in tandem with sustainable solutions.

This thesis showed that non-toxic DSSC can be remanufactured without negatively impacting the PCE and that their potential use in conventional glass recycling is promising. Both processes, remanufacturing and recycling, are essential for products that flow in a circular economy. Furthermore, it was pointed out that a circular business model, such as the performance model, is key to lift the DSSC technology to an industrial scale and reduce its environmental impact. Since there were no experiments on either remanufacturing or recycling, this work took the first step to fill this research gap.

The review results showed that rehydration with electrolytes can extend the lifetime of DSSCs and that the use of solid-electrolytes or gel-electrolytes is a solution to improve DSSCs further. Smartphone screens could be used as conductive substrate and graphite recycled from batteries, for instance, could be used for DSSC manufacturing. However, the price competitiveness of recycled materials has not yet been proven. In addition, ensuring a stable product quality and the migration of harmful substances to new products remain problems to be solved. Harmful substances can make the recycling process dangerous and unpredictable. Therefore, it is important to analyze the quality and composition of the recycled materials that are used.

The ICP-OES analysis revealed that the composition of the two glass substrates from different years had significant variations. For example, the Fe_2O_3 value of the glass substrate from 2018 was 0.009 wt% and that of the glass substrates from 2020 was 0.100 wt%. That is why, for managing a future recycling process, the glass composition should be easier to identify, for instance, via a material passport or a product label.

A recycling process for DSSCs containing ruthenium dyes has not been investigated. However, if a cleaning process were carried out to remove toxic components from the DSSCs prior to actual recycling, the materials could be fed into a glass recycling process. For every ton of DSSC cullet replacing virgin material, about EUR 84 and 0.13 tCO2 could be saved.

The results of the melting experiment are promising. The melts are visually similar and only minor differences in color can be identified. With the help of the simulated weathering process, organic compounds and residues were washed out of the DSSCs. Melt B was the only sample which went through a simulated weathering process and had the best glass quality. Overall, no significant differences can be observed between melts B to D and the reference sample melt A, neither in the melting behavior nor in the optical appearance. To ascertain whether DSSC cullets can be used in float or container glass production, further tests are required – material properties such as transparency, viscosity and chemical resistance must be investigated. The best use of DSSC glass or of glass from photovoltaic applications in general would be to reuse the iron poor glass for PV applications.

To further improve value retention, the glass substrate can be remanufactured instead of being recycled. For non-toxic DSSCs a successful remanufacturing approach was described. The PCE and long-term stability were not negatively affected. The highest PCE was achieved with a glass substrate from a batch from 2015 – a PCE of 0.09% was achieved.

The linear correlation calculation revealed positive correlations between the TiO_2 layer roughness and PCE and J_{sc}. However, further research is needed to determine the influence of the semiconductor morphology and the electric properties of the DSSC.

The washed off TiO_2 was recovered and reused. Furthermore, the remanufacturing process proved to outperform simply rehydrating the DSSCs in regards to PCE and long-term stability. This applies most significantly to old DSSCs in which the dye has already degraded. The described remanufacturing process could also be applied to DSSC containing ruthenium dyes. However, the toxic compounds make safe disassembly and cleaning difficult. Remanufacturing solutions for well-established PV technologies are still in the research stage and need to be further improved. At this point, it becomes clear that the

ability to recycle, remanufacture and reuse materials depends heavily on the design of the product.

The described Circo method is a useful tool for the transformation of a product and business model to become more circular. With value retention in focus, the reuse of the conductive glass substrate is most promising. To successfully recover the old DSSC materials, a performance-contracting business model was described. The Circo method is used by companies to start or improve the transformation of their products and business models towards a circular economy. In this case, only a fictitious DSSC module manufacturer was described, and thus the circular design principles and business models have been in focus, rather than the implementation of the ideas.

Most of the tools of the Circo method are of qualitative nature. To improve the results of the Circo method, tools such as cost-utility and Pestel analysis as well as a feasibility study should be used in addition. With these tools, specific and quantifiable results can be achieved as well as a more structured project plan.

Finally, a circular business model was described – performance contracting. Instead of selling the DSSC system, the company keeps ownership of the product. The system is integrated in the customers building. The customer is supplied with energy and pays a monthly fee. The product is upgradable and information from the use-phase are gathered and used to improve the product. Eventually, after the end of the contract or the useful life of the DSSC, the system is dismounted and a second life or recycling for the DSSC modules is realized.

With key processes of a circular business model, namely remanufacturing and recycling, material loops can be closed. In summary, non-toxic DSSCs are a promising technology for the use of green energy, which can potentially be integrated into the material cycles of the circular economy.

References

[1] IPCC. Climate Change 2022 Impacts, Adaption and Vulnerability. Technical report, The Intergovernmental Panel on Climate Change, 2022.

[2] Larry E. Erickson and Gary Brase. Paris Agreement on Climate Change. Technical report, 2019.

[3] Roland Pohl and Benedikt Heitmann. Aufarbeitung von Altmodulen und Rückführung von Wertstoffen in den Stoffkreislauf. Technical report, Reiling Glas Recycling GmbH & Co. KG, 2019.

[4] John A. Tsanakas, Arvid van der Heide, Tadas Radavičius, Julius Denafas, Elisabeth Lemaire, Ke Wang, Jef Poortmans, and Eszter Voroshazi. Towards a circular supply chain for PV modules: Review of today's challenges in PV recycling, refurbishment and re-certification. *Progress in Photovoltaics: Research and Applications*, 28(6):454–464, 2020.

[5] Lance Lambert. Why lumber prices are suddenly rising again | Fortune. https://fortune.com/2021/09/27/lumber-prices-rising-2021-covid/, last accessed 01/11/2023.

[6] Saheli Roy Choudhury. JPMorgan on semiconductor shortage and outlook for 2022, 2023. https://www.cnbc.com/2021/11/19/jpmorgan-on-semiconductor-shortage-and-outlook-for-2022-2023.html, last accessed 01/11/2023.

[7] The Ellen MacArthur Foundation. Towards the Circular Economy Vol. 1: an economic and business rationale for an accelerated transition. *Ellen MacArthur Found.*, 1:96, 2013.

[8] Ellen MacArthur Foundation. The Circular Economy In Detail. https://www.ellenmacarthurfoundation.org/explore/the-circular-economy-in-detail, last accessed 01/11/2023.

[9] Sophia Kohn, Christina Großerhode, Jan Lukas Storck, Georg Grötsch, Carsten Cornelißen, Almuth Streitenberger, Carsten Grassmann, Anne Schwarz-Pfeiffer, and Andrea Ehrmann. Commercially available teas as possible dyes for dye-sensitized solar cells. *Optik*, 185:178–182, 2019.

[10] Katrin Gossen, Jan Lukas Storck, and Andrea Ehrmann. Influence of solvents on Aloe vera gel performance in dye-sensitized solar cells. *Optik*, 180:615–618, 2019.

[11] Jan Lukas Storck, Timo Grothe, Marius Dotter, Sonia Adabra, Michelle Surjawidjaja, and Bennet Brockhagen. Long-term stability improvement of non-toxic dye-sensitized solar cells via poly(Ethylene oxide) gel electrolytes for future textile-based solar cells. *Polymers*, 12(12):1–15, 2020.

[12] Fabian Schoden, Alina Siebert, Alparslan Keskin, Konstantin Herzig, Majkel Straus, and Eva Schwenzfeier-Hellkamp. Building a wind power plant from scrap and raising public awareness for renewable energy technology in a circular economy. *Sustainability (Switzerland)*, 12(1):1–11, 2020.

[13] J Kawakita. Trends of research and development of dye-sensitized solar cells. *Sci Technol Trends*, 35:70–82, 2010.

[14] Nicole Mariotti, Matteo Bonomo, Lucia Fagiolari, Nadia Barbero, Claudio Gerbaldi, Federico Bella, and Claudia Barolo. Recent advances in eco-friendly and cost-effective materials towards sustainable dye-sensitized solar cells. *Green Chemistry*, 22(21):7168–7218, 2020.

[15] Huihui Yuan, Wei Wang, Di Xu, Quan Xu, Junjie Xie, Xinyu Chen, Tao Zhang, Changjun Xiong, Yunlong He, Yumei Zhang, Yan Liu, and Hujiang Shen. Outdoor testing and ageing of dye-sensitized solar cells for building integrated photovoltaics. *Solar Energy*, 165:233–239, 2018.

[16] Fabian Schoden, Marius Dotter, Dörthe Knefelkamp, Tomasz Blachowicz, and Eva Schwenzfeier-Hellkamp. Review of State of the Art Recycling Methods in the Context of Dye Sensitized Solar Cells. *Energies*, 14(13):3741, 2021.

[17] Andrea Ehrmann and Tomasz Błachowicz. Solarstrom aus Früchtetee. *Physik in unserer Zeit*, 51(4):196–200, 2020.

[18] Fabian Schoden, Marius Dotter, Dörthe Knefelkamp, Tomasz Blachowicz, and Eva Schwenzfeier-Hellkamp. Review of State of the Art Recycling Methods in the Context of Dye Sensitized Solar Cells. *Energies*, 14(13):3741, 2021.

[19] Paul Anastas and C. John Warner. *Green Chemistry: Theory and Practice*. Oxford University Press, 2000.

[20] M. L. Parisi, S. Maranghi, L. Vesce, A. Sinicropi, A. Di Carlo, and R. Basosi. Prospective life cycle assessment of third-generation photovoltaics at the pre-industrial scale: A long-term scenario approach. *Renewable and Sustainable Energy Reviews*, 121:109703, 2020.

[21] Kati Miettunen and Annukka Santasalo-Aarnio. Eco-design for dye solar cells: From hazardous waste to profitable recovery. *Journal of Cleaner Production*, 320:128743, 2021.

[22] M. J. de Wild-Scholten and A. C. Veltkamp. Environmental life cycle analysis of large area dye sensitized solar modules; status and outlook. *Presented at: 22nd European Photovoltaic Solar Energy Conference and Exhibition*, 3:3–7, 2007.

[23] M. S. Chowdhury, Kazi Sajedur Rahman, Vidhya Selvanathan, A. K.Mahmud Hasan, M. S. Jamal, Nurul Asma Samsudin, Md Akhtaruzzaman, Nowshad Amin, and Kuaanan Techato. Recovery of FTO coated glass substrate: Via environment-friendly facile recycling perovskite solar cells. *RSC Advances*, 11(24):14534–14541, 2021.

[24] Fabian Schoden, Anna Katharina Schnatmann, Emma Davies, Dirk Diederich, Jan Lukas Storck, Dörthe Knefelkamp, Tomasz Blachowicz, and Eva Schwenzfeier-Hellkamp. Investigating the recycling potential of glass based dye-sensitized solar cells – melting experiment. *Materials*, 14(21):6622, 2021.

[25] Fabian Schoden, Joscha Detzmeier, Anna Katharina Schnatmann, Tomasz Blachowicz, and Eva Schwenzfeier-Hellkamp. Investigating the Remanufacturing Potential of Dye-Sensitized Solar Cells. *Sustainability (Switzerland)*, 14(9):5670, 2022.

[26] Brian O'Regan and Michael Grätzel. A low-cost, high-efficiency solar cell based on dye-sensitized colloidal TiO2 films. *Nature*, 354:737–740, 1991.

[27] Henrik Pettersson, Kazuteru Nonomura, Lars Kloo, and Anders Hagfeldt. Trends in patent applications for dye-sensitized solar cells. *Energy and Environmental Science*, 5(6):7376–7380, 2012.

[28] Ana Belén Muñoz-García, Iacopo Benesperi, Gerrit Boschloo, Javier J. Concepcion, Jared H. Delcamp, Elizabeth A. Gibson, Gerald J. Meyer, Michele Pavone, Henrik Pettersson, Anders Hagfeldt, and Marina Freitag. Dye-sensitized solar cells strike back. *Chemical Society Reviews*, 50(22):12450–12550, 2021.

[29] Anders Hagfeldt, Gerrit Boschloo, Licheng Sun, Lars Kloo, and Henrik Pettersson. Dye-Sensitized Solar Cells. *Chem. Rev.*, 110:6595–6663, 2010.

[30] Solaronix SA. Solaronix. https://www.solaronix.com/, last accessed 01/11/2023.

[31] G24 Power. GCell. https://gcell.com/about-g24-power, last accessed 01/11/2023.

[32] Jason B. Baxter. Commercialization of dye sensitized solar cells: Present status and future research needs to improve efficiency, stability, and manufacturing. *Journal of Vacuum Science & Technology A: Vacuum, Surfaces, and Films*, 30(2):020801, 2012.

[33] Michael Grätzel. Dye-sensitized solar cells. *Journal of Photochemistry and Photobiology C: Photochemistry Reviews*, 4(2):145–153, 2003.

[34] R. Grünwald and H. Tributsch. Mechanisms of instability in ru-based dye sensitization solar cells. *Journal of Physical Chemistry B*, 101(14):2564–2575, 1997.

[35] Grand View Research. Dye Sensitized Solar Cell Market Size, Share & Trends Analysis Report By Application. Technical report, Grand View Research, 2020.

[36] Dan Zhang, Marko Stojanovic, Yameng Ren, Yiming Cao, Felix T. Eickemeyer, Etienne Socie, Nick Vlachopoulos, Jacques E. Moser, Shaik M. Zakeeruddin, Anders Hagfeldt, and Michael Grätzel. A molecular photosensitizer achieves a V oc of 1.24 V enabling highly efficient and stable dye-sensitized solar cells with copper(II/I)-based electrolyte. *Nature Communications*, 12(1):2–11, 2021.

[37] Geetam Richhariya, Bhim Charan Meikap, and Anil Kumar. Review on fabrication methodologies and its impacts on performance of dye-sensitized solar cells. *Environmental Science and Pollution Research 2021 29:11*, 29(11):15233–15251, 2022.

[38] Klaudia Pawlus and Tomasz Jarosz. Transition Metal Coordination Compounds as Novel Materials for Dye-Sensitized Solar Cells. *Applied Sciences*, 12(7):3442, 2022.

[39] Suphawit Udomrungkhajornchai, Irén Juhász Junger, and Andrea Ehrmann. Optimization of the TiO_2 layer in DSSCs by a nonionic surfactant. *Optik*, 203:163945, 2020.

[40] Florian Hölscher, Peer Robin Trümper, Irén Juhász Junger, Eva Schwenzfeier-Hellkamp, and Andrea Ehrmann. Raising reproducibility in dye-sensitized solar cells under laboratory conditions. *Journal of Renewable and Sustainable Energy*, 10(1):013506, 2018.

[41] Mario Alberto Sánchez-García, Xim Bokhimi, Sergio Velázquez Martínez, and Antonio Esteban Jiménez-González. Dye-Sensitized Solar Cells Prepared with Mexican Pre-Hispanic Dyes. *Journal of Nanotechnology*, 2018(1236878):8, 2018.

[42] Irén Juhász Junger, Agit Tellioglu, and Andrea Ehrmann. Refilling DSSCs as a method to ensure longevity. *Optik*, 160:255–258, 2018.

[43] Moon Sung Kang, Jong Hak Kim, Jongok Won, and Yong Soo Kang. Oligomer approaches for solid-state dye-sensitized solar cells employing polymer electrolytes. *Journal of Physical Chemistry C*, 111(13):5222–5228, 2007.

[44] Marius Dotter, Jan Lukas Storck, Michelle Surjawidjaja, Sonia Adabra, and Timo Grothe. Investigation of the long-term stability of different polymers and their blends with peo to produce gel polymer electrolytes for non-toxic dye-sensitized solar cells. *Applied Sciences (Switzerland)*, 11:5834, 2021.

[45] Katrin Gossen and Andrea Ehrmann. Glycerin-based electrolyte for reduced drying of dye-sensitized solar cells. *Optik*, 207:163772, 2020.

[46] Qifeng Zhang, Christopher S. Dandeneau, Xiaoyuan Zhou, and Cuozhong Cao. ZnO nanostructures for dye-sensitized solar cells. *Advanced Materials*, 21(41):4087–4108, 2009.

[47] K. Tennakone, V. P.S. Perera, I. R.M. Kottegoda, and G. R.R.A. Kumara. Dye-sensitized solid state photovoltaic cell based on composite zinc oxide/tin (IV) oxide films. *Journal of Physics D: Applied Physics*, 32(4):374–379, 1999.

[48] Okoye Ikechukwu Francis and Alaekwe Ikenna. Review of Dye-Sensitized Solar Cell (DSSCs) Development. *Natural Science*, 13(12):496–509, 2021.

[49] Yu Bai, Iván Mora-Seró, Filippo De Angelis, Juan Bisquert, and Peng Wang. Titanium dioxide nanomaterials for photovoltaic applications. *Chemical Reviews*, 114(19):10095–10130, 2014.

[50] Leinig Perazolli, Luciana Nuñez, Milady Renata Apolinário da Silva, Guilherme Francisco Pegler, Ademir Geraldo Cavalarri Costalonga, Rossano Gimenes, Márcia Matiko Kondo, and Maria Aparecida Zaghete Bertochi. TiO2/CuO Films Obtained by Citrate Precursor Method for Photocatalytic Application. *Materials Sciences and Applications*, 02(06):564–571, 2011.

[51] International Union, O F Pure, and Applied Chemistry. Recommendations for the characterization of porous solids (Technical Report). *Pure and Applied Chemistry*, 66(8):1739–1758, 1994.

[52] Seigo Ito, Takurou N. Murakami, Pascal Comte, Paul Liska, Carole Grätzel, Mohammad K. Nazeeruddin, and Michael Grätzel. Fabrication of thin film dye sensitized solar cells with solar to electric power conversion efficiency over 10%. *Thin Solid Films*, 516(14):4613–4619, 2008.

[53] Chia Yuan Chen, Mingkui Wang, Jheng Ying Li, Nuttapol Pootrakulchote, Leila Alibabaei, Cevey Ha Ngoc-Le, Jean David Decoppet, Jia Hung Tsai, Carole Grätzel, Chun Guey Wu, Shaik M. Zakeeruddin, and Michael Grätzel. Highly efficient light-harvesting ruthenium sensitizer for thin-film dye-sensitized solar cells. *ACS Nano*, 3(10):3103–3109, 2009.

[54] Hironobu Ozawa, Yu Okuyama, and Hironori Arakawa. Effective enhancement of the performance of black dye based dye-sensitized solar cells by metal oxide surface modification of the TiO_2 photoelectrode. *Dalton Transactions*, 41(17):5137–5139, 2012.

[55] Seigo Ito, Hidetoshi Miura, Satoshi Uchida, Masakazu Takata, Koichi Sumioka, Paul Liska, Pascal Comte, Peter Péchy, and Michael Grätzel. High-conversion-efficiency organic dye-sensitized solar cells with a novel indoline dye. *Chemical Communications*, (41):5194–5196, 2008.

[56] Jiabao Yang, Paramaguru Ganesan, Joël Teuscher, Thomas Moehl, Yong Joo Kim, Chenyi Yi, Pascal Comte, Kai Pei, Thomas W. Holcombe, Mohammad Khaja Nazeeruddin, Jianli Hua, Shaik M. Zakeeruddin, He Tian, and Michael Grätzel. Influence of the donor size in D-π-A organic dyes for dye-sensitized solar cells. *Journal of the American Chemical Society*, 136(15):5722–5730, 2014.

[57] Khushboo Sharma, Vinay Sharma, and S. S. Sharma. Dye-Sensitized Solar Cells: Fundamentals and Current Status. *Nanoscale Research Letters*, 13(1):1–46, 2018.

[58] Ji Hye Kim, Dong Hyuk Kim, Ju Hee So, and Hyung Jun Koo. Toward eco-friendly dye-sensitized solar cells (DSSCs): Natural dyes and aqueous electrolytes. *Energies*, 15(1):219, 2022.

[59] N. T.R.N. Kumara, Piyasiri Ekanayake, Andery Lim, Louis Yu Chiang Liew, Mohammad Iskandar, Lim Chee Ming, and G. K.R. Senadeera. Layered co-sensitization for enhancement of conversion efficiency of natural dye sensitized solar cells. *Journal of Alloys and Compounds*, 581:186–191, 2013.

[60] Mahmoud A.M. Al-Alwani, Abu Bakar Mohamad, Abd Amir H. Kadhum, and Norasikin A. Ludin. *Effect of solvents on the extraction of natural pigments and adsorption onto TiO_2 for dye-sensitized solar cell applications*, volume 138. Elsevier B.V., 2015.

[61] Puhong Wen, Yinfeng Han, and Weixing Zhao. Influence of TiO_2 nanocrystals fabricating dye-sensitized solar cell on the absorption spectra of N719 sensitizer. *International Journal of Photoenergy*, 2012(Ii):1–8, 2012.

[62] Aswani Yella, Hsuan Wei Lee, Hoi Nok Tsao, Chenyi Yi, Aravind Kumar Chandiran, Md Khaja Nazeeruddin, Eric Wei Guang Diau, Chen Yu Yeh, Shaik M. Zakeeruddin, and Michael Grätzel. Porphyrin-sensitized solar cells with cobalt (II/III)-based redox electrolyte exceed 12 percent efficiency. *Science*, 334(6056):629–634, 2011.

[63] Mingxing Wu and Tingli Ma. Platinum-free catalysts as counter electrodes in dye-sensitized solar cells. *ChemSusChem*, 5(8):1343–1357, 2012.

[64] Haider Iftikhar, Gabriela Gava Sonai, Syed Ghufran Hashmi, Ana Flávia Nogueira, and Peter David Lund. Progress on electrolytes development in dye-sensitized solar cells. *Materials*, 12(12):1998, 2019.

[65] Myung Jong Ju, In Yup Jeon, Hong Mo Kim, Ji Il Choi, Sun Min Jung, Jeong Min Seo, In Taek Choi, Sung Ho Kang, Han Seul Kim, Min Jong Noh, Jae Joon Lee, Hu Young Jeong, Hwan Kyu Kim, Yong Hoon Kim, and Jong Beom Baek. Edge-selenated graphene nanoplatelets as durable metal-free catalysts for iodine reduction reaction in dye-sensitized solar cells. *Science Advances*, 2(6):1–9, 2016.

[66] Jia Wei Shiu, Yen Cheng Chang, Chien Yi Chan, Hui Ping Wu, Hung Yu Hsu, Chin Li Wang, Ching Yao Lin, and Eric Wei Guang Diau. Panchromatic co-sensitization of porphyrin-sensitized solar cells to harvest near-infrared light beyond 900 nm. *Journal of Materials Chemistry A*, 3(4):1417–1420, 2015.

[67] Masud, Kyeong Min Kim, and Hwan Kyu Kim. Polymer Gel Electrolytes Based on PEG-Functionalized ABA Triblock Copolymers for Quasi-Solid-State Dye-Sensitized Solar Cells: Molecular Engineering and Key Factors. *ACS Applied Materials and Interfaces*, 12(37):42067–42080, 2020.

[68] Jan Lukas Storck, Marius Dotter, Bennet Brockhagen, and Timo Grothe. Evaluation of Novel Glycerol/PEO Gel Polymer Electrolytes for Non-Toxic Dye-Sensitized Solar Cellswith Natural Dyes Regarding Long-Term Stability and Reproducibility. *Crystals*, 10:1158, 2020.

[69] Thomas Stergiopoulos, Ioannis M. Arabatzis, Georgios Katsaros, and Polycarpos Falaras. Binary Polyethylene Oxide/Titania Solid-State Redox Electrolyte for Highly Efficient Nanocrystalline TiO_2 Photoelectrochemical Cells. *Nano Letters*, 2(11):1259–1261, 2002.

[70] M. S. Su'ait, M. Y.A. Rahman, and A. Ahmad. Review on polymer electrolyte in dye-sensitized solar cells (DSSCs). *Solar Energy*, 115:452–470, 2015.

[71] Yuan Li, Haoyuan Li, Cheng Zhong, Gjergji Sini, and Jean Luc Brédas. Characterization of intrinsic hole transport in single-crystal spiro-OMeTAD. *npj Flexible Electronics*, 1(1):1–7, 2017.

[72] Jessica Krüger, Robert Plass, Le Cevey, Marco Piccirelli, Michael Grätzel, and Udo Bach. High efficiency solid-state photovoltaic device due to inhibition of interface charge recombination. *Applied Physics Letters*, 79(13):2085–2087, 2001.

[73] Q. B. Meng, K. Takahashi, X. T. Zhang, I. Sutanto, T. N. Rao, O. Sato, A. Fujishima, H. Watanabe, T. Nakamori, and M. Uragami. Fabrication of an efficient solid-state dye-sensitized solar cell. *Langmuir*, 19(9):3572–3574, 2003.

[74] Iacopo Benesperi, Hannes Michaels, and Marina Freitag. The researcher's guide to solid-state dye-sensitized solar cells. *Journal of Materials Chemistry C*, 6(44):11903–11942, 2018.

[75] Julian Burschka, Amalie Dualeh, Florian Kessler, Etienne Baranoff, Ngoc Lê Cevey-Ha, Chenyi Yi, Mohammad K. Nazeeruddin, and Michael Grätzel. Tris(2-(1 H - pyrazol-1-yl)pyridine)cobalt(III) as p-type dopant for organic semiconductors and its application in highly efficient solid-state dye-sensitized solar cells. *Journal of the American Chemical Society*, 133(45):18042–18045, 2011.

[76] In Chung, Byunghong Lee, Jiaqing He, Robert P.H. Chang, and Mercouri G. Kanatzidis. All-solid-state dye-sensitized solar cells with high efficiency. *Nature*, 485(7399):486–489, 2012.

[77] Xiang Wu, Bo Wu, Zhiguo Zhu, Muhammad Tayyab, and Deqing Gao. Importance and Advancement of Modification Engineering in Perovskite Solar Cells. *Solar RRL*, 6(7):2200171, 2022.

[78] Mritunjaya Parashar, Mohin Sharma, and Anupama B. Kaul. Solution-Processed Perovskite Photoabsorbers with Mixed Cations for Improved Stability in Solar Cells. In *Minerals, Metals and Materials Series*, pages 1377–1384. Springer, Cham, 2022.

[79] Kai Li Wang, Yan Hui Lou, Meng Li, Xiao Mei Li, Igbari Femi, Ying Guo Yang, Xing Yu Gao, Heng Ma, and Zhao Kui Wang. Induced charge transfer bridge by

non-fullerene surface treatment for high-performance perovskite solar cells. *Applied Physics Letters*, 115:183503, 2019.

[80] Qiaohui Zhang, Cuncun Wu, and Lixin Xiao. Bi-based Lead-free Perovskite Solar Cells. In *Conference Proceedings of the IEEE Photovoltaic Specialists Conference*, pages 0077–0078. Institute of Electrical and Electronics Engineers Inc., 2020.

[81] Taihana Paula and Maria de Fatima Marques. Recent advances in polymer structures for organic solar cells: A review. *AIMS Energy*, 10(1):149–176, 2022.

[82] Annick Anctil, Callie Babbitt, Brian Landi, and Ryne P. Rafaelle. Life-Cycle Assessment of Organic Solar Cell Technologies. In *IEEE Photovoltaic Specialists Conference*, pages 742–747, Honolulu, 2010. IEEE.

[83] Harrison Ka Hin Lee, Jiaying Wu, Jérémy Barbé, Sagar M. Jain, Sebastian Wood, Emily M. Speller, Zhe Li, Fernando A. Castro, James R. Durrant, and Wing Chung Tsoi. Organic photovoltaic cells-promising indoor light harvesters for self-sustainable electronics. *Journal of Materials Chemistry A*, 6(14):5618–5626, 2018.

[84] Daniela C.A. Pigosso, Henrique Rozenfeld, and Tim C. McAloone. Ecodesign maturity model: A management framework to support ecodesign implementation into manufacturing companies. *Journal of Cleaner Production*, 59:160–173, 2013.

[85] Maria Laura Parisi, Simone Maranghi, and Riccardo Basosi. The evolution of the dye sensitized solar cells from Grätzel prototype to up-scaled solar applications: A life cycle assessment approach. *Renewable and Sustainable Energy Reviews*, 39:124–138, 2014.

[86] Samaneh Mozaffari, Mohammad Reza Nateghi, and Mahmood Borhani Zarandi. An overview of the Challenges in the commercialization of dye sensitized solar cells. *Renewable and Sustainable Energy Reviews*, 71:675–686, 2017.

[87] Nur Ifthitah Mustafa, Norasikin Ahmad Ludin, Norani Muti Mohamed, Mohd Adib Ibrahim, Mohd Asri Mat Teridi, Suhaila Sepeai, Azami Zaharim, and Kamaruzzaman Sopian. Environmental performance of window-integrated systems using dye-sensitised solar module technology in Malaysia. *Solar Energy*, 187:379–392, 2019.

[88] Matteo Bonomo Nicole Mariotti and Claudia Barolo. Emerging Photovoltaic Technologies and Eco- Design – Criticisms and Potential Improvements. In *Reliability and Ecological Aspects of Photovoltaic Modules*, pages 137–144. IntechOpen, 2020.

[89] Fabian Schoden, Anna Katharina Schnatmann, Tomasz Blachowicz, Hildegard Manz-Schumacher, and Eva Schwenzfeier-Hellkamp. Circular Design Principles Applied on Dye-Sensitized Solar Cells. *Sustainability (Switzerland)*, 14(22):15280, 2022.

[90] L'Ubomír Šooš, Miloš Matúš, Marcela Pokusová, Viliam Čačko, and Jozef Bábics. The recycling of waste laminated glass through decomposition technologies. *Recycling*, 6:26, 2021.

[91] Sylvia Ott-Welke and Achim Schiemann. Recycling von Polyvinylbutyral (PVB) aus Sicherheitsglas. Technical report, Ostfalia University of Applied Sciences, 2012.

[92] Michael Tupy, Pavel Mokrejs, Dagmar Merinska, Petr Svoboda, and Josef Zvonicek. Windshield recycling focused on effective separation of PVB sheet, 2014.

[93] Trosifol Solar. https://www.trosifol.com/, last accessed 01/11/2023.

[94] Anna Katharina Schnatmann, Fabian Schoden, and Eva Schwenzfeier-Hellkamp. Sustainable PV Module Design – Review of State-of-the-Art Encapsulation Methods. *Sustainability (Switzerland)*, 14:9971, 2022.

[95] NPC incorporated. PV Panel Recycling Service. https://www.npcgroup.net/eng/solarpower/reuse-recycle/recycle-service, last accessed 01/11/2023.

[96] ReProSolar. https://eitrawmaterials.eu/project/reprosolar/, last accessed 01/11/2023.

[97] Jörg Glatthaar, Emmanuel Kamdje, Ubbo Ricklefs, Ernst A Stadlbauer, J Glatthaar, E Kamdje, J B Barnickel, M Dax, V Schaub, H G Stevens, B Jehle, U Ricklefs, E A Stadlbauer, and H Weigand. Development of a modular cradle to cradle process-chain for c-Si-PV panel recycling. In *33rd European Photovoltaic Solar Energy Conference and Exhibition*, pages 1528–1532, 2017.

[98] pvXchange. https://www.pvxchange.com/, last accessed 01/11/2023.

[99] Second Sol. https://www.secondsol.com/, last accessed 01/11/2023.

[100] Rinovasol. https://www.rinovasol.de/, last accessed 01/11/2023.

[101] Solar-pur GmbH. https://www.solar-pur.de/, last accessed 01/11/2023.

[102] Lisa Krueger. Overview of First Solar's Module Collection and Recycling Program. https://www.bnl.gov/pv/files/prs_agenda/2_krueger_ieee-presentation-final.pdf, last accessed 01/11/2023.

[103] Vasilis Fthenakis, Clement Athias, Alyssa Blumenthal, Aylin Kulur, Julia Magliozzo, and David Ng. Sustainability evaluation of CdTe PV: An update. *Renewable and Sustainable Energy Reviews*, 123:109776, 2020.

[104] Parikhit Sinha, Sukhwant Raju, Karen Drozdiak, and Andreas Wade. Life cycle management and recycling of PV systems. www.pv-tech.org, last accessed 01/11/2023.

[105] E Saint-Sernin, R Einhaus, K Bamberg, and P Panno. Industrialisation of Apollon Solar's nice Module Technology. *Pv-Sec*, (January 2008):4, 2008.

[106] Nees Jan van Eck and Ludo Waltman. Software survey: VOSviewer, a computer program for bibliometric mapping. *Scientometrics*, 84(2):523–538, 2010.

[107] Carl Zeiss AG. ZEISS EVO. https://www.zeiss.com/microscopy/us/home.html, last accessed 01/31/2023.

[108] Thermo Fisher Scientific Inc. Pushing the boundaries of ICP performance with the iCAP 6000 Series – 66 Elements with detection limits less than 1μg/L. https://static.thermoscientific.com/images/D01567∼.pdf, last accessed 02/02/2023, 2008.

[109] Retsch GmbH. Mixer Mill MM 400. https://www.retsch.com/products/milling/ball-mills/mixer-mill-mm-400/, last accessed 02/02/2023.

[110] Memmert GmbH & Co.KG. UF260 Precise drying, heating, ageing, burn-in and hardening in research, science, industry and quality assurance. https://www.memmert.com/products/heating-drying-ovens/universal-oven/UF260/#technical-specification, last accessed 02/02/2023.

[111] CEM Corporation. Microwave MARS 6. https://cem.com/mars-6/, last accessed 02/02/2023.

[112] Carbolite Gero Ltd. Laboratory Chamber Furnace – CWF. https://www.carbolite-gero.com/products/chamber-furnaces/laboratory-furnaces/cwf-standard-chamber-furnaces/, last accessed 02/03/2023.

[113] ZEISS Microscopy. ZEISS SteREO Discovery.V20. https://www.zeiss.com/microscopy/en/products/light-microscopes/stereo-and-zoom-microscopes/stereo-discovery-v20.html, last accessed 02/03/2023.

[114] Antonis Nanakoudis. EDX Analysis with SEM: How Does it Work? https://www.thermofisher.com/blog/materials/edx-analysis-with-sem-how-does-it-work/, last accessed 01/31/2023.

[115] DC Bell and AJ Garratt-Reed. *Energy Dispersive X-ray Analysis in the Electron Microscope*. Taylor & Francis, 2003.

[116] DIN German Institute for Standardization. Microbeam analysis – Quantitative analysis using energy-dispersive spectrometry (EDS) for elements with an atomic number of 11 (Na) or above (ISO 22309:2011). November, 2015.

[117] Thermo Fisher Scientific Inc. iCAP 6300 ICP Spectrometer. http://www.nbg.kiev.ua/upload/image/scea/iCAP.pdf, last accessed 02/02/2023.

[118] DIN German Institute for Standardization. Testing of oxidic raw materials and materials for ceramics, glass and glazes – Part 2: Determination of Ag, As, B,..., W, Y, Yb, Zn, Zr by optical emission spectrometry with inductively coupled plasma (ICP OES). July, 2004.

[119] Neale Zachary. Inductively coupled plasma optical emission spectroscopy (ICP-OES) Overview. https://i.ytimg.com/vi/InFhIHPZYIc/maxresdefault.jpg, last accessed 02/02/2023.

[120] Richard D Beaty and Jack D Kerber. *Concepts , Instrumentation and Techniques in Atomic Absorption Spectrophotometry*. Perkin-Elmer Corporation, 1997.

[121] Nabertherm GmbH. Muffle Furnaces up to 1100 Â°C or 1200 Â°C. https://nabertherm.com/en/products/laboratory/muffle-furnaces/muffle-furnaces-1100-degc-or-1200-degc, last accessed 02/02/2023.

[122] Inc. Tektronix. Model 2450 SourceMeter. https://www.tek.com/en, last accessed 02/02/2023.

[123] Leistungselektronik JENA GmbH. Light Source LQ-XEAR 100DC. https://www.lej.de/lq-xear-100dc-234.html, last accessed 02/02/2023.

[124] Carl Zeiss Microscopy Deutschland GmbH. Axio Observer 7 materials. https://www.micro-shop.zeiss.com/en/de/system/axio+observer-axio+observer+7+materials-inverted+microscopes/10295/, last accessed 02/03/2023.

[125] Thermo Fisher Scientific Inc. UV-Vis spectrophotometer Genesys 10S. https://www.fishersci.de/de/en/home.html?change_lang=true, last accessed 02/03/2023.

[126] Nanosurf. The most flexible atomic force microscope for materials research. https://www.nanosurf.com/en/, last accessed 02/24/2023.

[127] Innovative Solutions Bulgaria Ltd. Tap190Al-G. https://www.budgetsensors.com/tapping-mode-afm-probe-long-cantilever-aluminum-tap190al, last accessed 03/01/2023.

[128] Bert Voigtländer. *Atomic Force Microscopy*. Springer Cham, 2 edition, 2019.

[129] David Nečas and Petr Klapetek. Gwyddion.

[130] ImageJ. ImageJ – Image Processing and Analysis in Java. https://imagej.net/ij/index.html, last accessed 03/06/2023.

[131] Conny Bakker, Marcel den Hollander, Ed van Hinte, and Yvo Zijlstra. *Products that last: product design for circular business models*. Marcel den Hollander, 1st edition, 2014.

[132] CIRCO. CIRCO method. https://www.circonl.nl/international/methodology/, last accessed 01/11/2023.

[133] Schott Ag. * DE102010023366B420170921 * patent, 2017.

[134] Maria Laura Parisi, Alessio Dessì, Lorenzo Zani, Simone Maranghi, Sanaz Mohammadpourasl, Massimo Calamante, Alessandro Mordini, Riccardo Basosi, Gianna Reginato, and Adalgisa Sinicropi. Combined LCA and Green Metrics Approach for the Sustainability Assessment of an Organic Dye Synthesis on Lab Scale. *Frontiers in Chemistry*, 8:214, 2020.

[135] Bastian Bohnenkamp, Jan Hendrik Linnemann, Irén Juhász Junger, Eva Schwenzfeier-Hellkamp, and Andrea Ehrmann. Influence of dyes and dying process parameters on the electrical properties of dye-sensitized solar cells. *Optik*, 168:282–286, 2018.

[136] Sakshi Sharma. Carbon Nanotubes in Emerging Photovoltaics : Progress and Limitations. *Journal of Photovoltaics*, 12(1):167–178, 2022.

[137] Zhexun Yu, Quanxin Zhang, Da Qin, Yanhong Luo, Dongmei Li, Qing Shen, Taro Toyoda, and Qingbo Meng. Highly efficient quasi-solid-state quantum-dot-sensitized solar cell based on hydrogel electrolytes. *Electrochemistry Communications*, 12(12):1776–1779, 2010.

[138] Christian Hellert, Christian Klemt, Uta Scheidt, Irén Juhász Junger, Eva Schwenzfeier-Hellkamp, and Andrea Ehrmann. Rehydrating dye sensitized solar cells. *AIMS Energy*, 5(3):397–403, 2017.

[139] C. C. Chen, F. C. Chang, C. Y. Liao, and H. Paul Wang. Copper nanowires on recycled conducting glass for DSSC electrodes. In *Technical Proceedings of the 2012 NSTI Nanotechnology Conference and Expo, NSTI-Nanotech 2012*, pages 18–21, 2012.

[140] Muhammad Ayaz, Jafar Khan Kasi, Ajab Khan Kasi, and Mustafa Ali. Toward Eco Green Energy: Fabrication of DSSC from Recycled Phone Screen. *The Open Access Journal of Resistive Economics International Journal of Resistive Economics*, 4(1):2345–4954, 2016.

[141] Stadtwerke Aachen Aktiengesellschaft. Photovoltaic for rent. https://www.stawag.de/produkte/photovoltaik-zum-mieten/, last accessed 01/11/2023.

[142] SwissTech Convention Center. SwissTech Convention Center. https://www.stcc.ch/, last accessed 02/16/2023.

[143] Martin Schachinger. PV-Magazine: Module Price Index. https://www.pv-magazine.com/module-price-index/, last accessed 01/11/2023, 2021.

[144] Gomesh Nair, Mohammad Shafawi, Muhammad Irwanto, Mohd Irwan Yusoff, Muhammad Fitra, and Norman Mariun. Performance improvement of dye sensitized solar cell by using recycle material for counter electrode. *Applied Mechanics and Materials*, 446-447:823–826, 2014.

[145] I. Daut, M. Fitra, M. Irwanto, N. Gomesh, and Y. M. Irwan. TiO_2 dye sensitized solar cells cathode using recycle battery. *Journal of Physics: Conference Series*, 36:333–340, 2013.

[146] Edigar Muchuweni, Bice S. Martincigh, and Vincent O. Nyamori. Recent advances in graphene-based materials for dye-sensitized solar cell fabrication. *RSC Advances*, 10(72):44453–44469, 2020.

[147] Weidong Zhu, Wenming Chai, Dandan Chen, He Xi, Dazheng Chen, Jingjing Chang, Jincheng Zhang, Chunfu Zhang, and Yue Hao. Recycling of FTO/TiO_2 Substrates: Route toward Simultaneously High-Performance and Cost-Efficient Carbon-Based, All-Inorganic $CsPbIBr_2$ Solar Cells. *ACS Applied Materials and Interfaces*, 12(4):4549–4557, 2020.

[148] Lenka Kuchariková, Eva Tillová, and Otakar Bokůvka. Recycling and properties of recycled aluminium alloys used in the transportation industry. *Transport Problems*, 11(2):117–122, 2016.

[149] Ruud Beerkens, Goos Kers, and Engelbert van Santen. Recycling of Post-Consumer Glass: Energy Saving, CO_2 Emission Reduction, Effects on Glass Quality and Glass Melting. In Charles H. Drummond, editor, *71st Conference on Glass Problems*, pages 167–194, Eindhoven, 2011.

[150] Dheeraj Devadiga, M. Selvakumar, Prakasha Shetty, and M. S. Santosh. Recent progress in dye sensitized solar cell materials and photo-supercapacitors: A review. *Journal of Power Sources*, 493:229698, 2021.

[151] M Mehedi Hasan, Didarul Islam, and Taslim Ur Rashid. Biopolymer-Based Electrolytes for Dye-Sensitized Solar Cells: A Critical Review. *Energy & Fuels*, 34(12):15634–15671, 2020.

[152] Rahul Singh, Anji Reddy Polu, B. Bhattacharya, Hee Woo Rhee, Canan Varlikli, and Pramod K. Singh. Perspectives for solid biopolymer electrolytes in dye sensitized solar cell and battery application. *Renewable and Sustainable Energy Reviews*, 65:1098–1117, 2016.

[153] Earle R Caley. The Action of Hydriodic Acid on Stannic Oxide. *Journal of the American Chemical Society*, 54(8):3240–3243, 1932.

[154] Egon. Wiberg, Nils. Wiberg, and A F Holleman. *Inorganic chemistry*. Academic Press; De Gruyter, San Diego; Berlin; New York, 2001.

[155] Helmut A. Schaefer and Roland Langfeld. *Werkstoff Glas Alter Werkstoff mit großer Zukunft*. Springer-Verlag, 2 edition, 2020.

[156] T. T. Volotinen, J. M. Parker, and P. A. Bingham. Concentrations and site partitioning of Fe^{2+} and Fe^{3+} ions in a soda-lime-silica glass obtained by optical absorbance spectroscopy. *Physics and Chemistry of Glasses: European Journal of Glass Science and Technology Part B*, 49(5):258–270, 2008.

[157] Malte Ruben Vogt, Harald Hahn, Hendrik Holst, Matthias Winter, Carsten Schinke, Marc Kontges, Rolf Brendel, and Pietro P. Altermatt. Measurement of the optical constants of soda-lime glasses in dependence of iron content and modeling of iron-related power losses in crystalline si solar cell modules. *IEEE Journal of Photovoltaics*, 6(1):111–118, 2016.

[158] Joseph M. Kuitche, Rong Pan, and Govindasamy Tamizhmani. Investigation of dominant failure mode(s) for field-aged crystalline silicon PV modules under desert climatic conditions. *IEEE Journal of Photovoltaics*, 4(3):814–826, 2014.

[159] Surendra K. Yadav, Sandheep Ravishankar, Sara Pescetelli, Antonio Agresti, Francisco Fabregat-Santiago, and Aldo Di Carlo. Stability of dye-sensitized solar cells under extended thermal stress. *Physical Chemistry Chemical Physics*, 19(33):22546–22554, 2017.

[160] Karuppannan Rokesh, Sambandam Anandan, and Kandasamy Jothivenkatachalam. Polymer Electrolytes in Dye Sensitized Solar Cells. *Materials Focus*, 4(4):262–271, 2015.

[161] S. L. Madorsicy and S. Straus. Thermal degradation of polyethylene oxide and polypropylene oxide. *Journal of Polymer Science*, 36(130):183–194, 1959.

[162] Jiawei Gong, Jing Liang, and K. Sumathy. Review on dye-sensitized solar cells (DSSCs): Fundamental concepts and novel materials. *Renewable and Sustainable Energy Reviews*, 16(8):5848–5860, 2012.

[163] Yi Fang Chiang, Ruei Tang Chen, Po Shen Shen, Peter Chen, and Tzung Fang Guo. Extension lifetime for dye-sensitized solar cells through multiple dye adsorption/desorption process. *Journal of Power Sources*, 225:257–262, 2013.

[164] Pabitra K. Nayak, Germà Garcia-Belmonte, Antoine Kahn, Juan Bisquert, and David Cahen. Photovoltaic efficiency limits and material disorder. *Energy and Environmental Science*, 5(3):6022–6039, 2012.

[165] Neeraj Tomar, Anupam Agrawal, Vijaypal Singh, and Praveen K Surolia. Ruthenium complexes based dye sensitized solar cells : Fundamentals and research trends. *Solar Energy*, 207:59–76, 2020.

[166] Geetam Richhariya and Anil Kumar. Natural dyes for dye sensitized solar cell : A review. *Renewable and Sustainable Energy Reviews*, 69:705–718, 2017.

[167] Khwanchit Wongcharee, Vissanu Meeyoo, and Sumaeth Chavadej. Dye-sensitized solar cell using natural dyes extracted from rosella and blue pea flowers. *Solar Energy Materials and Solar Cells*, 91(7):566–571, 2007.

[168] Zhaoke Zheng, Baibiao Huang, Zeyan Wang, Meng Guo, Xiaoyan Qin, Xiaoyang Zhang, Peng Wang, and Ying Dai. Crystal faces of Cu2O and their stabilities in photocatalytic reactions. *Journal of Physical Chemistry C*, 113(32):14448–14453, 2009.

[169] Norio Sato. *Electrochemistry at Metal and Semiconductor Electrodes*. Elsevier, 1998.

[170] European Commission. The European Green Deal. *European Commission*, 53(9):24, 2019.

[171] European Commission. Corporate sustainability due diligence | European Commission. https://ec.europa.eu/info/business-economy-euro/doing-business-eu/corporate-sustainability-due-diligence_en, last accessed 01/11/2023.

List of figures

List of tables

List of abbreviations

- Al – aluminum
- a-Si – amorphous silicon
- AFM – atomic force microscopy
- BIPV – building integrated photovoltaic
- C – carbon
- CdTe – cadmium telluride
- CED – cumulative energy demand
- CIS – copper indium diselenide
- cps – counts per second
- c-Si – PV crystalline silicon photovoltaic
- DSSC – dye-sensitized solar cell
- EPBT – energy payback time
- EVA – ethylene-vinyl acetate
- FF – fill factor
- FTO – fluorine-doped tin oxide
- GHG – greenhouse gas
- ICP-OES – inductively coupled plasma optical emission spectrometry
- J_{sc} – short circuit current
- LCA – life-cycle assessment

- MW – molecular weight
- Na – sodium
- O – oxygen
- PAN – polyacrylonitrile
- PCE – power conversion efficiency
- PEO – polyethylene oxide
- Pestel – political, economic, social, technological, environmental and legal
- P_M – power at the maximum power point
- PVB – polyvinyl butyral
- R_q – root mean square roughness
- SEM-EDX – scanning electron microscopy energy dispersive X-ray
- Si – silicon
- Sn – tin
- SnO_2 – tin oxide
- TCO – transparent conductive oxide
- TFT-LCD – transistor liquid crystal displays
- Ti – titanium
- TiO_2 – titanium dioxide
- UV-Vis – ultraviolet–visible
- V_{oc} – circuit voltage

- WBS – work breakdown structure
- ZnO – zinc oxide

Appendix – detailed technical information about the equipment

In figures 55 and 56 the detailed technical information about the Carl Zeiss EVO MA10 are shown.

		ZEISS EVO 10
Resolution: High Vaccum Mode	2 nm, 3 nm @ 30 kV SE with LaB_6, W	
	6 nm, 8 nm @ 3 kV SE with LaB_6, W	
	9 nm, 15 nm @ 1 kV SE with LaB_6, W	
	3.8 nm, 4 nm @ 30kV BSE with LaB_6, W	
Resolution: VP Mode	3 nm, 3.4 nm @ 30 kV SE VP mode with LaB_6, W	
Acceleration Voltage	0.2 to 30 kV	
Probe Current	0.5 pA to 5 µA	
Magnification		< 7 – 1,000,000×
Field of View	6 mm at Analytical Working Distance (AWD)	
X-ray Analysis	8.5 mm AWD and 35° take-off angle	
OptiBeam(1) Modes	Resolution, Depth, Analysis, Field, Fisheye(2)	
Pressure Range	10 – 133 Pa (EasyVP) 10 - 400 Pa (Variable Pressure)	
	10 – 3000 Pa (Extended Pressure)	
Available Detectors	SE – Everhart-Thornley Secondary Electron Detector (supplied as standard)	
	HDBSD / BSD1 – Solid State Backscattered Electron, 5 quadrants YAG-BSD – YAG Crystal Backscattered Electron Detector	
	VPSE-G4 – Variable Pressure Secondary Electron Detector C2D – Cascade Current Detector Detector C2DX – Extended Range Cascade Current Detector	
	SCD – Specimen Current Detector	
	STEM – Scanning Transmission Electron Microscopy Detector	
	CL – Cathodoluminescence Detector	
	ZEISS SmartEDX – Energy Dispersive Spectrometer (EDS)	
	WDS – Wavelength Dispersive Spectrometer	
	EBSD – Electron Backscatter Diffraction Detector	

Figure 55: Technical Specifications: Carl Zeiss EVO MA10 Part 1 [107].

		ZEISS EVO 10
Chamber Dimensions		310 mm (Ø) x 220 mm (h)
5-Axes Motorized Specimen Stage	Stage control by mouse or optional joystick and control panel	X = 80 mm, Y = 100 mm, Z = 35 mm, T = -10° to 90°, R = 360° (continuous)
Maximum Specimen Height		100 mm
Future Assured Upgraded Paths[2]	BeamSleeve, Extended Pressure, Water vapor VP and EP	
Image Framestore	32,000 x 24,000 pixels, signal acquisition by integration and averaging (scan speed 2 or above)	
System Control	SmartSEM[3] GUI operated by mouse and keyboard	
	SmartSEM Touch[2] GUI operated by 23" touchscreen, mouse and optional hardware control panel	
	Hardware control panel with rotary controls for improved manual feedback and more intuitive control during imaging	
	Ease of use features – auto saturation, auto align, sample selection & automated imaging	
	Windows® 10 multilingual operating system	
Utility Requirements	100 – 240 V, 50 or 60 Hz single phase, no water cooling requirement	

[1] Optibeam – active column control for best resolution, best depth of field or best field of view
[2] Optional upgrade
[3] SmartSEM – Sixth generation SEM control Graphical User Interface

Figure 56: Technical Specifications: Carl Zeiss EVO MA10 Part 2 [107].

In figure 57 the detailed technical information about the SmartEDX are shown.

Detector	
Type	Silicon Drift
Cooling	Peltier (LN-free)
Active Area	30 mm^2
Window	Silicon Nitride (Si_3N_4)
Mount	Fixed or Slide (optional, recommended for particle analysis)
Detection Range	Be (4) to Am (95)

Pulse Processor	
Amplification Time	Three settings: Resolution, Middle and Speed
Best Energy Resolution	129 eV for Mn Ka
Input Count Rate (ICPS)	Up to 1.000.000 CPS
Output Count Rate (OCPS)	Up to 300.000 CPS (Speed amp time)
	Up to 40.000 CPS (Resolution amp time)

Key Features	
Peak Deconvolution	Included
Quantitative Analysis	Standardless, ZAF corrected. Spectrum Matching
Multipoint Analysis	Included
Elemental Linescan	Intensities (CPS) or Quant
Elemental Mapping	Intensities (CPS) or Quant
Drift Correction	Standard
Spectrum Matching	Optional

Figure 57: Technical Specifications: SmartEDX [107].

In figure 57 the detailed technical information about the SmartEDX are shown.

Spectrometer	Echelle type 52.91 grooves/mm ruled grating 383 mm effective focal length 9.5 ° UV fused silica cross dispersion prism
Wavelength range	166 - 847 nm
Spectral bandpass	7 pm at 200 nm
Detector	High performance CID86 chip
RF source	27.12 MHz solid state 750 - 1500 watts output power (Duo restricted to 1350 watts)
Sample pump	3-channel, 12 roller peristaltic Speed 0 - 125 rpm
Plasma gas	Fixed 12 L/min, argon
Nebulizer gas	Pressure control, from 0 - 0.4 MPa
Auxiliary gas	4 fixed flows, 0, 0.5, 1.0 and 1.5 L/min
Standard sampling kit	Concentric glass nebulizer Glass cyclone spray chamber Semi-demountable EMT torch 1.5 mm bore quartz injector (Radial) 2 mm bore quartz injector (Duo)
Dimensions	840 W x 750 D x 590 H

Figure 58: Technical Specifications: Thermo Scientific iCAP 6300 Duo [117].

In figure 59 the detailed technical information about the Mixer Mill MM 400 are shown.

TECHNICAL DATA	
Applications	size reduction, mixing, homogenization, cell disruption, cryogenic grinding
Field of application	agriculture, biology, chemistry / plastics, construction materials, electronics, environment / recycling, food, geology / metallurgy, glass / ceramics, mechanosynthesis, medicine / pharmaceuticals
Feed material	hard, medium-hard, soft, brittle, elastic, fibrous
Size reduction principle	impact, friction
Material feed size*	<= 8 mm
Final fineness*	~ 5 µm
Batch size / feed quantity*	max. 2 x 20 ml
No. of grinding stations	2
Setting of vibrational frequency	digital, 3 - 30 Hz (180 - 1800 min-1)
Typical mean grinding time	30 s - 2 min
Dry grinding	yes
Wet grinding	yes
Cryogenic grinding	yes
Cell disruption with reaction vials	yes, up to 20 x 2.0 ml
Self-centering clamping device	yes
Type of grinding jars	screw top design
Material of grinding tools	hardened steel, stainless steel, tungsten carbide, agate, zirconium oxide, PTFE
Grinding jar sizes	1.5 ml / 5 ml / 10 ml / 25 ml / 35 ml / 50ml
Setting of grinding time	digital, 10 s - 99 min
Storable SOPs	9
Electrical supply data	100-240 V, 50/60 Hz
Power connection	1-phase
Protection code	IP 30
Power consumption	150 W
W x H x D closed	371 x 266 x 461 mm
Net weight	~ 26 kg
Standards	CE

*depending on feed material and instrument configuration/settings

Figure 59: Technical Specifications: Mixer Mill MM 400 [109].

In figures 60 and 61 the detailed technical information about the Universal oven UF260 are shown.

Temperature

Working temperature range	at least 5 (UN/UNplus/UNm/UNmplus) or 10 (UF/UFplus/UFm/UFmplus) above ambient temperature to +300 °C
Setting accuracy temperature	up to 99.9 °C: 0.1 / from 100 °C: 0.5
Setting temperature range	+20 to +300 °C
Temperature sensor	1 Pt100 sensor DIN class A in 4-wire-circuit

Control technology

Language setting	German, English, Spanish, French, Polish, Czech, Hungarian
ControlCOCKPIT	SingleDISPLAY. Adaptive multifunctional digital PID-microprocessor controller with high-definition TFT-colour display
Timer	Digital backwards counter with target time setting, adjustable from 1 minute to 99 days
Function SetpointWAIT	the process time does not start until the set temperature is reached
Calibration	three freely selectable temperature values
adjustable parameters	temperature (Celsius or Fahrenheit), fan speed, air flap position, programme time, time zones, summertime/wintertime

Ventilation

Fan	forced air circulation by quiet air turbine, adjustable in 10 % steps
Fresh air	Admixture of pre-heated fresh air by electronically adjustable air flap
Vent	vent connection with restrictor flap

Communication

Documentation	programme stored in case of power failure
Programming	AtmoCONTROL software for reading out, managing and organising the data logger via Ethernet interface (temporary trial version can be downloaded). USB stick with AtmoCONTROL software available as accessory (on demand).

Safety

Temperature control	adjustable electronic overtemperature monitor and mechanical temperature limiter TB, protection class 1 according to DIN 12880 to switch off the heating approx. 20°C above nominal temperature
Autodiagnostic system	for fault analysis

Standard equipment

Works calibration certificate	Calibration at +160°C
Door	fully insulated stainless steel door with 2-point locking (compression door lock)
Internals	2 stainless steel grid(s), electropolished

Figure 60: Technical Specifications: Universal oven UF260 part I [110].

Stainless steel interior

Dimensions	$w_{(A)}$ x $h_{(B)}$ x $d_{(C)}$: 640 x 800 x 500 mm (d less 39 mm for fan)
Interior	easy-to-clean interior,made of stainless steel, reinforced by deep drawn ribbing with integrated and protected large-area heating on four sides
Volume	256 l
Max. number of internals	9
Max. loading of chamber	300 kg
Max. loading per internal	20 kg

Textured stainless steel casing

Dimensions	$w_{(D)}$ x $h_{(E)}$ x $d_{(F)}$: 824 x 1183 x 684 mm (d +56mm door handle)
Housing	rear zinc-plated steel

Electrical data

Voltage **Electrical load**	230 V, 50/60 Hz approx. 3400 W
Voltage **Electrical load**	115 V, 50/60 Hz approx. 1800 W

Ambient conditions

Set Up	The distance between the wall and the rear of the appliance must be at least 15 cm. The clearance from the ceiling must not be less than 20 cm and the side clearance from walls or nearby appliances must not be less than 5 cm.
Altitude of installation	max. 2,000 m above sea level
Ambient temperature	+5 °C to +40 °C
Humidity rh	max. 80 %, non-condensing
Overvoltage category	II
Pollution degree	2

Packing/shipping data

Transport information	The appliances must be transported upright
Customs tariff number	8419 8998
Country of origin	Federal Republic of Germany
WEEE-Reg.-No.	DE 66812464
Dimensions approx incl. carton	w x h x d: 930 x 1380 x 930 mm
Net weight	approx. 110 kg
Gross weight carton	approx. 161 kg

Figure 61: Technical Specifications: Universal oven UF260 part II [110].

In figures 62 and 63 the detailed technical information about the microwave MARS6 are shown.

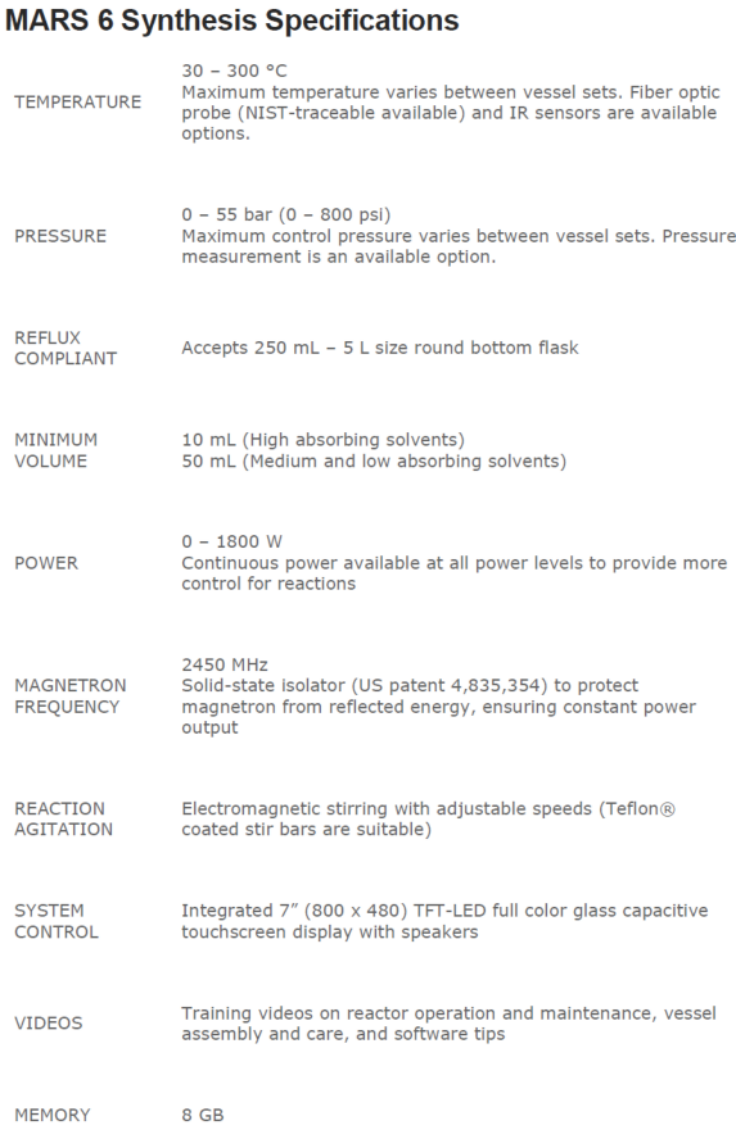

MARS 6 Synthesis Specifications

TEMPERATURE	30 – 300 °C Maximum temperature varies between vessel sets. Fiber optic probe (NIST-traceable available) and IR sensors are available options.
PRESSURE	0 – 55 bar (0 – 800 psi) Maximum control pressure varies between vessel sets. Pressure measurement is an available option.
REFLUX COMPLIANT	Accepts 250 mL – 5 L size round bottom flask
MINIMUM VOLUME	10 mL (High absorbing solvents) 50 mL (Medium and low absorbing solvents)
POWER	0 – 1800 W Continuous power available at all power levels to provide more control for reactions
MAGNETRON FREQUENCY	2450 MHz Solid-state isolator (US patent 4,835,354) to protect magnetron from reflected energy, ensuring constant power output
REACTION AGITATION	Electromagnetic stirring with adjustable speeds (Teflon® coated stir bars are suitable)
SYSTEM CONTROL	Integrated 7" (800 x 480) TFT-LED full color glass capacitive touchscreen display with speakers
VIDEOS	Training videos on reactor operation and maintenance, vessel assembly and care, and software tips
MEMORY	8 GB

Figure 62: Technical Specifications: microwave MARS 6 part I [111].

PRINTER	On-board thermal printer and USB-B compatible printer port
PORTS	5 USB, 1 USB-B, 2 Ethernet, 1 RS-232
CAVITY DESIGN	Heavy-duty 316 solid steel cavity with multi-layer Teflon® coating
SAFETY FEATURES	Three independent door safety interlocks, including an interlock monitoring system plus three independent thermal switches, are used in each instrument to prevent instrument operation and microwave emissions in case of improper door closure or misalignment. The instrument complies with HHS standards under 21 CFR, Part 1030.10, Subparts (C)(1), (C)(2) and (C)(3). Reactiguard continuously monitors the cavity and disables the magnetron if disturbances occur inside the cavity.
SAFETY APPROVALS	Conforms to Globally Harmonized EN61010-1 Standard for Safety Requirements for Electric Equipment for Measurement, Control, and Laboratory Use Part 1: General Requirements (CAN/CSA-C22.2 No. 1010.1-1992).
WEIGHT	140 lbs (63.6 kg)
DIMENSIONS	21"W x 25"D x 25" H (53.3 cm x 63.5 cm x 63.5 cm)
ELECTRICAL	200/208/230 VAC (200-253 VAC), 60 Hz, 15A @ 230 VAC (United States, Canada, Japan) 220/240 VAC (202-250 VAC), 50 Hz, 15A @ 240VAC
APPLICATIONS	Synthetic chemistry, acid digestion (sample prep for elemental analysis), solvent extraction, distillation, peptide synthesis

Figure 63: Technical Specifications: microwave MARS 6 part II [111].

In figure 64 the detailed technical information of the laboratory chamber furnace-CWF from Carbolite Gero GmbH & Co. KG are shown.

Technical data

CGH Model	Max. temp. [°C]	Heat-up time [mins]	Max. continuous operating temperature [°C]	Dimensions: Usable chamber H x W x D [mm]	Dimensions: External H x W x D [mm]	Dimensions: External with door open H x W x D [mm]	Temperature uniformity of ±5°C within H x W x D [mm]	Volume [litres]	Max. power [W]	Weight [kg]
Standard Chamber Furnaces										
CWF 11/5	1100	47	1000	135 x 140 x 250	585 x 375 x 485	800 x 375 x 485	85 x 90 x 110	5	2400	30
CWF 11/13	1100	76	1000	200 x 200 x 325	655 x 435 x 610	905 x 435 x 610	120 x 120 x 185	13	3100	47
CWF 11/23	1100	36	1000	235 x 245 x 400	705 x 505 x 675	990 x 505 x 675	155 x 165 x 285	23	7000	68
CWF 12/5	1200	51	1100	135 x 140 x 250	585 x 375 x 485	800 x 375 x 485	85 x 90 x 125	5	2400	30
CWF 12/13	1200	88	1100	200 x 200 x 325	655 x 435 x 610	905 x 435 x 610	120 x 120 x 200	13	3100	47
CWF 12/23	1200	45	1100	235 x 245 x 400	705 x 505 x 675	990 x 505 x 675	155 x 165 x 325	23	7000	68
CWF 12/36	1200	37	1100	250 x 320 x 450	810 x 690 x 780	1105 x 690 x 780	170 x 240 x 357	36	9000	100
CWF 12/65	1200	40	1100	278 x 388 x 595	885 x 780 x 945	1245 x 780 x 945	178 x 288 x 455	65	14000	165
CWF 13/5	1300	75	1200	135 x 140 x 250	585 x 375 x 485	800 x 375 x 485	85 x 90 x 150	5	2400	30
CWF 13/13	1300	121	1200	200 x 200 x 325	655 x 435 x 610	905 x 435 x 610	120 x 120 x 225	13	3100	47
CWF 13/23	1300	55	1200	235 x 245 x 400	705 x 505 x 675	990 x 505 x 675	155 x 165 x 340	23	7000	68
CWF 13/36	1300	47	1200	250 x 320 x 450	810 x 690 x 780	1105 x 690 x 780	170 x 240 x 400	36	9000	100
CWF 13/65	1300	45	1200	278 x 388 x 595	885 x 780 x 945	1245 x 780 x 945	178 x 288 x 520	65	14000	165

Figure 64: Technical Specifications: laboratory chamber furnace-CWF from Carbolite Gero GmbH & Co. KG [112].

In figure 65 the detailed technical information of the ZEISS SteREO Discovery.V20 from Carl Zeiss AG are shown.

		SteREO Discovery.V8					
		SteREO Discovery.V12					
		SteREO Discovery.V20					
Objectives		Eyepieces					
		WPL 10×/23 Br. foc.		WPL 16×/16 Br. foc.		W 25×/10 foc.	
Designation	Free working distance (FWD in mm)	Magnification	Field of view (mm)	Magnification	Field of view (mm)	Magnification	Field of view (mm)
PlanApo S 0.63×	81	6.3 x ... 50.4 x	36.5 ... 4.6	10.1 x ... 80.6 x	25.4 ... 3.2	15.8 x ... 126 x	15.9 ... 2.0
		5 x ... 63 x	45.6 ... 3.7	8 x ... 100.8 x	28.5 ... 2.3	12.6 x ... 157.5 x	18.3 ... 1.5
		4.7 x ... 94.5 x	48.7 ... 2.4	7.6 x ... 151 x	33.9 ... 1.7	11.8 x ... 236 x	21.1 ... 1.1
PlanApo S 1.0×	60	10 x ... 80 x	23.0 ... 2.9	16 x ... 128 x	16.0 ... 2.0	25 x ... 200 x	10.0 ... 1.3
		8 x ... 100 x	28.8 ... 2.3	12.8 x ... 160 x	18.0 ... 1.4	20 x ... 250 x	11.5 ... 0.9
		7.5 x ... 150 x	30.7 ... 1.5	12 x ... 240 x	21.3 ... 1.1	18.8 x ... 375 x	13.3 ... 0.7
PlanApo S 1.5×	30	15 x ... 120 x	15.3 ... 1.9	24 x ... 192 x	10.7 ... 1.3	37.5 x ... 300 x	6.7 ... 0.8
		12 x ... 150 x	19.2 ... 1.5	19.2 x ... 240 x	12.0 ... 1.0	30 x ... 375 x	7.7 ... 0.6
		11.3 x ... 225 x	20.4 ... 1.0	18 x ... 360 x	14.2 ... 0.7	28.1 x ... 563 x	8.9 ... 0.4
PlanApo S 2.3×	10	23 x ... 184 x	10.0 ... 0.7	36.8 x ... 294.4 x	6.3 ... 0.8	57.5 x ... 460 x	4.0 ... 0.5
		18.4 x ... 230 x	12.5 ... 1.0	29.4 x ... 368 x	7.8 ... 0.6	46 x ... 575 x	5.0 ... 0.4
		17.3 x ... 345 x	13.3 ... 0.7	27.6 x ... 552 x	9.3 ... 0.5	43.1 x ... 863 x	5.8 ... 0.3
PlanApo S 3.5× mono	16	35 x ... 280 x	6.6 ... 0.8	56 x ... 448 x	4.1 ... 0.5	87.5 x ... 700 x	2.6 ... 0.3
		28 x ... 350 x	8.2 ... 0.7	44.8 x ... 560 x	5.1 ... 0.4	70.5 x ... 875 x	3.3 ... 0.3
		26.3 x ... 525 x	8.8 ... 0.4	42 x ... 840 x	5.5 ... 0.27	65.6 x ... 1312.5 x	3.5 ... 0.18
Plan S 1.0×	81	10 x ... 80 x	23.0 ... 2.9	16 x ... 128 x	16.0 ... 2.0	25 x ... 200 x	10.0 ... 1.3
		8 x ... 100 x	28.8 ... 2.3	12.8 x ... 160 x	18.0 ... 1.4	20 x ... 250 x	11.5 ... 0.9
		7.5 x ... 150 x	30.7 ... 1.5	12 x ... 240 x	21.3 ... 1.1	18.8 x ... 375 x	13.3 ... 0.7
Achromat S 0.3×	253	3 x ... 24 x	76.7 ... 9.6	4.8 x ... 38.4 x	53.3 ... 6.7	7.5 x ... 60 x	33.3 ... 4.2
		2.4 x ... 30 x	95.8 ... 7.7	3.8 x ... 48 x	59.9 ... 4.8	6 x ... 75 x	38.3 ... 3.1
		2.3 x ... 45 x	102 ... 5.1	3.6 x ... 72 x	71.1 ... 3.6	5.6 x ... 113 x	44.4 ... 2.2
Achromat S 0.5×	151	5 x ... 40 x	46.0 ... 5.8	8 x ... 64 x	32.0 ... 4.0	12.5 x ... 100 x	20.0 ... 2.5
		4 x ... 50 x	57.5 ... 4.6	6.4 x ... 80 x	35.9 ... 2.9	10 x ... 150 x	23.0 ... 1.8
		3.8 x ... 75 x	61.3 ... 3.1	6 x ... 120 x	42.7 ... 2.1	9.4 x ... 188 x	26.7 ... 1.3
Achromat S 0.63×	115	6.3 x ... 50.4 x	36.5 ... 4.6	10.1 x ... 80.6 x	25.4 ... 3.2	15.8 x ... 126 x	15.9 ... 2.0
		5 x ... 63 x	45.6 ... 3.7	8 x ... 100.8 x	28.5 ... 2.3	12.6 x ... 157.5 x	18.3 ... 1.5
		4.7 x ... 94.5 x	48.7 ... 2.4	7.6 x ... 151 x	33.9 ... 1.7	11.8 x ... 236 x	21.1 ... 1.1
Achromat S 1.0×	69	10 x ... 80 x	23.0 ... 2.9	16 x ... 128 x	16.0 ... 2.0	25 x ... 200 x	10.0 ... 1.3
		8 x ... 100 x	28.8 ... 2.3	12.8 x ... 160 x	18.0 ... 1.4	20 x ... 250 x	11.5 ... 0.9
		7.5 x ... 150 x	30.7 ... 1.5	12 x ... 240 x	21.3 ... 1.1	18.8 x ... 375 x	13.3 ... 0.7
Achromat S 1.25×	50	12.5 x ... 100 x	18.4 ... 2.3	20 x ... 160 x	12.8 ... 1.6	31.3 x ... 250 x	8.0 ... 1.0
		10 x ... 120 x	23.0 ... 1.9	16 x ... 200 x	16.0 ... 1.3	25 x ... 313 x	10.0 ... 0.8
		9.4 x ... 188 x	24.5 ... 1.2	15 x ... 192 x	17.0 ... 0.9	23.5 x ... 469 x	10.6 ... 0.5
Achromat S 1.5×	28	15 x ... 120 x	15.3 ... 1.9	24 x ... 192 x	10.7 ... 1.3	37.5 x ... 300 x	6.7 ... 0.8
		12 x ... 150 x	19.2 ... 1.5	19.2 x ... 240 x	12.0 ... 1.0	30 x ... 375 x	7.7 ... 0.6
		11.3 x ... 225 x	20.4 ... 1.0	18 x ... 360 x	14.2 ... 0.7	28.1 x ... 563 x	8.9 ... 0.4

Figure 65: Technical Specifications: ZEISS SteREO Discovery.V20 [113].

In figure 66 the detailed technical information of the Nabertherm L5/11 oven from Nabertherm GmbH are shown.

Model	Tmax	Inner dimensions in mm			Volume	Outer dimensions[2] in mm			Temperature uniformity of +/- 5K in the empty workspace[5]			Connected load	Electrical	Weight	Heating time
	in °C[1]	w	d	h	in l	W	D	H[3]	w	d	h	in kW	connection*	in kg	in min[4]
L(T) 3/11	1100	160	140	100	3	385	330	405+155	110	50	50	1.2	1-phase	20	40
L(T) 5/11	1100	200	170	130	5	385	390	460+205	170	80	90	2.4	1-phase	30	50
L(T) 9/11	1100	230	240	170	9	415	455	515+240	180	150	120	3.0	1-phase	35	65
L(T) 15/11	1100	230	340	170	15	415	555	515+240	180	250	120	3.2	1-phase	40	75
L(T) 24/11	1100	280	340	250	24	490	555	580+320	230	250	200	4.5	3-phase	55	70
L(T) 40/11	1100	320	490	250	40	530	705	580+320	270	400	200	6.0	3-phase	65	75
L 1/12	1200	90	115	110	1	290	280	430	45	60	40	1.5	1-phase	10	25
L(T) 3/12	1200	160	140	100	3	385	330	405+155	110	50	50	1.2	1-phase	20	45
L(T) 5/12	1200	200	170	130	5	385	390	460+205	170	80	90	2.4	1-phase	30	60
L(T) 9/12	1200	230	240	170	9	415	455	515+240	180	150	120	3.0	1-phase	35	75
L(T) 15/12	1200	230	340	170	15	415	555	515+240	180	250	120	3.2	1-phase	40	85
L(T) 24/12	1200	280	340	250	24	490	555	580+320	230	250	200	4.5	3-phase	55	80
L(T) 40/12	1200	320	490	250	40	530	705	580+320	270	400	200	6.0	3-phase	65	85

[1]Recommended working temperature for processes with longer dwell times is 1000 °C (L.../11) rsp. 1100 °C (L.../12)*Please see page 75 for more information about supply voltage
[2]External dimensions vary when furnace is equipped with additional equipment. Dimensions on request.
[3]Including opened lift door (LT models)
[4]Heating time of the empty and closed furnace up to Tmax -100 K (connected to 230 V 1/N/PE rsp. 400 V 3/N/PE)
[5]Temperature uniformity of +/- 5 K with closed fresh-air inlet in empty work space according to DIN 17052-1 at working temperatures above 800 °C

Figure 66: Technical Specifications: Nabertherm L5/11 oven from Nabertherm GmbH [121].

In figure 67 the detailed technical information of Keithley 2450 source meter from Tektronix Incorporated are shown.

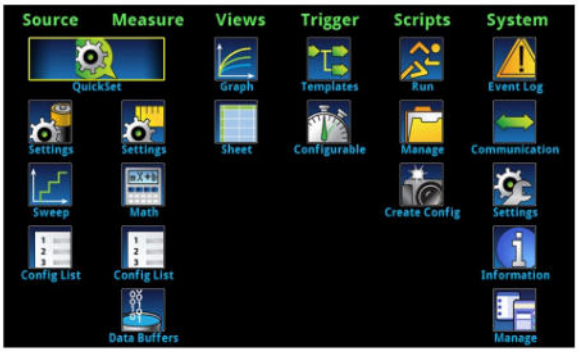

2450 icon-based menu.

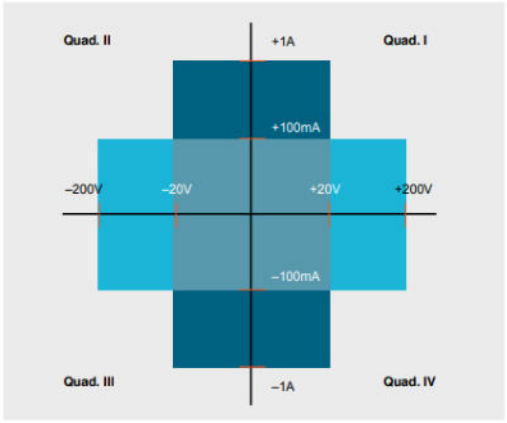

2450 power envelope.

Comparison Table: 2400 vs 2450

Model 2400	Model 2450
V-Ranges: 200 mV – 200 V	V-Ranges: 20 mV – 200 V
I-Ranges: 1 µA – 1 A	I-Ranges: 10 nA – 1 A
0.012% Basic Accuracy	0.012% Basic Accuracy
Wideband Noise: 4 mV_{rms} Typ.	Wideband Noise: 2 mV_{rms} Typ.
Sweep Types: Linear, Log, Custom, Source-Memory	Sweep Types: Linear, Log, Dual Linear, Dual Log, Custom, Source-Memory (SCPI 2400 Mode)
5000 Point Reading Buffer	>250,000 Point Reading Buffer
>2000 Readings/Second	>3000 Readings/Second
SCPI Programming	SCPI (2400 + 2450) + TSP Programming
GPIB	GPIB, USB, Ethernet (LXI)
Front/Rear Banana Jacks	Front: Banana Jacks, Rear: Triax

Figure 67: Technical Specifications: Keithley 2450 source meter [122].

In figure 68 the detailed technical information of the LS0500 solar simulator from LOT-Quantum Design GmbH are shown.

Electrical connection	
Mains voltage	100 up to 240 VAC ± 10 %, 50 up to 60 Hz
Power input	max. 175 VA
Configuration	
Bulb	Xenon short-arc reflector lamp
Filter	Bandpass 400 - 800 nm
Shutter	Frequency max. 40 Hz, switching time approx. 6 ms triggering via external switch, USB or CAN-Bus connection
Dimming	mechanically, 5 steps 0 ... 100%
operating hour meter	display of lamp operation hours, resettable
desktop device	
Dimensions (HxWxD)	210 x 138 x 290 in mm
Weight	5,2 kg
Safety	**as per EN 61010-1**
Equipment class	I
Protection class	IP 20 (EN 60529)
Safety circuit	Yes
Excess temperature protection	Yes
Glare shield	Yes
EMC	
Interference	EN 61326 (class B)
Immunity	EN 61326 appendix A
Voltage fluctuations, flicker	EN 61000-3-3
Harmonic current emissions	EN 61000-3-2
Environmental conditions	
Ambiente temperature	0 °C to 40 °C
Storage temperature	- 20 °C to + 85 °C
Conformity	
	CE
	RoHS
Approvals	
	NRTL on request

Figure 68: Technical Specifications: LS0500 solar simulator [123].

In figures 69 and 70 the detailed technical information of the Axio Observer 7 materials microscope from Carl Zeiss GmbH are shown.

Dimensions (width x depth x height)

Axio Observer 3 materials, 5 materials, 7 materials stand..... approx. 295 mm x 805 mm x max. 707 mm

Weight

Axio Observer 3 materials..... approx. 27 kg
Axio Observer 5 materials ..... approx. 30 kg
Axio Observer 7 materials..... approx. 36 kg

Operating data for Axio Observer 3 materials and 5 materials, manual with integrated power supply unit, and motorized Axio Observer 7 materials with external power supply unit VP232-2.

Operating area..... Enclosed rooms
Protection class..... I
Ingress protection rating..... IP 20
Electrical safety .....DIN EN 61010-1 (IEC 61010-1)
and CSA and UL regulations
Overvoltage category II
Suppression of interference ..... acc. to EN 55011 Class B
Noise immunity..... acc. to DIN EN 61326-1
Line voltage (Axio Observer 3 materials and 5 materials) ... 100 V to 127 V and 200 V to 240 VAC ±10 %
Line voltage of external power supply unit of Axio Observer 7 materials ..... 100 V to 240 VAC ±10 %
A change of the line voltage is not required!
Mains frequency ..... 50 Hz to 60 Hz
Power consumption of Axio Observer 3 materials and 5 materials, manual ..... max. 300 VA
Power consumption of external power supply unit of Axio Observer 7 materials, mot..... max. 190 VA

Power supply unit (ballast unit) HBO 100

Operating area..... Enclosed rooms
Protection class..... I
Ingress protection rating..... IP 20
Line voltage ..... 100 V to 240 VAC
Mains frequency ..... 50 Hz to 60 Hz
Power consumption if operating with HBO 100 .....155 VA

Fuses in accordance with IEC 127

Microscope stand Axio Observer 3 materials and 5 materials, manual ..... T 5 A/H / 250 V, 5x20 mm
Power supply unit VP232-2 for Axio Observer ..... T 4.0 A/H / 250 V, 5x20 mm
HBO 100 power supply unit (ballast unit)..... T 2.0 A/H / 250 V, 5x20 mm

Figure 69: Technical Specifications: Axio Observer 7 materials microscope part I [124].

Light sources

HBO 50W/AC mercury vapor short-arc lamp

Output	50 W
Average service life	100 h
HBO 103 W/2 mercury vapor short-arc lamp	100 W

Optical-mechanical data

Stand with stage focussing	with coarse focusing drive approx. 2mm/rotation and fine focusing drive approx. 1/10 coarse/fine focus transmission ratio, Total travel approx. 10 mm, 13 mm also possible
Change of objective	via 6-objective revolver
Objectives	with M27 screw thread
Eyepieces	Plug-in diameter 30 mm, field number 23

Optical risk group classification acc. to DIN EN 62471:2009

HBO 100	Risk group 2 acc. to DIN EN 62471:2009
XBO 75	Risk group 2 acc. to DIN EN 62471:2009
HXP 120	Risk group 2 acc. to DIN EN 62471:2009
HAL 100	Risk group 1 acc. to DIN EN 62471:2009
VIS-LED	Risk group 1 acc. to DIN EN 62471:2009
MicroLED	Risk group 1 acc. to DIN EN 62471:2009

Figure 70: Technical Specifications: Axio Observer 7 materials microscope part II [124].

In figure 71 the detailed technical information of the UV-Vis spectrophotometer Genesys 10S from Fisher Scientific GmbH are shown.

	GENESYS 10S UV-Vis	GENESYS 10S Vis
Optical Design	Dual-Beam – Internal Reference Detector	Single-Beam
Spectral Bandwidth	1.8 nm	5.0 nm
Light Source (Typical Lifetime)	Xenon Flash Lamp (5 years, 3 years guaranteed)	Tungsten-Halogen Lamp (1000 hrs.)
Detectors	Dual Silicon Photodiodes	Silicon Photodiode
Wavelength		
Range	190–1100 nm	325–1100 nm
Accuracy	±1.0 nm	
Repeatability	±0.5 nm	
Slew Speed	11,000 nm/min	
Scan Speed	Up to 3600 nm/min	
Data Interval for Scanning	0.1, 0.2, 0.5, 1.0, 2.0, 5.0 nm	1.0, 2.0, 3.0, 5.0 nm
Photometric		
Linear Range	Up to 3.5 A at 260 nm	Up to 3.0 A at 340 nm
Display	-0.1 A; -1.5–125%T; ±9999 C	-0.1–3.0 A; -0.3–125%T; ±9999 C
Accuracy	±0.005 A at 1.0 A 0.010 A $K_2Cr_2O_7$	0.5% or ±0.005 A, whichever is greater up to 2 A
Noise	<0.00025 at 0.0 A; <0.00050 at 1.0 A; <0.00080 at 2.0 A; RMS at 260 nm	<0.001 A at 0.0 A <0.002 A at 2.0 A Peak-to-peak at 340 nm
Drift	<0.0005 A/hr	0.002 A/hr after warm-up
Stray Light	<0.08%T at 220, 340 nm (NaI, $NaNO_2$); <1.0%T 198–200 nm (KCl)	<0.1%T at 340, and 400 nm
Display	Graphical with LCD backlight; 9.7 × 7.1 cm (3.8 × 2.8 in)	
Keypad	Sealed Membrane with tactile response keys	
Printer (optional)	40 column Internal (text and graphics); External USB printer (HP PCL 3.0 and greater)	
Connectivity	USB Type A port for USB memory device (front panel) USB Type B port for optional computer connectivity (rear panel) USB Type A port for external printer (rear panel)	
Dimensions	30 W × 40 D × 25 H cm (11.8 × 15.7 × 9.8 in)	
Weight	8.6 kg (19 lbs)	
Power Requirements	Selected Automatically 100–240 V; 50–60 Hz	

Figure 71: Technical Specifications: UV-Vis spectrophotometer Genesys 10S [117].

In figures 72 and 73 the detailed technical information of the FlexAFM from Nanosurf AG are shown.

Standard functionality

Standard imaging modes	Static force, dynamic force, phase contrast, MFM, friction force, force modulation, spreading resistance
Imaging functions	Up to 8000×8000 data points with 24-bit zoom in 8 acquisition channels with dynamic digital filters X/Y sample slope correction
Standard spectroscopy modes	Force–distance, amplitude–distance, phase–distance Tip currentt–tip voltage
Spectroscopy functions	Setup wizard for each spectroscopy mode XY-position table: point, line, and grid (max. 64 positions) 3 distinct spectroscopy phases
Standard lithography modes	Free vector objects drawing or real-time drawing by mouse Tip lift or force control during movement from point to point
Sample approach	Fast home, retract, and advance movement Automatic approach with definable final end position Continuous or step-by-step approach mode

C3000i controller — hardware specifications

X/Y/Z-axis scan and position controller	3× 24-bit DAC (200 kHz)
X/Y/Z-axis position measurement	1× 24-bit ADC (200 kHz)
Excitation & modulation outputs	2× 16-bit DAC (20 MHz)
Analog signal input bandwidth	0–5 MHz
Main input signal capturing	2× 16-bit ADC (20 MHz) 2× 24-bit ADC (200 kHz)
Additional user signal inputs	1× 24-bit ADC (200 kHz)
Digital synchronization	Sync Out 1/2: digital outputs, signal range 0/5V TTL pulses
FPGA module and embedded processor	ALTERA FPGA, 32-bit NIOS-CPU, 80 MHz, 256 MB RAM, multitasking OS
Communication	USB 2.0 hi-speed to PC
System clock	Internal quartz (10 MHz) or external clock
Power	90–240 V AC, 70 W, 50/60Hz

Figure 72: Technical Specifications: FlexAFM part I [126].

In figure 74 the detailed technical information of cantilever Tap190Al-G from Innovative Solutions Bulgaria Ltd. are shown.

Scan head specifications

FlexAFM 5 scan head features

General design	Tripod stand-alone scan head with tip scanner; Flexure-based electro-magnetically actuated XY-scanner with superb linearity; Piezo-based Z-actuator; Optical Z-position sensor; Closed loop Z-control
Laser / detector	High-speed, low-noise 4-quadrant photodiode detector; Choice between red laser and near-infrared SLD; Laser on/off through software and scan head tilting; Optical filters for use with optical microscope phase contrast and fluorescence
Approach	Approach with continuous DC-motor; Up/down arrows on scan head for manual approach; Software-driven automated final approach
Cantilever holder	Automatic self-alignment for cantilevers with alignment grooves. Manual laser adjustment possible for special cantilevers.
Sample observation	Top and side view in air and liquid; White LEDs (brightness 0–100%); Axial illumination for top view
Operating modes	Static Force, Lateral Force, Dynamic Force, Phase Contrast, MFM, EFM, KPFM, Piezo Force, Force Modulation, Scanning Thermal, Spreading Resistance, Multiple Spectroscopy modes, Lithography and Manipulation modes. Some modes may require additional hardware and/or activating of the respective C3000i controller options.

FlexAFM 5 scan head with C3000i controller

Scan head type	100-µm	10-µm
Sample size	Unlimited w/o sample stage 100 mm on sample stage	
Maximum Petri dish height (fluid level)	9 mm (6 mm)	
Manual height adjustment range	6 mm	
Motorized approach range (at tip position)	2 mm	
Maximum scan range	100 µm (1)	10 µm (1)
Maximum Z-range	10 µm (2)	3 µm (1)
XY-linearity mean error	< 0.1%	
XY-flatness at maximum scan range	typ. 5 nm	typ. 1 nm
Detector bandwith	DC – 4 MHz	
Detector noise level	typ. 60 pm / max. 100 pm (3,4)	
Z-sensor noise level (RMS)	typ. 180 pm / max. 200 pm (3)	
Z-measurement noise level (RMS, static mode in air)	typ. 100 pm / max. 200 pm	
Z-measurement noise level (RMS, dynamic mode in air)	typ. 35 pm / max. 50 pm	
Scan head dimensions	143 × 158 × 53 mm	
Scan head weight	1.25 kg	

(1) Manufacturing tolerances ± 5%
(2) Manufacturing tolerances ± 10%
(3) Measured at 2 kHz
(4) Measured with XYContr cantilever

Software options

Stage control option

Drivers	Direct control for all supported stage controllers
Manual move	Via buttons in the C3000i control software
Batch Manager	Automated movement via position list and scripts

Cantilever calibration option

Spring constant calibration	Free resonance detection via thermal tuning Q-Factor calculation Spring constant calculation by Sader method FFT spectrum analyzer, many windowing modes, averaging
Deflection sensitivity calibration	Wizard for deflection sensitivity calculation from force–distance measurements Automatic mode or user-defined parameters

Advanced spectroscopy option

Additional spectroscopy functions	Additional "Stop by input value reached" modulation mode Automatic cantilever drift recalibration Unlimited number of spectroscopy data points 5 distinct spectroscopy phases

Advanced lithography option

Additional lithography modes	Vector-based lithography with objects on layers with different lithography parameters Bitmap-based lithography Nano printing

Scripting interface option

Internal scripting	Visual Basic script editor Ribbon drop-down menu to access user scripts
COM-API	Control of measurement process and data analysis
Compatibility	All applications that support the Microsoft COM Automation standard: Python, C++, LabVIEW, C#, and more.

Advanced modes option

Additional operating modes	Enables advanced measurement modes via an additional digital 2-channel Lock-In. Measure amplitude and phase of an additional signal from many inputs. (e.g higher harmonics, higher resonances, torsional cantilever oscillations, tip voltage modulation, etc.) during imaging and spectroscopy
Secondary lock-in amplifier	Frequency range: 1 kHz–5 MHz Demodulation bandwidth: 11 Hz–23 kHz Amplitude resolution: 20 bit; Phase range: ±180° Reference phase shift: 0–360° (digital) Excitation: tip voltage, 2× user output

KPFM work package

Extends the advanced modes option with the Kelvin probe force microscopy (KPFM) mode. In addition to the Lock-In, it provides a tip voltage feedback controller through a special user interface. In addition to the standard signals, contact potential can be measured during imaging and spectroscopy.

PFM work package

Extends the advanced modes option with the Piezoresponse force microscopy (PFM) mode through a special user interface. In addition to the standard signals, amplitude and phase of the piezo response signal can be measured during imaging and spectroscopy

Advanced dual pass option

Unlocks the contour-following mode and advanced AFM parameter settings for the second scan pass

FluidFM pressure control option

Unlocks nanofluidic pressure control for FluidFM integration.

Figure 73: Technical Specifications: FlexAFM part II [126].

AFM Tip

SHAPE	HEIGHT	SETBACK	RADIUS	HALF CONE ANGLE
Rotated	17 µm (15 - 19 µm)*	15 µm (10 - 20 µm)*	10 nm	20°-25° along cantilever axis, 25°-30° from side, 10° at the apex

AFM Cantilever

Cantilever A	
Shape	Beam
Force Constant	48 N/m (28 - 75 N/m)*
Resonance Frequency	190 kHz (160 - 220 kHz)*
Length	225 µm (215 - 235 µm)*
Width	38 µm (33 - 43 µm)*
Thickness	7 µm (6 - 8 µm)*

* typical range

Figure 74: Technical Specifications: cantilever Tap190Al-G [127]